Analysis of the Impact of Impulse Noise in Digital Subscriber Line Systems

Nedko H. Nedev

A thesis submitted for the degree of Doctor of Philosophy.
The University of Edinburgh.
March 2003

Abstract

In recent years, Digital subscriber line (DSL) technology has been gaining popularity as a high speed network access technology, capable of the delivery of multimedia services. A major impairment for DSL is impulse noise in the telephone line. However, evaluating the data errors caused by this noise is not trivial due to its complex statistical nature, which until recently had not been well understood, and the complicated error mitigation and framing techniques used in DSL systems. This thesis presents a novel analysis of the impact of impulse noise and the DSL framing parameters on transmission errors, building on a recently proposed impulse noise model. It focuses on errors at higher protocol layers, such as asynchronous transfer mode (ATM), in the most widely used DSL version, namely Asymmetric DSL (ADSL).

The impulse noise is characterised statistically through its amplitudes, duration, inter-arrival times, and frequency spectrum, using the British Telecom / University of Edinburgh / Deutsche Telekom (BT/UE/DT) model. This model is broadband, considers both the time and the frequency domains, and accounts for the impulse clustering. It is based on recent measurements in two different telephone networks (the UK and Germany) and therefore is the most complete model available to date and suited for DSL analysis. A new statistical analysis of impulse noise spectra from DT measurements shows that impulse spectra can be modelled with three spectral components with similar bandwidth statistical distributions. Also, a novel distribution of the impulse powers is derived from the impulse amplitude statistics.

The performance of a generic ADSL modem is investigated in an impulse noise and crosstalk environment for different bit rates and framing parameters. ATM cell and ADSL frame error rates, and subjective MPEG2 video quality are used as performance metrics. A new modification of a bit loading algorithm is developed to enable stable convergence of the algorithm with trellis coding and restricted subtone constellation size. It is shown that while interleaving brings improvement if set at its maximum depth, at intermediate depths it actually worsens the performance of all considered metrics in comparison with no interleaving. No such performance degradation is caused by combining several symbols in a forward error correction (FEC) codeword, but this burst error mitigation technique is only viable at low bit rates. Performance improvement can also be achieved by increasing the strength of FEC, especially if combined with interleaving. In contrast, trellis coding is ineffective against the long impulse noise error bursts. Alien as opposed to kindred crosstalk degrades the error rates and this is an important issue in an unbundled network environment. It is also argued that error free data units is a better performance measure from a user perspective than the commonly used error free seconds.

The impact of impulse noise on the errors in DSL systems has also been considered analytically. A new Bernoulli-Weibull impulse noise model at symbol level is proposed and it is shown that other models which assume Gaussian distributed impulse amplitudes or Rayleigh distributed impulse powers give overly optimistic error estimates in DSL systems. A novel bivariate extension of the Weibull impulse amplitudes is introduced to enable the analysis of orthogonal signals. Since an exact closed-form expression for the symbol error probability of multi-carrier QAM assuming Bernoulli-Weibull noise model does not exist, this problem has been solved numerically. Multi-carrier QAM is shown to perform better at high signal-to-noise ratio (SNR), but worse at low SNR than single carrier QAM, in both cases because of the spreading of noise power between subcarriers. Analytical expressions for errors up to frame level in the specific case of ADSL are then derived from the impulse noise model, with good agreement with simulation results. The Bernoulli-Weibull model is applied to study the errors in single-pair high-speed DSL (SHDSL). The performance of ADSL is found to be better when the burst error mitigation techniques are used, but SHDSL has advantages if low bit error rate and low latency are required.

Declaration of originality

I hereby declare that the research recorded in this thesis and the thesis itself was composed and originated entirely by myself in the School of Engineering and Electronics at The University of Edinburgh.

The software used to perform the simulations was written by myself with the following exceptions:

> The routines in the ADSL simulation performing interleaving/deinterleaving, RS coding/decoding, and finding the root of a function are modified versions of code written by Dr. David I. Laurenson.

Nedko H. Nedev

Acknowledgements

First of all, I would like to thank my supervisors, Stephen McLaughlin and David Laurenson, for their outstanding guidance, support, and advice at all stages of this work. Also thanks to Keith Jones, Robert Daley, and Graham Cope from Fujitsu Telecommunications Europe Ltd. for their continued interest, comments, and suggestions.

I am thankful to all of my colleagues in the Institute for Digital Communications for the enjoyable atmosphere and for their help, with particular mention to: Martin Luna Rivera for the advice about trellis coding; David Levey for the useful discussions about impulse noise statistics and generation; Iain Mann for providing impulse generation software; Michael Bennett for proof–reading this thesis. Thanks also to the guys from IT services and Unai Garro for the excellent computer support.

I gratefully acknowledge the financial support of Fujitsu Telecommunications Europe Ltd.

I would like to express my deepest gratitude to my parents, Veska and Hristo, for their dedication, love, and support in all my endeavours.

Бих искал да изкажа дълбоката ми благодарност към моите родители, Веска и Христо, за тяхната преданост, обич и подкрепа във всички мои начинания.

Contents

List of figures

List of tables

Acronyms and abbreviations

AAL	ATM adaptation layer
ACF	Auto-correlation function
ADSL	Asymmetrical DSL
AMI	Alternate mark inversion
ANFP	Access network frequency plan
ANSI	American National Standards Institute
ATM	Asynchronous transfer mode
ATU/-C/-R	ADSL transceiver unit / at the central office end / at the remote terminal end
BER	Bit error rate
BRI	Basic rate ISDN
BT	British Telecom
CAP	Carrierless amplitude/phase
ccdf	Complementary cumulative distribution function
cdf	Cumulative distribution function
cf	Characteristic function
CG	Coding gain
CRC	Cyclic redundancy check
DAVIC	Digital audio-visual council
DFT	Discrete Fourier transform
DMT	Discrete multi-tone
DT	Deutsche Telekom
DWMT	Discrete wavelet multi-tone
DSL	Digital subcriber line (loop)
ETSI	European Telecommunications Standards Institute
FDD	Frequency division duplexing
FDM	Frequency division multiplexing
FEC	Forward error correction
FEXT	Far-end crosstalk
FFT	Fast Fourier transform

FIR	Finite impulse response
FSAN	Full Service Access Network
FTTB/C/Cab/N	Fibre-to-the-building / curb / cabinet / neighbourhood
HDSL	High-speed DSL
IDFT	Inverse discrete Fourier transform
IE	Impulse event
IN	Impulse noise
IP	Internet protocol
ISDN	Integrated services digital network
ITU	International Telecommunications Union
kbps	kilobits per second
MC-QAM	Multi-carrier QAM
MNLT	memoryless nonlinear transform
Mbps	Megabits per second
MPEG	Moving Picture Experts Group
MRP	Markov renewal process
NEXT	Near-end crosstalk
ONU	Optical network units
PAM	Pulse amplitude modulation
PCM	Pulse code modulation
pdf	Probability density function
POTS	Plain old telephone service
PSD	Power spectral density
QAM	Quadrature amplitude modulation
QASK	Quadrature amplitude shift keying
QoS	Quality of service
RADSL	Rate adaptive DSL
RS	Reed - Solomon
SBR	Signal-to-background noise ratio
SC-QAM	Single carrier QAM
SER	Symbol error rate
SHDSL	Single-pair high-speed DSL
SIR	Signal-to-impulse noise ratio

SM	service guarantee margin
SNR	Signal-to-noise ratio
STM	Synchronous transfer mode
TCP	Transmission control protocol
TC-PAM	Trellis coded PAM
TDD	Time-division duplexing
UDP	User datagram protocol
UE	University of Edinburgh
UTP	Unshielded twisted pair
VDSL	Very high-speed DSL
VoIP	Voice over IP

Nomenclature

$a(m)$	transmitted symbol
b	scale parameter of Weibull distribution
$b(n)$	number of bits in DMT subcarrier n
b_{bias}	number of bits in subcarriers loaded with one bit
$b_{DSLframe}$	number of bits in an ADSL frame
b_{target}	target number of bits in a DMT symbol (during bit loading)
b_{total}	total number of bits in a DMT symbol
$b_{trellis}$	number of trellis redundancy bits
$bnl(m)$	Bernoulli process
B	impulse duration pdf parameter
B_{data}/B_{err}	length of data block / error burst in bytes
$C(D)$	check polynomial
d	distance between constellation points
D	interleaving depth
D_i	probability for correct detection of symbol points
$\mathrm{erf}/\mathrm{erfc}$	error function / complementary error function
$\mathcal{E}_s$	symbol energy
$\mathcal{E}_{av}$	average symbol energy
$\mathcal{E}_n$	transmit energy in DMT subcarrier n
$\mathcal{E}_{target}$	target energy in a DMT symbol during bit loading
$\mathcal{E}_{total}$	total energy in a DMT symbol
$f_{exp/ge/par/wb}(x)$	univariate exponential / generalised exponential / pareto / Weibull pdf
$f_l(x)$	impulse lengths pdf
$f_{nI,MC/nII,MC}(x_1, x_2)$	Weibull type I / type II noise pdf for multi-carrier QAM
$f_{n,PAM}(x)$	noise pdf for PAM
$f_{n,SC}(x_1, x_2)$	noise pdf for single carrier QAM
$f_{Ti}(t)$	pdf for the T_i impulse inter-arrival time interval
$f_{wb,I/wb,II/g}(x_1, x_2)$	bivariate Weibull of type I / Weibull of type II / Gaussian pdf
$F(x)$	univariate cumulative density function

$F_{wb,I/wb,II}(x_1, x_2)$	bivariate Weibull cumulative density of type I / type II
$\mathcal{F}$	Fourier transform operator
$g(m)$	Gaussian process
g_n	channel gain for DMT subcarrier n
$G(D)$	generator polynomial
$\|H_{fext/next}\|^2$	FEXT or NEXT power transfer function
$\|H_{line}\|$	line transfer function
$H_n(z)$	Hermite polynomial of n-th degree
k	number of bits in the signal constellation
$k_{fext/next}$	FEXT or NEXT coupling coefficients
M	number of points in the signal constellation
$M(D)$	message polynomial
$n(m)$	noise in the symbol domain
$n_f(m)$	noise in the subcarrier domain
n_R/n_I	real and imaginary noise components
N	number of subcarriers in DMT modulation
N_{cw}	FEC codeword size in bytes
N_S	number of states in the Markov inter-arrival times model
p	impulse probability
p_{ij}	probability of transition from state i to state j in the Markov chain
P_0	parameter in the impulse power pdf
P_{2st}/P_{4st}	2- or 4-state Markov transition probability matrix
P_b/P_B	bit / byte error probability
P_{burst}	probability of data block error in case of an error burst
P_{data}/P_F	data block / frame error probability
P_{fail}	probability of FEC decoding failure
P_{mar}	Markov transition probability matrix
P_M	error probability of symbols with M signal points
$P_{s/s,PAM/s,QAM}$	symbol error probability / for PAM / for QAM
P_u	normalised impulse power
P_{user}	probability of user (non-synchro) ADSL frame
$\mathcal{Q}(x)$	the $\mathcal{Q}$-function
$r(m)$	received symbol

R	user data rate in SHDSL
R	number of Reed-Solomon redundancy bytes in ADSL
$R_G(t)$	input Gaussian correlation coefficients for MNLT
$R_{xx}(\tau)$	impulse auto-correlation function
s_1, s_2	impulse duration pdf parameters
$S_{fext/next}(f)$	FEXT or NEXT power spectral density
$S_{src}(f)$	PSD of the crosstalk source
$S_{xx}(f)$	impulse power spectral density
$\bar{t}$	mean inter-arrival time
t_0	scale parameter of Pareto distribution
T_i	time interval in the Markov inter-arrival times model
u	voltage
u_R/u_I	real and imaginary voltage components
u_0	scale parameter of the generalised exponential distribution
$w(m)$	Weibull process
$\langle y(0)y(t)\rangle$	output Weibull correlation coefficients for MNLT
α	shape parameter of Weibull distribution
α_i	oscilation frequency of the i-th impulse ACF component
β_i	decay rate of the i-th impulse ACF component
γ_m	system performance SNR margin
Γ	gap between the practically achievable and the Shannon SNR limit
$\Gamma(z)$	gamma function
λ	shape parameter of Poisson distribution
π, π_i	steady-state probability vector / probabilities of the Markov chain
σ^2/σ_a^2	power / signal power
σ_g^2/σ_i^2	background / impulse noise power
$\bar{\tau}/\tau_{1/2}$	mean / median impulse duration
τ_1, τ_2	impulse duration pdf parameters
$\tau_{s/adsl/shdsl}$	symbol duration / of ADSL / of SHDSL
θ	shape parameter of Pareto distribution
$\Phi_{n_f/wb/g}(\omega_1, \omega_2)$	characteristic function of the combined noise / Weibull / Gaussian distribution
χ^2	chi-squared value

Chapter 1
Introduction

This thesis is concerned with the impact of impulse noise in the local loop and resulting data errors in digital subscriber line (DSL) systems. DSL is a technology that provides transport of high-bit-rate digital information over telephone subscriber lines. The telephone network reaches virtually every home and workplace in the industrialised world, and the majority of the lines are capable of supporting DSL without the need for major modifications to the outside plant facilities [6]. The vast potential customer base and the economic advantages of leveraging the existing loop infrastructure simply by enabling it with the right technology creates a very strong business case for the promotion of DSL. This factor, combined with the exponential growth of digital communications and required bandwidth, has lead to the popularity and ever increasing demand for this technology.

Motivation

It has been recognised since the first DSL field trials that impulse noise, alongside other telephone line impairments such as attenuation and crosstalk, is a major limiting factor for the reach and achievable bit rate of DSL systems [7]. Impulse noise consists of energy spikes with random amplitudes and spectra, and which occur in a random fashion. It can be induced in the loop by both man-made and natural electromagnetic events, e.g. communication equipment, electrical appliances, vehicles, lightning discharges etc.

Because of its non-stationary unpredictable nature, impulse noise does not lend itself easily to a statistical description. Although the earliest impulse noise studies date from the 1960s [8, 9], it is only recently that a model was proposed [3] which is particularly suited for DSL analysis. This model, developed by British Telecom / University of Edinburgh / Deutsche Telekom (BT/UE/DT) teams, has been derived from broadband noise measurements made in the telephone networks in the UK and Germany, and is the most complete impulse noise model presented to date.

Evaluating the impact of impulse noise on data transmitted over DSL is not straightforward

due to both the complexity of the impulse noise statistics and the use of sophisticated digital transmission techniques in DSL to compensate for the impairments of the telephone lines. Each DSL technology has a unique organisation of the physical layer, which may differ significantly from the others.

Of particular interest is asymmetric DSL (ADSL), since it is the most widely used DSL version, but it has one of the most complicated framing formats among the DSL technologies. ADSL is based on discrete multi-tone (DMT) modulation, employs numerous noise mitigation techniques and sophisticated framing, and can potentially achieve data rates of up to 9 Mbps downstream (network to subscriber) and 1 Mbps upstream (subscriber to network) [1]. The reliable delivery of high-bit-rate services other than simple Internet to a larger proportion of the loop plant is still an open question for ADSL, despite its wide deployment. The results from the analysis of ADSL are also relevant to the next generation of DSL technologies - very high-speed DSL (VDSL), since some VDSL versions are expected to have a physical layer organisation similar to that of ADSL [10]. Therefore, ADSL is the main focus of attention in this work and is studied in detail both theoretically and through simulation.

In comparison with ADSL, single-pair high-speed DSL (SHDSL) has a much simpler physical layer organisation [2]. It uses trellis-coded pulse amplitude modulation (TC-PAM) and offers up to 2.3 Mbps symmetric (both downstream and upstream) service. SHDSL is expected to prove particularly popular with business users, and will be discussed briefly in this study.

Another point of difficulty in evaluating the impulse noise impact on data transmission is that the user requirements to link performance are usually related to higher level protocols and applications. DSL technology may be used for voice, data, or integrated voice/data access, where data usually refers to TCP/IP, asynchronous transfer mode (ATM), frame relay or other packet protocols. Other applications include video transmission, and increasingly, gaming. From a user perspective, metrics such as ATM cell or IP packet error rates, or video image quality, are more representative of the system performance than simple bit or byte error rates.

Contributions

The aim of this work is to investigate the data errors caused by impulse noise in DSL (with emphasis on ADSL) and how these errors affect higher layers of the protocol stack. In order to achieve this, two approaches have been followed - simulation and theoretical analysis.

The simulation analysis in this work combines a model of a generic ADSL modem [1, 11] with impulse noise [3] and crosstalk models. The ADSL modem implementation supports all framing functions relevant to error mitigation, i.e. interleaving, forward error correction (FEC), trellis coding, and combining several ADSL frames in one FEC codeword. The aims pursued in the simulations are to evaluate the impact of impulse noise on higher level protocols and to find appropriate framing parameters for efficient noise mitigation. For this purpose, simulations are run for different values of the framing parameters, bit rates, and crosstalk scenarios. The performance metrics used are ATM cell and ADSL frame error rates and error-free intervals, and subjective MPEG2 bit stream video quality. These metrics have been chosen as representative of the errors in higher level protocols and end user applications.

The simulation results show that interleaving should either be set to maximum if high latency can be tolerated, or not used at all for low latency requirements. Intermediate interleaving depths only worsen the error performance of higher layers. Combining multiple ADSL frames in one FEC codeword is a better alternative to interleaving, but under the ADSL standard's constraints it can only bring benefits at low bit rates. FEC should be used at all times, whereas trellis coding as implemented in ADSL is not efficient against impulse noise. One impulse event may cause a train of errored ATM cells, between which there are "good" cells that can be used by certain applications. Therefore, a measure of error-free intervals between errored data blocks is more appropriate from the point of view of higher layers than error-free seconds. However, the headers of the ATM cells are affected less by impulse noise than the ATM payloads, which may have implications in payload error detection if such "good" cells were to be discovered and used. Also, it is shown that crosstalk from alien systems may worsen the error performance and should be taken into account in an unbundled local loop.

Analytically, the impact of impulse noise in telephone lines at symbol level is evaluated using a Bernoulli-Weibull impulse noise model. Other impulse noise models, which assume Gaussian or Rayleigh distributed impulse amplitudes or powers [12–14], give overly optimistic results if applied to local loop analysis. Although the Bernoulli-Weibull model is not mathematically tractable in the case of the multi-carrier quadrature amplitude modulation (QAM), which is used in ADSL, it is possible to evaluate the symbol errors numerically. Although the multi-carrier QAM signal performs better in impulse noise at high single-to-noise ratios (SNR), it has a worse symbol error probability at low SNR in comparison with single carrier QAM. Building on the Bernoulli-Weibull model and the temporal characteristics of impulse noise, the higher

level errors in ADSL and SHDSL are analysed. When compared to SHDSL, ADSL downstream has superior performance for maximum interleaving depth, but is worse if a low latency and low byte error rate is required.

The achievements of the work described in this thesis are fourfold. Firstly, work on the impulse noise model has lead to new results for the spectral statistics of impulses and novel extensions of the impulse amplitude model to two dimensions and to a distribution of the impulse powers. Secondly, separate from the impulse noise issues, a new modification of a bit loading algorithm has been developed, which offers stable convergence of the algorithm with a trellis coding constellation expansion and a constraint on the minimum number of bits per constellation. Thirdly, the error performance at higher layers of ADSL in impulse noise has been analysed through simulation, and conclusions about the optimum parameter settings and the error patterns at higher layers have been made. And finally, a novel framework for the analysis of DSL systems in impulse noise has been proposed, and ADSL and SHDSL have been considered as an example. The latter two contributions will also be applicable to VDSL systems with modulation and framing similar to that of ADSL. In summary, the impact of impulse noise in DSL systems is significant and the best approach to its mitigation depends on the requirements of the end user application.

1.1 Thesis layout

The remainder of this chapter describes the layout of the thesis, which is organised into a further five chapters.

Chapter 2 starts with a brief discussion of high-speed access technologies and the evolution of digital subscriber line systems, to provide a general description of the technological solutions and potential problems in DSL transmission. It then presents the various data types and protocol stacks that may be found in DSL systems, to demonstrate the diversity of data as viewed from a user perspective. Three common or promising DSL systems are then examined, concentrating on the most widely used technology - ADSL. The complexity of ADSL modulation and framing is demonstrated, followed by an overview of SHDSL and VDSL. It is concluded that there is still a requirement for the study of the impact of impulse noise on the errors at higher layers in DSL systems.

In Chapter 3, the background to the various telephone line noise impairments is presented.

Earlier impulse noise studies are outlined, followed by a discussion of the BT/UE/DT impulse noise model. A new analysis of the statistics of impulse spectra from DT measurements is presented, which can be used for refining the impulse noise model to generate impulses with a more complex spectral contents. Also, the impulse amplitudes statistics are used to derive a novel distribution of the impulse powers. The problem of crosstalk generated by the various DSL technologies is then considered with a special attention to summing crosstalk from mixed sources, which is a likely scenario in an unbundled telephone network. The chapter concludes with some comments about radio frequency interference and its impact on DSL.

Chapter 4 deals with simulation analysis of the errors caused by impulse noise in ADSL downstream. The simulation platform is described in detail, including a new modification of a bit loading algorithm to ensure convergence with simultaneous trellis code constellation expansion and constraints on the minimum number of bits per constellation. The impact of various ADSL framing parameters on impulse noise mitigation is investigated, using as performance measures ATM cell errors, ADSL frame errors, and MPEG2 video quality. Conclusions about the efficiency of the various noise mitigation techniques in ADSL for user applications with different requirements are drawn. The error patterns in an ATM stream and their effect on different applications are also discussed.

In Chapter 5, a Bernoulli-Weibull impulse noise model at symbol level is introduced to allow for theoretical analysis of the impact of impulse noise on DSL systems. A comparison with other models assuming Gaussian distributed impulse amplitudes shows that they give an overly optimistic error estimates when used for DSL analysis. A numerical method to find the error probability of multi-carrier QAM is proposed to overcome the fact that no closed-form analytical expression for the Bernoulli-Weibull model exists. A comparison between single and multi-carrier QAM is then presented, showing that the latter performs better at high SNR, and the former - at low SNR. A framework for calculating the errors at higher levels in ADSL and SHDSL is developed, and the advantages and disadvantages of these DSL technologies for different user requirements are underlined.

Finally, in Chapter 6, the main contributions of the thesis are highlighted, certain limitations of the work are identified, and areas for possible further work are suggested.

Chapter 2
Background to xDSL systems

2.1 Introduction

Digital subscriber line (DSL) technologies enable transmission of high-speed data to and from customer premises over existing unshielded twisted pair (UTP) telephone networks. These networks were often built decades ago and were designed to carry only voice within a bandwidth of less than 4 kHz. The local loop as a broadband transmission media is therefore strongly impaired by noise and attenuation. In order to mitigate the line impairments, the DSL technologies (collectively referred to as xDSL) have a complicated organisation in their physical layer, which differs significantly for each of the various DSL systems. At higher layers xDSL systems are expected to carry various types of data ranging from direct bit stream to complex packet protocols. The impact of line impairments on the data and consequently the services transmitted over xDSL is the motivation behind this work.

After an overview of the various access media and the evolution of DSL technologies, this chapter will concentrate on the specifics of the physical layer of the most common DSL systems. Besides the already accepted DSL standards, proposals for new standards are also discussed. Attention is also given to the possible data formats carried over DSL.

2.2 High-speed access technologies

The telephone line is only one of four principal technologies for transmission of high-speed data to and from customer premises. The alternative media are coaxial cable, optical fibre and wireless. There is certainly no universal transmission medium that best serves all applications and locations, as can be seen from the summary of the advantages and weaknesses of different media below.

Telephone loop. Telephone lines have a very high penetration among the population in countries with developed communications infrastructure. Therefore DSL potentially has a very large

customer base. However, typically between 5% and 10% of the total loop plant are unsuitable for DSL due to excessive loop length, presence of load coils, or because a large number of bridge taps exist on the line. DSL also suffers from noise and interference on the line and has a poor broadcast efficiency.

Coaxial cable. Coaxial cable networks were originally installed for unidirectional video broadcast systems but are being increasingly upgraded and used for interactive services such as voice and data. Cable providers have had some success by bundling broadcast, data and voice services. A drawback of coaxial cable networks is that they reach mainly residential customers but much fewer businesses, so the coaxial cable customer base is restricted.

Optical fibre. Optical fibres have an impressive bandwidth-distance product and can deliver large bit rates over large distances. However, economics and logistical challenges hold back their wide deployment. Fibre optic lines are now common to major business sites and are on the increase in residential areas. However, entirely optical networks are still rare and the last hundreds meters normally use copper technologies such as DSL, coaxial cables, or Ethernet.

Wireless. Wireless access offers higher customer location flexibility than cable access solutions. Wireless may also be preferable in areas where building cable infrastructure can be too costly, such as remote areas or busy cities. However, wireless access is restricted by limited radio spectrum bandwidth and faces challenges of placing radio transceivers (either on earth or in orbit). Wireless links are also subject to substantial noise interference. Connections to satellites at medium and high earth orbit suffer excessive delays due to the geographical distance.

2.3 Evolution of DSL telephony

It is arguable when the subscriber loop was first used for data transmission - was it the telegraph, or the first voice-band modems? The term *digital subscriber line* was first conceived to describe the digital connection between subscribers and the integrated services digital network (ISDN). Since then various DSL systems have evolved in reflection to different user requirements and technological advances. An outline of the DSL versions follows below.

Basic-rate access DSL

The acronym DSL was originally used to refer to this technology, also known as basic-rate access transmission for ISDN (ISDN-BA or BRI). The development of ISDN started in the 1970s, with first ISDN trials in 1985. DSL provides full-duplex access to ISDN at 160 kbps over a single telephony pair. The DSL payload is usually two 'B' or Bearer channels of 64 kbps each, one 'D' or signalling channel at 16 kbps, which can sometimes be used for packet data, as well as a 16 kbps channel for framing and line control. The ITU Recommendation G.961 [15] defines three different systems:

- *Appendix I:* 2B1Q coding with echo cancellation, used in North America and much of Europe. It is also standardised as ANSI T1.601 [16] and ETSI TS 102 080 [17].
- *Appendix II:* 4B3T coding with echo cancellation, used in some European countries (primarily Germany). As well as in G.961 it is also standardised in Annex B of ETSI TS 102 080 [17].
- *Appendix III:* alternate mark inversion (AMI) coding with synchronised time-division duplexing (TDD), used in Japan.

ISDN was once hailed as the ultimate replacement of the plain old telephone service (POTS). It enjoyed, however, only limited success. The more notable exception is Germany, where ISDN deployment was accelerated by government mandate. ISDN was focused on telephony services and lower-speed packet-switched data. However, the driving market force behind the roll out of digital subscriber loops turns out to be the Internet. ISDN networks were poorly suited for high-speed packet-switched data and long holding times, which are characteristic of Internet access. Therefore, in countries where deployment was driven by market demand the ISDN service failed to pick up.

T1/E1

Although originally T1/E1 were designed and installed for trunk transmission of 24 or 32 multiplexed 64 kbps pulse code modulation (PCM) voice channels between central offices, nowadays they have been replaced almost completely for that use by fibre and microwave. Since the 1970s, however, they have also been used for high-speed links between central offices and customer sites and should arguably also be considered DSLs. Although T1/E1 have been made

obsolete by newer DSL technologies, already installed systems used as DSL are unlikely to be replaced in the short term. *T1* is a 1.544 Mbps dual simplex system on two pairs using AMI or B8ZS (bipolar, with 8-zero substitution) coding and repeaters every 6,000 ft (≈1.83 km), used in North America. *E1* is similar to T1, but at 2.048 Mbps with HDB3 (high density bipolar order 3) or AMI coding and repeaters spaced approximately every 2 km, used everywhere else in the world. T1 is standardised as ANSI T1.403 [18] and E1 - as ITU Recommendation G.703 [19].

High-speed DSL (HDSL)

HDSL is generally used as a substitution for T1/E1 with the advantage that it has a longer maximum reach without the use of repeaters than T1/E1 (12,000 ft / 3.66 km as opposed to 6,000 ft / 1.83 km). The work on HDSL started in the mid 1980s, with first service launched in 1992. The earlier HDSLs are 1.536 Mbps two-pair or 2.048 Mbps two- and three-pair, full-duplex systems using 2B1Q coding and echo cancellation. HDSL using carrierless amplitude phase (CAP) modulation has also been standardised. Later versions of HDSL with 2B1Q, CAP or trellis coded pulse amplitude modulation (TC-PAM) line coding use only one pair and are sometimes referred to as SDSL (single-pair or symmetric DSL) or HDSL2 (second generation HDSL). HDSL is standardised in ANSI T1.TR.28 [20] and ANSI T1.418 [21], ITU Recommendation G.991.1 [22], and ETSI TS 101 135 [23].

Asymmetric DSL (ADSL)

ADSL is a home user-oriented technology that allows downstream (towards customer) bit rates of up to about 9 Mbps, and upstream (towards network) of up to 1 Mbps. At the same time ADSL leaves the possibility for using analogue voice (POTS) and ISDN services at baseband frequencies. The ADSL development began in the early 1990s and the first field trials took place in 1995. ADSL is based on discrete multi-tone (DMT) modulation and was initially standardised as ANSI T1.413 [11]. ITU G.992.1 [1] uses ANSI T1.413 as a core system but is expanded through annexes to meet regional needs. ETSI TS 101 388 [24] is based on G.992.1 but defines European specific requirements. ITU G.992.2 [25] and ANSI T1.419 [26] (also known as ADSL “lite”) define a simpler system than the standard ADSL that is line compatible with G.992.1 and T1.413.

ADSL systems based on single carrier modulation such as carrierless amplitude and phase (CAP) and quadrature amplitude modulation (QAM) also exist. The most prominent single carrier ADSL is the rate adaptive DSL (RADSL) based on CAP. RADSL was submitted for standardisation at ANSI as document no. T1E1/97-104R2a when competing with T1.413 for approval. At the moment a CAP-RADSL standard does exist under the number ANSI T1.TR.59 [27] but is much less common than its DMT counterpart. Note that the DMT-ADSL also provides the capability for rate-adaptive operation.

ADSL has achieved a much wider deployment than ISDN-BA and the number of ADSL connections is still growing at a fast rate due to several factors. ADSL offers a much higher downstream bit rate in comparison with ISDN. ADSL is also much more flexible in carrying different protocols on top without being tied up to a specific network architecture. The success of ADSL has also been enhanced by the ever increasing need for faster Internet connections.

Single-pair high-speed DSL (SHDSL)

SHDSL belongs to the family of symmetric DSL and covers applications traditionally served by HDSL and T1/E1 systems. It is believed SHDSL will repeat the success of ADSL and prove popular with customers that require symmetric services. SHDSL is a product of the standardisation efforts of ITU which began in the late 1990s and the final version of the standard was released in 2001. SHDSL achieves higher bit rate or reach in comparison with older HDSL systems. It also offers better spectral compatibility with other DSL systems. It can transport from 192 kbps to 2.3 Mbps over a single-pair or 384 kbps to 4.6 Mbps over two pairs and is the first standardised multi-rate symmetric DSL. SHDSL uses TC-PAM line coding and adheres to ITU G.991.2 [2], ETSI TS 101-524 [28] and ANSI T1.422 [29].

Very high-speed DSL (VDSL)

VDSL is an extension of DSL to higher rates and will be able to carry up to 58 Mbps aggregate (up plus downstream) data rate both in symmetric and asymmetric modes. At such high bit rates the loop length is severely restricted. Therefore VDSL will be used primarily in hybrid fibre/copper systems to connect optical network units (ONU) to the customer premises. VDSL ranges vary between 300 m and 2 km depending on the scenario, e.g. fibre to the neighbourhood (FTTN), FTTC(urb), or FTTB(uilding).

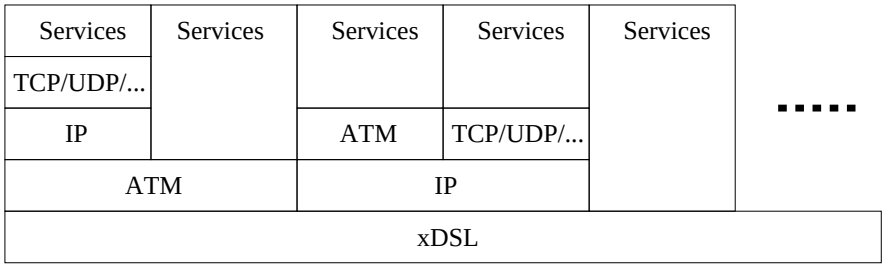

Figure 2.1: *Protocol stacks over xDSL.*

VDSL is expected to capitalise on the growing deployment of optical fibre networks around the world. It combines the ease of working with copper with the high bit rate offered by fibre. VDSL is in the process of standardisation and a discussion is going on about the physical layer specifications. The relevant standards in development are ANSI T1.424 - Trial Use [10], ITU Recommendation G.993.1 [30], and ETSI TS 101 270 - 1 [31].

A summary of the features of the most common xDSL systems is presented in table 2.1. Later sections of this chapter will make a more detailed overview of the most prolific and/or promising DSL versions, namely ADSL, SHDSL and VDSL.

2.4 Protocol stacks over xDSL

Most xDSL systems can be regarded as “bit pipes” that work in a synchronous transfer mode (STM) and are not confined to a specific protocol. A more notable exception is ISDN, which has standardised signalling and transfer modes geared towards the ISDN network. ADSL is another exception and has a standardised asynchronous transfer mode (ATM). ATM is only an option alongside STM in the “full” ADSL version [1, 11], but is compulsory in the “light” ADSL version [25] (see section 2.5.5, p. 24).

The services that an xDSL system may transport include high-speed access to Internet, ATM or frame relay networks, virtual private networks, remote access to corporate local area networks (LANs), digital voice telephony, video streaming, retrieval or video on demand. In the general case there is a variety of possible protocol stack scenarios that can carry these services over a DSL link (Figure 2.1). Two main transport modes can be differentiated: bit stream and packet data.

xDSL	Standard(s)	Modulation	No. of pairs	Line bit rate	Freq. band
T1	ANSI T1.403	AMI or B8ZS	two	1.544 Mbps symmetric	up to 1.544 MHz
E1	ITU G.703	HDB3 or AMI	two	2.048 Mbps symmetric	up to 2.048 MHz
ISDN	ITU G.961 ANSI T1.601 ETSI TS 102 080	2B1Q or 4B3T	one	160 kbps symmetric	up to 80 kHz
HDSL	ITU G.991.1 ETSI TS 101 135 ANSI T1.TR.28	2B1Q	two	1.544 Mbps symmetric	up to 370 kHz
HDSL2	ANSI T1.418	16 TC-PAM	one	1.544 Mbps symmetric	up to 300 kHz upstream up to 440 kHz downstream
ADSL	ANSI T1.413 ITU G.992.1 ETSI TS 101 388	DMT	one	max 1 Mbps upstream max 9 Mbps downstream	up to 138 kHz up to 1.104 MHz
ADSL lite	ITU G.992.2 ANSI T1.419	DMT	one	max 1 Mbps upstream max 1.5 Mbps downstream	up to 138 kHz up to 552 kHz
RADSL	ANSI T1.TR.59	CAP	one	max 1 Mbps upstream max 8 Mbps downstream	up to 138 kHz up to 1.104 MHz
SHDSL SDSL	ITU G.991.2 ANSI T1.422 ETSI TS 101 524	16 TC-PAM	one	max 2.312 Mbps symmetric	up to 400 kHz
VDSL	ANSI T1.424 trial-use ITU G.993.1 ETSI TS 101 270	DMT or QAM	one	max 13 Mbps upstream max 23 Mbps downstream max 28 Mbps symmetric	up to 12 MHz

Table 2.1: *Common broadband copper loop transmission systems.*

2.4.1 Bit stream

In this approach the transmitted data is carried directly by the xDSL bit stream in synchronous mode. Telephony is transmitted either in a direct 64 kbps PCM stream or at reduced rate with some type of compression, digital video is carried as an MPEG bit stream, and network protocols are transmitted directly over the link.

2.4.2 Packet data

Another possibility is to use a packet layer as an intermediate protocol to transfer data. Two packet protocols are fighting for dominance in xDSL - ATM and IP, although frame relay and other packet protocols are found in some DSL implementations.

IP is gaining popularity because it is the underlying protocol for one of the most common DSL applications - Internet access. The increase in voice over IP (VoIP) usage also contributes to its case. IP can carry other protocols on top, such as TCP, UDP and even encapsulated ATM (although many would question the rationale behind the latter solution).

ATM, on the other hand, is favoured by the telcos because it enables them to extend their ATM backbones directly to the customers. In this way the telcos can take advantage of economies of scale and no protocol conversion at the network interfaces is needed. Voice telephony over ATM is carried using ATM adaptation layer 5 (AAL5), AAL2, or a structured circuit emulation service. Digital video is transmitted as MPEG over AAL5, and video conferencing - over AAL5 or AAL1. It is also common to encapsulate IP over ATM, from where further protocols can be built on top of IP.

There is no standard protocol stack scenario over xDSL. This work considers some bit stream applications as representative of the STM mode, and ATM as representative of packet data. However, the results could be extended to other protocol scenarios.

2.5 Overview of ADSL systems

Asymmetric digital subscriber line (ADSL) is a telephone loop technology which provides downstream (towards customer) bit rates of up to approximately 9 Mbps and upstream (towards network) bit rates of up to 1 Mbps over one twisted pair. The term *asymmetric* reflects

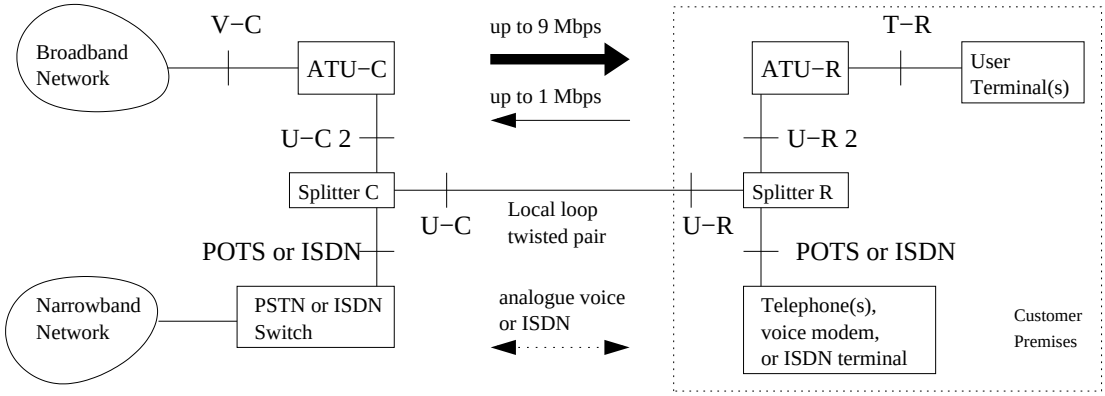

Figure 2.2: *Reference model of an ADSL system.*

the fact that the available bit rate towards the customer is much greater than that from the customer. ADSL also allows for POTS or ISDN to be transmitted at baseband frequencies. The POTS/ISDN signal is combined with the ADSL data transmission via a filter commonly called a "splitter" (Figure 2.2). The splitter consists of a low-pass filter on the POTS/ISDN side and a high-pass filter on the ADSL side, although there are simplified designs that contain only the low-pass filter and count on the input filters of the ADSL modem to do the high-pass filtering.

This section will concentrate on ADSL features relevant to noise impact modelling and analysis. Full ADSL specifications can be found in ANSI T1.413 [11], ITU G.992.1 [1], ETSI TS 101 388 (Europe specific requirements only) [24], and ITU G.992.2[25].

2.5.1 ADSL architecture and transport capabilities

ADSL supports up to four downstream simplex bearer channels named AS0 to AS3, and up to three duplex bearer channels named LS0 to LS2 (Figure 2.3). The signalling downstream channels are operations, administration and maintenance (OAM), embedded operations channel and ADSL overhead control (EOC/AOC), indicator bits (ib) and the optional network timing reference (NTR). In the upstream direction ADSL only provides the duplex bearers LS0 to LS2 through input interface T-R, as well as the EOC/AOC channel. ATM transport is supported at least over bearer channel AS0 downstream and LS0 upstream.

There are two paths between the multiplexer Mux/Sync control and Tone ordering. Both paths are protected from transmission errors by cyclic redundancy checks (CRC), forward error cor-

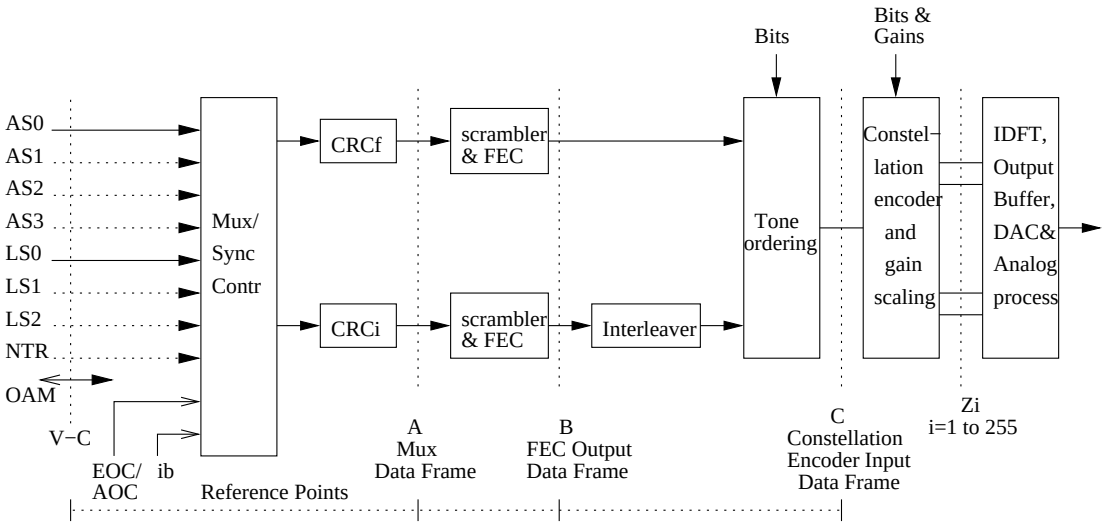

Figure 2.3: *Block diagram of a generic ADSL modem [1] - downstream transmitter.*

rection (FEC), and are scrambled to randomise the data stream. In one of the paths the data is also interleaved. The interleaved path provides a lower error rate but higher latency in comparison with the non-interleaved "fast" path. A bearer channel can be allocated by the multiplexer either to the fast or the interleaved path. The data from both paths is then encoded into a discrete multi-tone (DMT) symbol with a maximum of 256 tones downstream and 32 tones upstream. The modulation may also be trellis coded (TC) and many implementations use TC although it is optional in the standards.

ADSL supports a net data rate of at least 6.144 Mbps downstream and 640 kbps upstream. Higher bit rates are possible but optional in the standards. The maximum bit rates mentioned in the literature are 8 or 9 Mbps downstream and 1 Mbps upstream [6, 32–34].

2.5.2 ADSL framing

The ADSL superframe and frame structures are shown in Figure 2.4. An ADSL superframe is composed of 68 data frames, which are encoded and modulated into DMT symbols (one data frame is mapped onto one DMT symbol). At the end of each superframe the modulator inserts a synchronisation symbol, which carries no user or signalling data and whose function is to establish superframe boundaries. From the bit-level perspective, the DMT symbol rate is 4000 baud (symbol duration 250 μs), but because of the insertion of the synchronisation symbol the

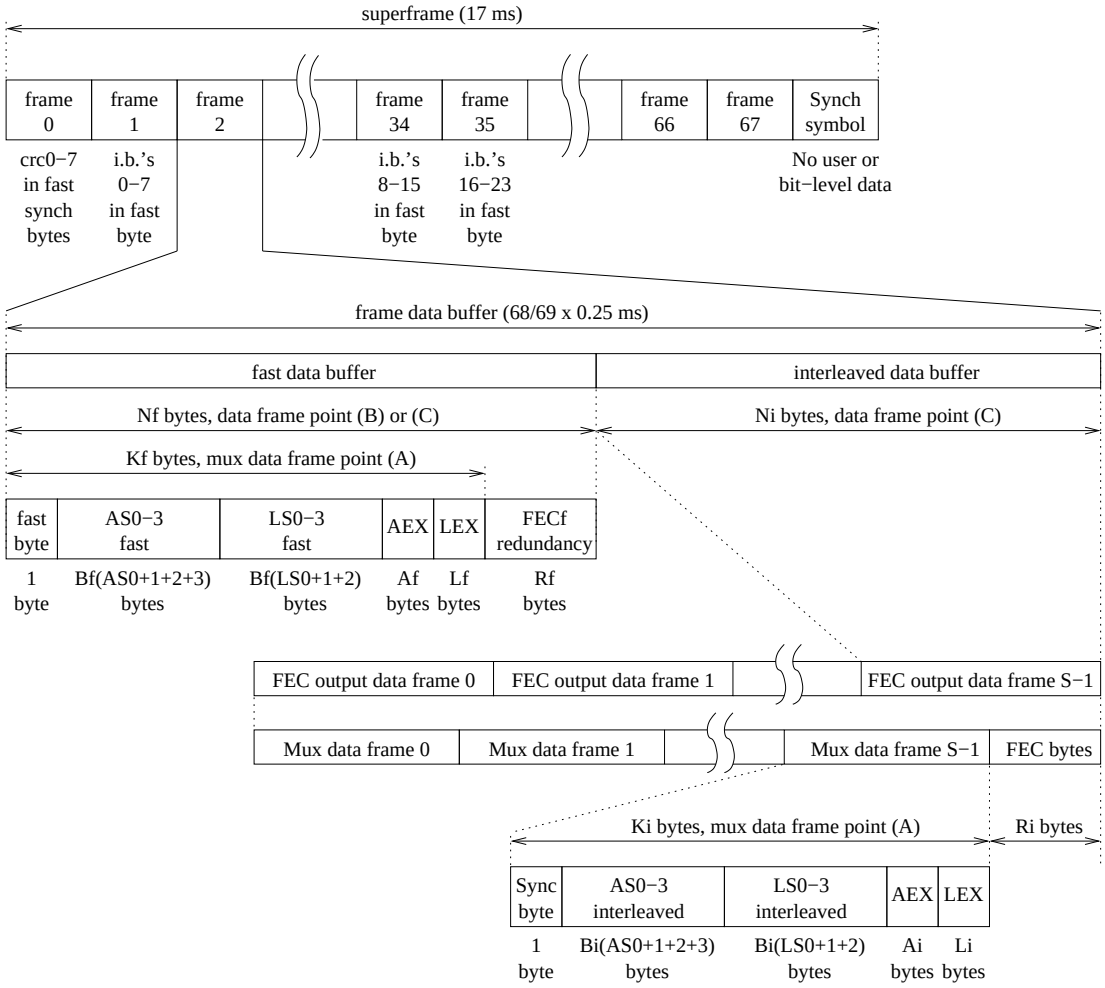

Figure 2.4: *ADSL frame structure [1] - downstream, full overhead.*

actual transmitted DMT symbol rate is 69/68 x 4000 baud.

Each frame within the superframe carries data from both the fast and interleaved buffer. The fast data buffer contains the user data from those channels AS0-3 and LS0-2, which have been assigned by the multiplexor to the fast path. The overhead consists of a fast synchronisation byte, used to carry CRC, ib, EOC and synchronisation control bits, as well as AEX and LEX bytes if the buffer contains data from the AS or the LS channels respectively. FEC redundancy bytes are appended to the end of the fast buffer frame. Even when no user data is transmitted along the fast path, it contains at least the fast synchronisation byte.

The interleaved buffer frame is also composed of a synchronisation byte carrying CRC, AOC,

and synchronisation control bits, user data assigned to the interleaved path, and AEX/LEX bytes. However, one FEC codeword of the interleaved path may comprise several mux frames of reference point A. The FEC output is divided into FEC output data frames (reference point B) and the FEC output data frames are interleaved at a specified depth to produce the interleaved frames in reference point C. As with the fast buffer, the interleaved buffer should contain at least the synchronisation byte even when no user data is transmitted over it.

The ADSL frame structure as described above contains the full possible overhead. The framing overhead can be reduced by eliminating the AEX/LEX bytes (reduced overhead framing with separate fast and sync bytes). If one of the paths is not used (single latency mode) it is also possible to eliminate its synchronisation byte and operate in reduced overhead framing with merged fast and sync bytes.

2.5.3 Coding and interleaving techniques in ADSL

Due to the considerable noise impairments of telephone lines (see chapter 3, p. 32), ADSL uses numerous error detection/mitigation techniques. Only an outline of these techniques will be given here. For full details of their ADSL implementation see [1, 11, 25].

Cyclic redundancy check (CRC). This error detection technique is implemented separately for the fast and the interleaved buffer. Eight bits per buffer are generated for each superframe of 68 data frames. The CRC bits are then transmitted in the first frame of the following superframe. The bits covered by CRC include all the data in the mux frames (reference point A) except the previous CRC bits.

Scramblers. Scrambling is related indirectly to error correction because it randomises the data stream, which benefits various digital signal processing algorithms at the receivers (e.g. equalisers, echo cancellers etc.). ADSL uses a self-synchronising scrambler (see e.g. [35]) and as a consequence the bit error rate is actually multiplied after descrambling (tripled in the ADSL case). Scrambling is applied separately to the fast and the interleaved buffers in ADSL, and both scrambling and descrambling are performed on the serial data streams without reference to any framing or symbol synchronisation.

Forward error correction (FEC). Reed-Solomon coding (see e.g. [36]) has been chosen as the error correction technique in ADSL. Reed-Solomon (RS) code arithmetic executes in Galois Field GF(2^8) and allows for up to 16 bytes to be corrected in a codeword of up to 255 bytes.

If the K message bytes $m_i,\ i = 0 \ldots K-1$, and the R check bytes $c_i,\ i = 0 \ldots R-1$ are represented through their polynomials $M(D) = m_0 D^{K-1} + m_1 D^{K-2} + \cdots + m_{K-2} D + m_{K-1}$ and $C(D) = c_0 D^{R-1} + c_1 D^{K-2} + \cdots + c_{R-2} D + c_{R-1}$ respectively, then the check bytes can be computed from:

$$C(D) = M(D) D^R \bmod G(D), \tag{2.1}$$

where $G(D) = \prod_{i=0}^{R-1} (D + \alpha^i)$ is the generator polynomial of the RS code, and α is a primitive element that satisfies the primitive binary polynomial $x^8 + x^4 + x^3 + x^2 + 1$. A data byte $(d_7, d_6, \ldots, d_1, d_0)$ is identified with the Galois Field element $d_7\alpha^7 + d_6\alpha^6 + \cdots + d_1\alpha + d_0$. The ADSL standard requires support of all even numbers from 0 to 16 of redundancy bytes per codeword for both the fast and the interleaved buffer. For RS decoding and correction algorithms see e.g. [37].

Interleaving. The Reed-Solomon codewords in the interleaved buffer are convolutionally interleaved in a bid to overcome burst errors. By spreading the error bursts over several Reed-Solomon (RS) codewords it is hoped that the number of errors will become small enough to allow for error correction by the RS code. In the ADSL version each byte b_i of a frame at the input of the interleaver is delayed by $(D-1) \times i$ bytes, where D is the interleave depth. ADSL supports interleave depth which is a power of two from 1 to 64.

Number of frames per RS codeword. Combining several mux frames in a single RS codeword can also be considered a burst error mitigation technique as it effectively "spreads" the codeword over several ADSL frames. The number of frames per codeword S in ADSL can be any power of 2 between 1 and 16. S=1/2 is optional to allow for bit rates higher than 8 Mbps to be transmitted in the interleaved path downstream.

The last three techniques are aimed at neutralising the impact of impulse noise in ADSL. The influence of their parameters is a subject of detailed study in this work. A summary of the minimum FEC capabilities required by the ADSL standards [1, 11, 25] is presented in table 2.2. It should be noted that as a result of the error mitigation techniques, the interleaved data buffer at the receiver will be delayed with respect to the fast data buffer by (number of mux frames per FEC codeword x interleave depth x 250) μs.

Trellis coding is another ADSL coding technique and will be discussed in the next section.

Parameter	Fast buffer	Interleaved buffer
Redundancy bytes per RS codeword - R	0,2,4,6,8,10,12,14,16	0,2,4,6,8,10,12,14,16
Mux frames per RS codeword - S	1	1, 2, 4, 8, 16
Interleave depth - D	1	1, 2, 4, 8, 16, 32, 64

Note that R $>$ 0 only if user data is transmitted over the respective buffer. Also, R must be an integer multiple of S.

Table 2.2: *Minimum FEC coding capabilities for ADSL.*

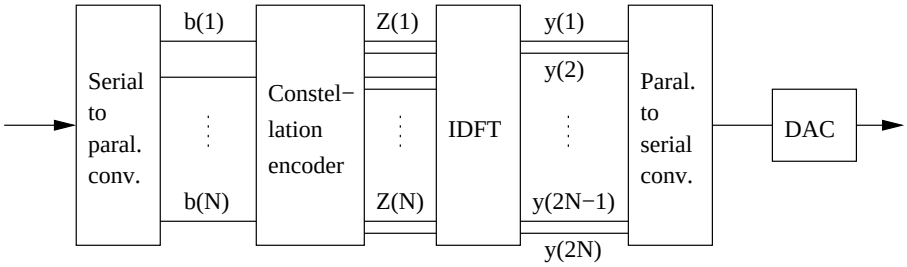

Figure 2.5: *Simplified diagram of a DMT transmitter.*

2.5.4 DMT modulation

The ANSI T1.E1.4 Working Group, which developed the original ADSL T1.413 standard [11], took the decision to base the ADSL line code on multicarrier modulation where each subcarrier uses quadrature amplitude modulation (QAM). This multicarrier version is commonly known as discrete multi-tone (DMT)[1].

DMT was first suggested by Weinstein and Ebert [39] and its implementation is based on discrete Fourier transform (DFT) techniques. The DMT modulation consists in dividing the data into blocks and encoding it into a set of N multibit complex symbols Z_i. Inverse DFT (IDFT) is then applied on the set of complex symbols (equation 2.2). In the end 2N real samples are generated and passed through a digital-to-analogue converter (DAC) as shown in figure 2.5.

$$Y_n = \sum_{k=0}^{N-1} Z_k e^{\frac{j2\pi nk}{N}} \tag{2.2}$$

Modulation via an IDFT is equivalent to multicarrier quadrature amplitude shift keying (QASK), in which the modulating baseband pulse shape is a rectangle and as a result the spectra of the

[1]The usage of DMT for ADSL was first proposed in 1991 [38] and two years later, not without heated debates, was chosen to be the basis of the ADSL standard.

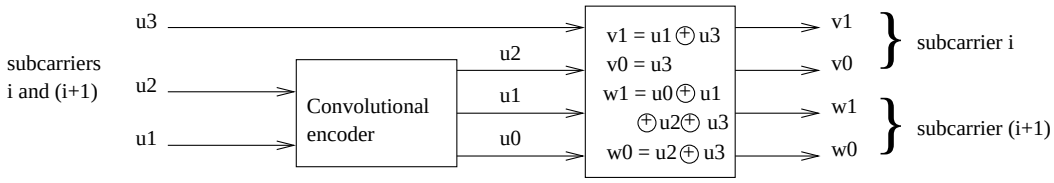

(a) Conversion of (u3,u2,u1) to (v1,v0) and (w1,w0)

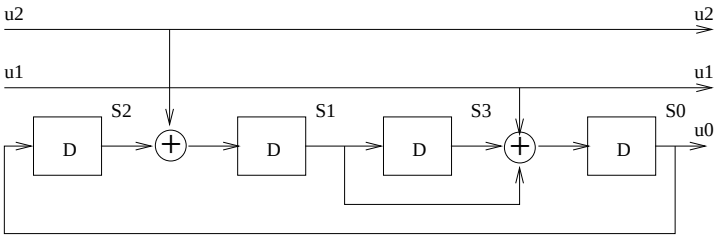

(b) Finite state machine for Wei's convolutional encoder

Figure 2.6: *Trellis coding in ADSL.*

individual subcarriers are sinc functions. The advantage of this approach is that both the transmitter and receiver can be implemented using efficient fast Fourier transform (FFT) techniques. No passband filtering is required at the output of the constellation encoders as opposed to other multicarrier modulation techniques [39, 40].

Trellis coding

The ADSL standard gives as an option the possibility to trellis code the modulation. The standardised convolutional encoder is based on Wei's 16-state 4-dimensional trellis code [41]. The encoding is carried out from one subcarrier to the next, as proposed by Decker et al. [42], and the state of the encoder is forced back to zero at the end of each DMT symbol [1, 11, 25]. The subcarriers are grouped in pairs and the three least significant bits (u1,u2,u3) from two successive subcarriers are coded, which reflects a constellation expansion of 1 bit per four dimensions (figure 2.6). That is, the trellis code in the ADSL standard protects only the two most vulnerable (with least Hamming distance) bits in each constellation. The output coded bits (v1,v0) and (w1,w0) are dimensions in the vectors of the two successive constellations.

Bit loading

One of the advantages of multicarrier modulation is that the number of bits and the energy transmitted over each subchannel can be set adaptively. In this way noisy regions of the spectrum can be "loaded" with fewer bits or avoided altogether. The emitted power spectral density (PSD) can also be easily controlled, which is useful for spectral management in the local loop.

The algorithms for assigning data and energy to each of the subcarriers, commonly known as *loading* algorithms in the multicarrier technology, are based on analysis of the channel capacity. It can be shown that for subchannel n the number of bits $b(n)$ can be approximated by [6, 32]:

$$b(n) = log_2\left[1 + \frac{SNR(n)}{\Gamma}\right] = log_2\left(1 + \frac{\mathcal{E}_n.g_n}{\Gamma\sigma_n^2}\right) \tag{2.3}$$

where $SNR(n)$ is the signal-to-noise ratio, $\mathcal{E}_n$ is the transmit energy, g_n is the channel gain, σ_n^2 is the noise power, and Γ is the *gap* defined for QAM modulation with the approximate expression [32]:

$$\Gamma = \frac{SM}{3CG}[\mathcal{Q}^{-1}(P_s/4)]^2 \tag{2.4}$$

where SM is a service guarantee margin (typically 6dB for ADSL [32]), CG is the coding gain of error correction codes used in the system (in ADSL considered 2 dB for the Reed-Solomon plus 2 dB if there is trellis coding [32]), P_s is the symbol error probability, and the function $\mathcal{Q}(x)$ is defined as:

$$\mathcal{Q}(x) = \frac{1}{\sqrt{2\pi}}\int_x^\infty e^{-y^2/2}dy. \tag{2.5}$$

The total number of bits over N channels $b_{total} = \sum_{n=0}^{N-1} b(n)$ is maximised for a fixed total energy $\mathcal{E}_{total} = \sum_{n=0}^{N-1} \mathcal{E}_n$ by the so-called *water-filling* solution:

$$\mathcal{E}_n + \frac{\Gamma.\sigma_n^2}{g_n} = const \tag{2.6}$$

In general the number of bits assigned to each subcarrier may be chosen according to two possible requirements:

- Maximum data rate at a given Γ, i.e. at a pre-defined error rate, margin and coding gain. An extra requirement may be imposed such that the data rate is an integer multiple of N $\times$ the symbol rate.
- Minimum error rate at a given data rate, margin and coding gain, i.e. maximum Γ at a

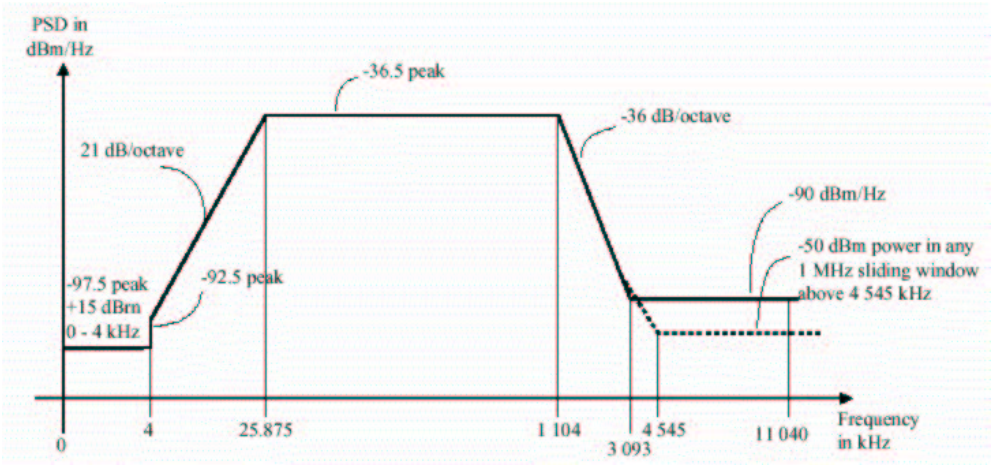

Figure 2.7: *Power spectral mask for the downstream transmit signal of ADSL over POTS (as defined in [1]).*

defined data rate.

Due to crosstalk considerations (see Section 3.3, p. 59) the transmit power of the system may be limited. The restrictions may be imposed on the transmit power spectral density (PSD) or on the total transmit power depending on the specific requirements. ADSL in particular is PSD limited and figure 2.7 shows the transmit downstream PSD mask for ADSL operating over analogue telephony (POTS).

The practical implementation of the water-filling solution is somewhat problematic as it assumes infinite granularity in the constellation size. The first finite-granularity multicarrier loading algorithm was developed for voiceband modems by Hughes-Hartogs [43]. However, this algorithm is very slow for applications like ADSL, where a large number of bits have to be loaded onto a large number of channels [44]. Numerous works suggest practical loading algorithms which are suitable for ADSL. Some algorithms deliver potentially suboptimal solutions but at a significantly increased convergence rate [44–47]. Other loading algorithms ensure optimum solution at reduced complexity in comparison with Hughes-Hartogs [47–51]. The work presented in [52, 53] derives necessary and sufficient conditions for optimality of bit assignment and applies these conditions to construct fast loading algorithms.

The services transmitted over ADSL may have different quality of service (QoS) requirements, where QoS usually (but not always) refers to latency and bit/byte error rate. By means of an appropriate bit loading a DMT system can provide multiple error rates simultaneously. The

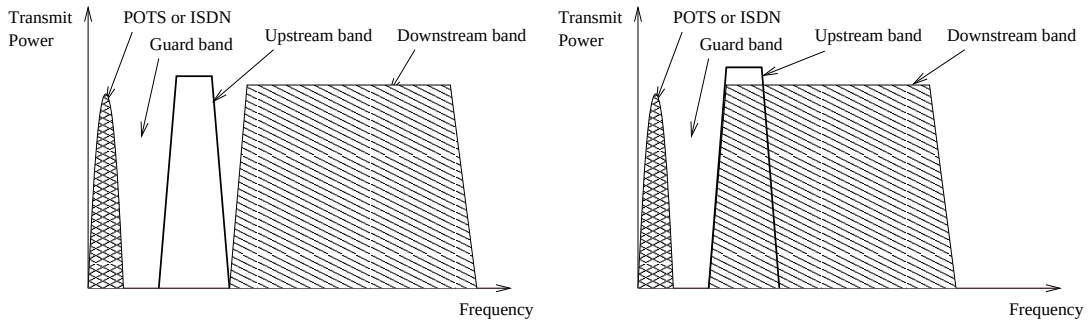

(a) FDD **(b)** Echo cancellation

Figure 2.8: *Frequency spectrum usage by ADSL with* (a) *frequency division duplexing and* (b) *echo cancellation.*

task of assigning data with different error rate requirements to the DMT subchannels has been considered in [54–57]. The multiple QoS idea has also been used in [58] for image and video transmission, whereby the data bits are allocated according to their perceptual importance to subchannels with different error rates. A superframe-based bit allocation algorithm has been proposed in [59].

ADSL frequency band

The subcarriers in the ADSL modulation are spaced at Δf = 4.3125 kHz. In the downstream direction the maximum number of carriers is $N_{DS} = 255$, which are placed at frequencies $n\Delta f$, n = 1 to 255. One of the carriers should be left unmodulated as a pilot tone. In the upstream direction the maximum number of carriers is N_{US} = 31, placed at frequencies $n\Delta f$, n = 1 to 31. The downstream frequency spectrum may go up to 1.1 MHz, and the upstream spectrum - up to 138 kHz. The lower limit of the frequency band for the upstream depends on the service option selected, e.g. whether the system is ADSL with POTS, ADSL with ISDN, or only ADSL. The lower limit of the downstream frequency band depends on both the service and duplexing option selected. Several duplexing methods may be used in ADSL:

- Frequency division duplexing (FDD). In this strategy the downstream is placed in a frequency band separate from the upstream (figure 2.8(a)). In this way self-crosstalk is prevented but the available bandwidth is not used very efficiently.

- Echo cancellation. Another approach is to place the upstream within the downstream band and use echo cancellation to remove the reflection of the locally transmitted signal (figure 2.8(b)). However, the level of induced kindred near-end crosstalk (NEXT) (see section 3.3, p.59) is so high in ADSL that the echo cancellation duplexing may be undesirable even at low frequencies [32]. Besides, echo cancellation increases the complexity of digital signal processing in the receivers.

- Mixed FDD/echo cancellation. In this strategy duplex transmission is used up to a certain frequency, and simplex with FDD above that.

2.5.5 ADSL "lite"

ITU Recommendation G.992.2 [25], previously known as G.lite, specifies an ADSL system which is less complex than but line compatible with G.992.1. The ANSI version of the standard is published as ANSI T1.419 [26]. ADSL lite has the following main characteristics:

- It is designed for "always on" operation and therefore has provisions for:
  - power saving modes of the ADSL transceiver unit (ATU) at both the central office (ATU-C) and the customer premises (ATU-R);
  - short wake-up times from standby mode when transmission is needed;
  - a fast retraining mechanism is added to permit rapid recovery from noise pulses, such as on/off hook events.
- The low-pass part of the POTS splitter should not be needed.
- The number of tones in the DMT symbol is reduced from 256 to 128, and the maximum number of bits per tone is reduced from 15 to 8.
- Only transport of asynchronous transfer mode (ATM) is supported.
- Range is more important than bit rate - ADSL "lite" aims at delivering service to larger distances albeit at potentially lower data rate.

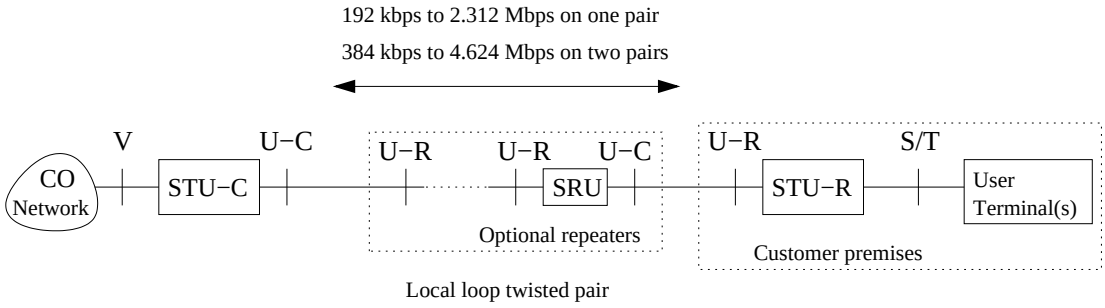

Figure 2.9: *SHDSL reference model.*

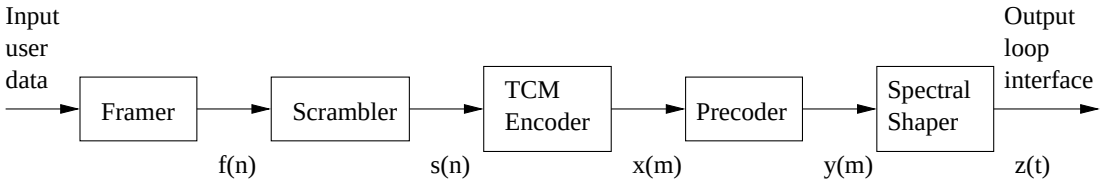

Figure 2.10: *Block diagram of a generic SHDSL transmitter (after [2]).*

2.6 Overview of SHDSL systems

Single-pair high-speed digital subscriber line (SHDSL) is a DSL technology designed for businesses that require fast symmetric data transfer. SHDSL supports data rates from 192 kbps to 2.312 Mbps and works in *symmetric* mode, i.e. the downstream data rate is equal to the upstream data rate. SHDSL can also operate over two pairs, in which case the available data rate becomes 384 kbps to 4.624 Mbps. SHDSL is the first standardised multi-rate symmetric DSL.

The SHDSL standards ITU G.991.2 [2], ETSI TS 101-524 [28], and ANSI T1.422 [29] leave an option for repeaters (SRU) in its reference model (figure 2.9). Unlike ADSL, SHDSL does not provide the possibility for sharing the pair with POTS or ISDN service. If needed, telephony and fax signals are transmitted in a digitised form in the data stream provided by SHDSL.

2.6.1 SHDSL architecture and transport capabilities

Figure 2.10 shows the block diagram of an SHDSL transmitter, where n represents bit time, m represents symbol time, and t represents analogue time. The input user bit stream is framed, scrambled to ensure higher level of randomisation, and encoded to 16-level trellis-coded pulse

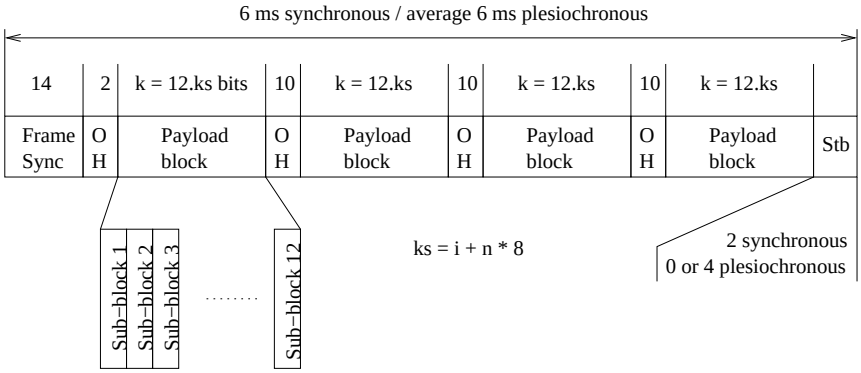

Figure 2.11: *SHDSL frame structure.*

amplitude modulation (TC-PAM). Since SHDSL uses a single carrier modulation, the spectrum of the modulated signal is relatively large. Therefore a precoder is needed to compensate the channel distortion that broadband signals generally suffer in transmission channels. The spectral shaper is related to the spectrum compatibility of SHDSL and is subject to regional requirements.

The allowed user data rates R in single-pair SHDSL are defined by $R = n \times 64 + i \times 8$ kbps, where $3 \leq n \leq 36$ and $0 \leq i \leq 7$, for $n = 36$, i is restricted to values 0 or 1. That is, the allowed data rates are 192 kbps to 2.312 Mbps in increments of 8 kbps. Alternatively for two-pair SHDSL the allowed data rates are 384 kbps to 4.624 Mbps in increments of 16 kbps.

2.6.2 SHDSL framing

An SHDSL frame starts with synchronisation bits, followed by four groups of overhead (OH) and payload blocks, and ends with several vendor dependent “stuff” bits (Stb), as shown in Figure 2.11. Each payload block has $k = 12(i + n \times 8)$ bits and is divided into 12 sub-blocks of $k_s = (i + n \times 8)$ bits each. The overhead contains a cyclic redundancy check (CRC), embedded operations channel (EOC) information, and the so-called “stuff” bits. The total framing overhead in synchronous mode is 48 bits per frame or 8 kbps regardless of the user data rate. The total frame duration in synchronous mode is 6 ms.

For the optional two-pair mode, the above details represent the framing of each pair. Both pairs operate at the same payload rate and the transmitters maintain frame alignment within some specified limits. A payload block will then contain $2k$ bits and each sub-block - $2k_s$ bits.

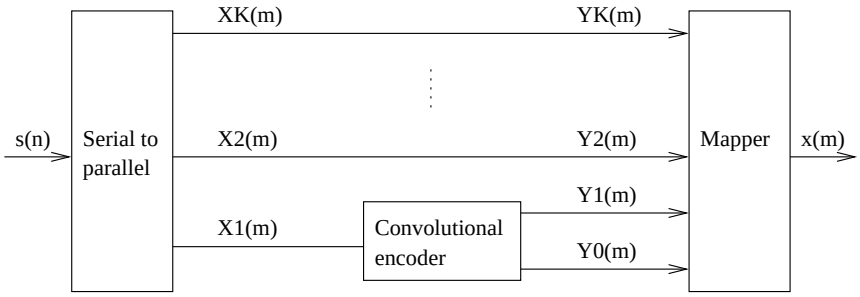

Figure 2.12: *Block diagram of the modulation encoder in SHDSL.*

The framing organisation of SHDSL - without long FEC codewords or interleaving, allows SHDSL to achieve much lower latency than ADSL. However, this comes at the price of poorer error protection in SHDSL especially against burst errors.

2.6.3 Coding and TC-PAM modulation in SHDSL

SHDSL uses cyclic redundancy checks (CRC) as an error detection mechanism. The CRC sums are calculated during framing and transmitted in the overhead bits of the following frame. The bits covered are all payload data plus some of the overhead except the synchronisation bits, CRC bits and the Stb. The scrambler used in SHDSL is self-synchronising and therefore multiplies bit errors.

SHDSL relies for error correction on trellis coding implemented in the encoder (Figure 2.12). One bit in a symbol is convolutionally encoded in which process the symbol is expanded by one bit. The resulting word is mapped to some pre-determined levels. The structure of the convolutional encoder is specified but the coefficients it uses are vendor specific. According to annexes A and B in [2] SHDSL uses 16-level TC-PAM[2], a symbol carries 3 bits expanded after the trellis coding to four bits and is mapped to 16 levels. The symbol rate is given as $(R+8)/3$ where $R = n \times 64 + i \times 8$ is the payload data rate.

The frequency band that PAM takes up depends on the symbol rate and therefore on the data rate. The nominal PSDs for several data rates are shown in Figure 2.13. Because of spectral compatibility issues the SHDSL standard also defines power spectral density masks [2, 28, 29].

[2]SHDSL has inherited the TC-PAM from earlier versions of HDSL2. CAP and DMT were also considered when discussing the SHDSL standard, but in the end PAM was chosen as a compromise

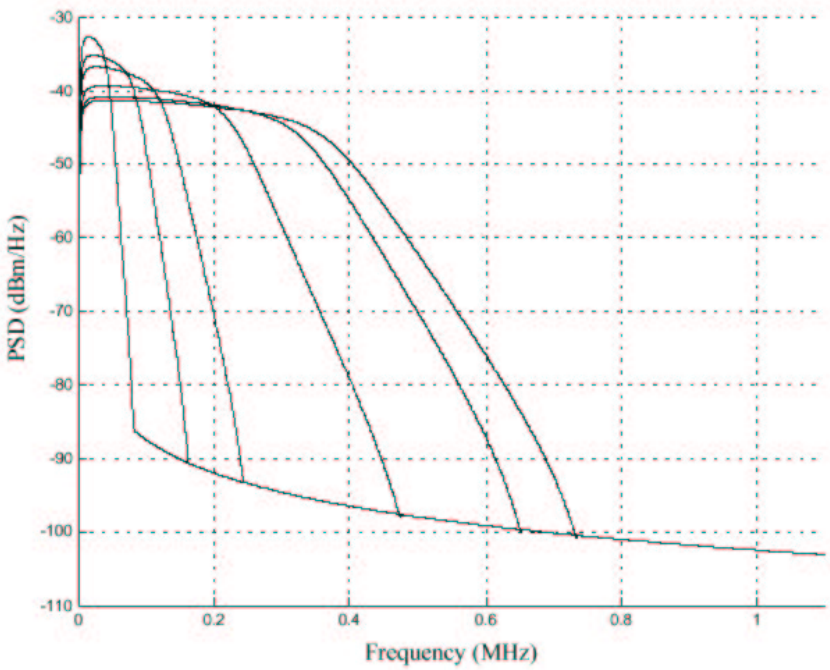

Figure 2.13: *Nominal PSDs of SHDSL for 256, 512, 768, 1536, 2048, and 2304 kbps respectively for the graphs from left to right (as defined in [2]).*

2.7 Development of VDSL systems

Very high-speed digital subscriber line (VDSL) is a subscriber loop technology which is still in the process of development, although single carrier VDSL systems have been deployed in Korea. VDSL is intended to be incorporated in hybrid fibre-copper systems that combine the large bandwidth of optic fibre technology and the ease of deployment and use of copper.

In the VDSL reference model (Figure 2.14) an optic fibre to the neighbourhood (FTTN), the curb (FTTC), the cabinet (FTTCab), or the building (FTTB) will feed an optical network unit (ONU). VDSL will provide high-speed connection of up to 58 Mbps aggregate (upstream + downstream) from the ONU to the end users over twisted-pair subscriber loops. VDSL is also expected to support analogue telephony (POTS) or ISDN on the same pair in a fashion similar to ADSL. The frequency band of VDSL would be placed above that of POTS or ISDN and a filter (splitter) will separate the VDSL from POTS/ISDN signals.

VDSL is expected to be able to operate in both asymmetric and symmetric mode. The data rate requirements vary across the different documents. E.g. the rates specified in [31] allow up to 23 Mbps downstream and up to 4 Mbps upstream in asymmetric mode. Again according to

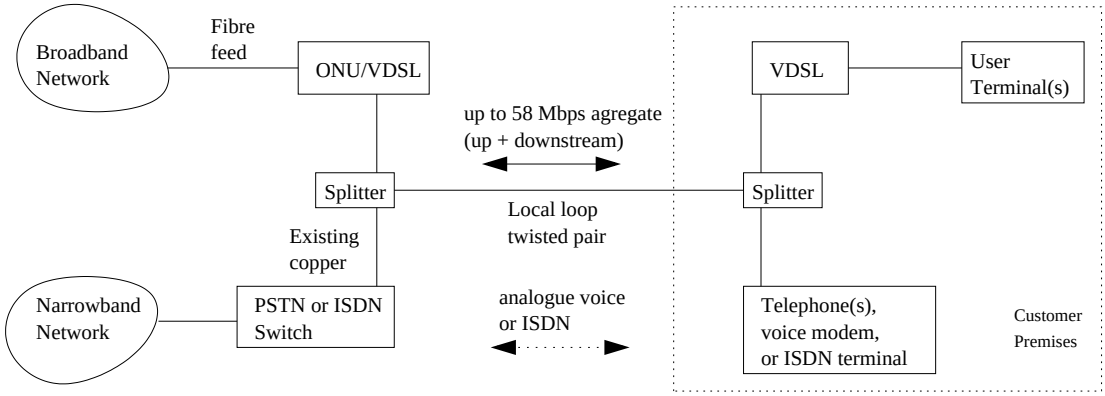

Figure 2.14: *VDSL reference model.*

[31], in symmetric mode VDSL should provide data rates of up to 28 Mbps in each direction. Other specifications give 52 Mbps downstream and 6.4 Mbps upstream for asymmetric, and 34 Mbps two-way for symmetric [32]. Due to the interference and attenuation at such high bit rates, VDSL will only have a reach between 300m and 2 km and will be able to operate at the top speeds only on the shortest loops.

Another requirement is that VDSL should be able to support both synchronous transfer mode (STM) and asynchronous transfer mode (ATM) [31].

2.7.1 Proposed line codes

The line codes have been the subject of much debate in the process of VDSL standardisation. Here are the main choices that can be made:

Single carrier vs. multicarrier modulation. The principal choice in the VDSL development is whether to use single carrier or multicarrier modulation. Arguments have been given in favour of each type of modulation [6, 32, 60]. Both modulations have advantages and weaknesses [61] and a careful consideration has to be made as to which modulation would suit better the VDSL environment.

Which single carrier modulation? Should single carrier modulation be chosen, there are two possible options. One possibility is to use carrierless amplitude phase modulation/quadrature amplitude modulation (CAP/QAM), the other is to use a simple line code such as a version of four-level signalling.

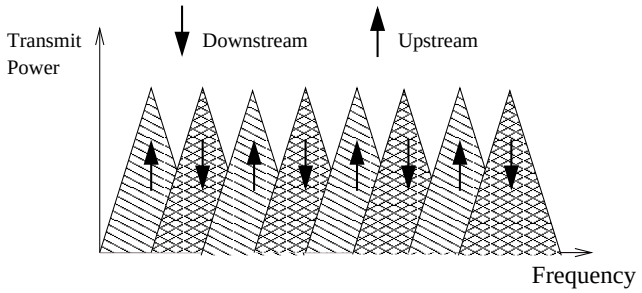

Figure 2.15: *The zipper principle of duplexing.*

Which multicarrier modulation? If multicarrier modulation is preferred, then the "classical" discrete multitone (DMT) modulation generated by Fourier transform is one possibility. Another option is the so-called discrete wavelet multitone (DWMT), where the modulated signal is obtained by wavelet transform. Some works argue that in DWMT the spectral overlap between subcarriers is lower than that in DMT [62–64]. Therefore, the DWMT subcarriers can be more tightly packed with a lower guard band between them, thus allowing for more efficient use of the channel bandwidth than can be achieved with DMT. A third multi-carrier version is obtained by filter banks and is known as filtered multitone (FMT). The results reported in [65–67] suggest that FMT offers advantages over other modulations in terms of spectrum management and duplexing.

Which duplexing method? In most discussions it is agreed that echo cancellation is not a viable option for VDSL because the benefits it offers are insignificant - about 10% over the other multiplexing technologies but only at frequencies up to 3 MHz and on short loops [32]. Two other options remain - time division duplexing (aka ping-pong), where the upstream and downstream are transmitted alternately, or frequency division duplexing, where the upstream and downstream are placed in separate frequency bands. An added twist to the frequency division in DMT is to extend it to zipper duplexing as opposed to normal bandwidth separation (Figure 2.15). It has been argued that the zipper method provides benefits in terms of crosstalk interference and noise robustness [68–71].

2.7.2 Standards status

Several organisations take interest in the development of a VDSL standard. Those are ANSI, ITU, ETSI, the digital audio-visual council (DAVIC), the ATM Forum, and the ADSL forum.

DAVIC and the ATM Forum address the higher level protocols, the ADSL Forum deals with the network, protocol and architecture aspects of VDSL, and the VDSL metallic interface and transceiver protocols are developed by ANSI, ITU, and ETSI. The VDSL standards are still largely in the process of development. ANSI has released a TrialUse version of the VDSL standard under the number T1.424 [10]. ETSI TS 101 270 [31] defines the functional requirements to VDSL systems. ITU has also published a document on VDSL foundation under number G.993.1 [30].

2.8 Summary

In this chapter a brief overview of the historical development of the digital subscriber line technology has been presented. This provides an explanation of the reasoning behind various technological decisions and restrictions in the DSL standards. A short description of possible protocol stack scenarios of services carried over DSL has also been outlined. Following this, a detailed review of some common DSL systems has been made. The emphasis has been placed on features in the standards affecting the error rate, such as framing, error mitigation techniques, and modulation, since system error performance is the area of interest in this work.

Two of the considered systems - ADSL and SHDSL, have been shown to have completely different physical layer specifications. ADSL has a particularly complicated metallic interface with numerous error mitigation techniques, a complex framing format and an elaborate modulation. It is therefore not a trivial task to evaluate the impact of errors in ADSL. SHDSL has much simpler physical characteristics, however it lacks in extensive error protection particularly against burst errors. Therefore, there is still a need to analyse thoroughly the error performance of DSL systems. The results of such an analysis can contribute both to finding optimal parameter settings of existing systems, and to choosing appropriate specifications for the next generation in the DSL family - VDSL.

Chapter 3
xDSL line noise impairments

3.1 Introduction

In this chapter, the sources of noise on telephone lines and the respective noise models are introduced, since they will form the basis of this work. Firstly, the statistical nature and modelling of impulse noise on local loops is presented as impulse noise is one of the major impairments to DSL systems. After introductory notes on the historical development of impulse noise models, the discussion concentrates on the latest advancements in the statistical description of impulse noise on the local loop. The salient statistics of impulse noise include inter-arrival times, impulse durations, impulse amplitudes, and frequency spectrum. The problem of generation of impulses with appropriate statistics is also discussed. Some new work on impulse power statistics and more accurate impulse frequency spectrum modelling is presented here.

Following this, an overview of the sources of crosstalk and the crosstalk models is made. Mixing crosstalk from various sources and the administrative measures undertaken to restrict crosstalk are discussed.

Finally, the issue of radio frequency interference to and from DSL systems is presented.

3.2 Impulse noise

Impulse noise is a non-stationary stochastic electromagnetic interference which consists of random occurrences of energy spikes with random amplitude and spectral content. The causes of impulse noise on the telephone line are diverse and vary from telephone on/off-hook events, through noise from home, office, and industrial electrical appliances, and transport vehicles, to atmospheric noise from electrical discharges. The resulting interference into the telephone twisted pairs is a major impairment for DSL systems. It is therefore essential to know the statistical nature of impulse noise in order to be able to evaluate its impact on transmission technologies.

3.2.1 Historical perspective on impulse noise

In order to address the specifics of the impulse noise non-stationarity, virtually all studies up to now divide its statistical properties in two groups. The description of impulse statistics, such as voltage distributions, lengths, or spectra, is considered separately from the impulse inter-arrival times.

Impulse statistics

The emergence of digital transmission over telephone lines prompted several studies of the statistics of impulse noise and the errors caused by it in the 1960s and 1970s. Mertz proposed a higher-order hyperbolic distribution to model the impulse noise amplitudes on telephone lines [8]. In [72], Fennick used an exponential function to describe the amplitude densities in the extreme tails. Stuck and Kleiner considered amplitude density models with symmetric stable distributions, log-normal distribution, and Rayleigh distribution [73].

The first field trials of DSL systems showed that impulse noise is one of the major limiting factors in a DSL transceiver's achievable performance. However, earlier impulse models, although probably suitable for voice-band digital transmission over telephone lines, were not necessarily applicable to DSL systems, which use larger bandwidth and work at higher bit rates than their voice-band counterparts. This triggered a wave of DSL-oriented surveys of impulse noise on the loop plant in the 1980s. The measurements mostly concentrated on the ISDN frequency band and rarely exceeded several hundred kilohertz. More important works include [74–76] and a summary of the early results is presented in [7]. In [75, 77], a hyperbolic distribution for the impulse amplitudes was proposed, in a form which is a special case of the general hyperbolic distribution discussed in [8].

New surveys in an increased frequency band accompanied the development of ADSL in the early 1990s. Valenti and Kerpez of Bellcore reported results from measurements on telephone lines in [78], but the number of sampled impulses was insufficient to derive statistical properties of the noise. Cook of British Telecom (BT) proposed an analytical model of impulse noise after studying data from a wide-scale survey on the BT telephone network [79, 80]. This model, which is now usually referred to as the Cook pulse, defines a continuous-time mathematically abstract symbolic pulse. A drawback of the Cook pulse is that its shape is unrealistic, and a single symbolic pulse cannot represent the statistical properties of a stochastic process.

Another impulse noise model was proposed by Henkel and Kessler of Deutsche Telekom (DT) based on measurements in the German telephone network [81–83]. It includes probability density functions of impulse amplitudes (generalised exponential) and lengths (log-normal mixture), as well as mean power spectral density and phase. However, both the Cook and the Henkel/Kessler models only deal with mean power spectral densities and do not reflect the fact that each impulse has a unique power spectrum.

The latter issue has been tackled in a recent impulse noise model [3, 4], which is based on measurements conducted independently by BT together with the University of Edinburgh [84–87] and DT [81–83, 88, 89]. This model combines the Henkel/Kessler densities for impulse amplitude and length with a spectral model and impulse generation method proposed by Mann and McLaughlin, and inter-arrival times model presented by Levey and McLaughlin. The Mann/McLaughlin spectral model [3, 4] is based on the spectral features of the impulse autocorrelation function, which then allows the use of a technique proposed by Tough and Ward [90] for impulse generation with appropriate time domain and spectral characteristics. The Levey/McLaughlin inter-arrival times model [5, 84, 86] will be discussed below.

Inter-arrival statistics

From the first studies of impulse noise in the early 1960s, it has been observed that the error events in data transmitted on telephone lines tend to occur in groups (bursts). Mertz presented a model with Poisson distributed spacing between error bursts and a random distribution of errors within a burst [8]. Berger and Mandelbrot [9] proposed a model for inter-error intervals that is based on the Pareto distribution and belongs to the class of renewal processes [91, 92]. Mandelbrot went on to conclude in [93] that even if the error events in communication circuits were independent and identically distributed (iid), the errors themselves exhibited self-similar clustering, i.e. errors were grouped in bursts, which in turn were grouped in bursts of bursts and so on. This self-similarity [93] of error clusters is an indication of the invariance of the generating mechanism with respect to multiplication of time by a constant.

In subsequent analysis Sussman [94] and Fennick [72] confirmed that the Berger/Mandelbrot model showed a very good agreement with inter-arrival data from network measurements. Fano also derived a complementary distribution of inter-arrival times with a Pareto-type component multiplied by an exponential density [95], although he started from a completely different assumption that impulse noise reverberates in the telephone network. Fano also noted that the

measurement results presented in studies are inconsistent with the assumption that the inter-arrival times are Poisson distributed. Stuck and Kleiner [73] also admit that a simple Poisson process cannot approximate well the empirical inter-arrival distributions. Nevertheless, they finally assumed exactly the Poisson model, the reason being that the alternatives considered by them - a p-th order autoregressive process, and a doubly stochastic Poisson process, performed even worse. Valenti and Kerpez [78] followed [8] and [73] and also assumed Poisson distribution for inter-arrival statistics. So did Cook [79, 80], who also included a separate probability for impulse noise caused by ringing cadences. A generalised Poisson law was used for daytime statistics of inter-arrival times by Henkel and Kessler as well [81–83].

Fennick pointed out in [72] that while the Berger/Mandelbrot model seems to be the best presented to date, a mathematically more tractable model based on partitioned Markov chain was proposed by Fritchman [96]. The approaches of [9] and [96] were combined by Levey and McLaughlin, who argued that an inter-arrival time model based on Markov renewal process would account well for the clustering of inter-arrival times and the distribution heavy tails they observed in [5, 84, 86]. This inter-arrival times description was adopted in the joint DT/BT/University of Edinburgh (UE) impulse noise model [3, 4].

It should be noted that there is a subtle difference between different inter-arrival models. Some models, such as that of Berger and Mandelbrot, concern inter-error intervals between errored bits in a data stream, whereas impulse noise is related to the inter-arrival times between impulses. Indeed, the errors in the inter-error models are caused by impulse events, however, not all impulse events are necessarily error-inducing.

3.2.2 Impulse noise model

It is evident from the previous sections that the BT/UE/DT approach to impulse noise modelling [3, 4] has clear advantages over other impulse noise studies because it:

- gives a full description of the impulse statistics in the time and frequency domain, and the inter-arrival times between impulse events;
- enables generation of impulses with statistically appropriate both time domain and spectral characteristics ;
- takes into account the clustering and heavy-tailed distribution of intervals between im-

pulse events, and the fact that the distributions of impulse amplitudes and lengths are also heavy-tailed;

- is based on recent measurements and reflects the current statistics of impulse noise in telephone networks. It is well known that in the past a major source of impulse noise in telephone lines were mechanical switches and dialing pulses, whereas nowadays most networks use digital switches and tone dialing and the character of impulse noise is not necessarily the same as several decades ago;
- is based on wide-band measurements (15 MHz for BT/UE, 5 MHz for DT) and can be applied to analysis of systems transmitting signals with large (for a telephone line) bandwidth, such as ADSL (1.1 MHz) and VDSL (12 MHz);
- agrees with empirical statistics from two different networks in different countries (UK and Germany), demonstrating that the impact of loop topology on the noise statistics is quantitative rather than qualitative. That is, although the scaling of the impulse statistics does change, the type of distributions remains invariant regardless of the network topology. Therefore it can be assumed that the model represents accurately the statistical nature of impulse noise in general.

In the next four sections, the different aspects of this impulse noise model will be described in some detail, since the model forms the basis of the analysis in this work. Complete description of the model is to be found in [3, 4], as well as [81–83, 85, 88, 89] for impulse amplitudes and lengths and [5, 84, 86] for inter-arrival times.

3.2.3 Impulse modelling in time domain

In the time domain, impulse noise is characterised with the impulse voltage amplitudes, impulse durations, and inter-arrival times. This section will present the individual impulse statistics, i.e. amplitudes and lengths, as well as a novel analysis of the impulse powers, and finally some notes on impulse detection. The inter-arrival times will be discussed later in a separate section because of their specifics.

Impulse amplitudes

The impulse amplitude model is based on an approach originally proposed by Henkel and Kessler in [81–83], which consists of approximating the voltage histograms with a generalised exponential distribution of the form:

$$f_{ge}(u) = \frac{1}{240u_0} e^{-|u/u_0|^{1/5}}, \tag{3.1}$$

where u is the voltage and u_0 - a scaling parameter. This model reflects well the fact that voltage distributions are heavy-tailed [85] and offers a good approximation for all measured impulse noise voltage amplitude distributions collected in the networks of both DT [81–83, 89] and BT [3]. Nevertheless, a Weibull density has also been investigated as a possible alternative in [3] because it is mathematically more tractable when using the results of Tough and Ward [90] to generate random noise with prescribed amplitude and spectral characteristics (see section 3.2.5, p.50). In the statistics literature the Weibull density function is defined as (see e.g. [97]):

$$f_{wb}(y) = \begin{cases} \alpha b y^{\alpha-1} e^{-by^{\alpha}} & \text{if } y \geq 0, \\ 0 & \text{elsewhere}, \end{cases} \tag{3.2}$$

where $\alpha > 0$ and $b > 0$ are shape parameters. For the purposes of this model (3.2) has been modified in [3] to a double Weibull density to make it symmetrical:

$$f_{wb}(u) = \frac{1}{2}\alpha b |u|^{\alpha-1} e^{-b|u|^{\alpha}}. \tag{3.3}$$

A comparison between the two approaches for data measured at the customer premises of a BT line is shown in Figure 3.1. It can be seen that the generalised exponential and the Weibull approximation densities virtually overlap. However, it has been reported in [3] that DT data required scaling of the Weibull distribution in order to achieve good fit. Example values of model parameters for both densities measured at customer premises (CP) on BT and DT lines, as well as at a DT central office (CO) as given in [3] are presented in Table 3.1. A binding reference for such model parameters can be found in [4].

Derivation of impulse power statistics

From the probability density function for impulse amplitudes it is possible to derive a distribution of the impulse power. The impulse power relates directly to the signal-to-noise ratio, which

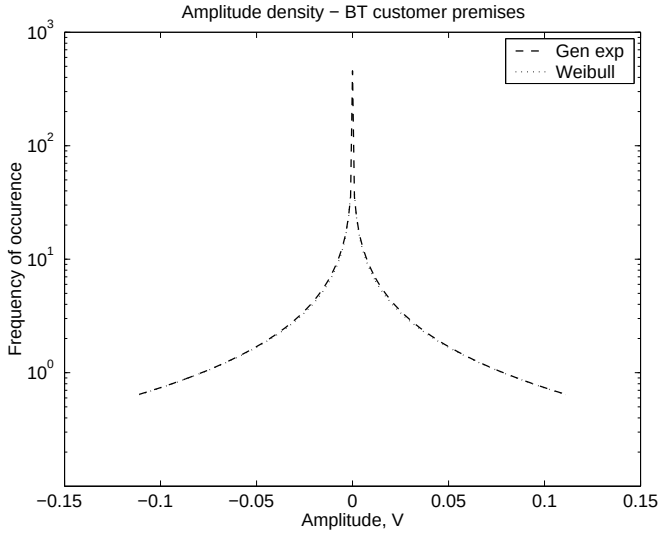

Figure 3.1: *Generalised exponential and Weibull approximations of voltage density measured at customer premises by BT.*

	Weibull		Gen exp
	α	b	u_0
BT(CP)	0.263	4.77	9.12 μV
DT(CP)	0.486	44.40	23.23 nV
DT(CO)	0.216	12.47	30.67 nV

Note that α and b are computed such that u is in volts.

Table 3.1: *Model parameters for the Weibull and generalised exponential voltage densities from BT and DT measurements (after [3]).*

can be used further for evaluating the impact of impulse noise on communications systems. This novel extension of the impulse noise model was obtained by means of variate transformation.

If $F(x)$ and $f(x)$ are respectively the distribution function and density function of the random variable x, and $x = x(y) \Leftrightarrow y = y(x)$ is a one-to-one relation such that y is continuous and differentiable in x and vice versa, it can be shown [98] that:

$$dF(y) = f\{x(y)\}\frac{dx}{dy}dy. \tag{3.4}$$

Let us consider the normalised power $P_u = u^2$, noting that an extension to the general case when the resistance $R \neq 1$ is trivial. Using the generalised exponential density from Equa-

tion 3.1 in Equation 3.4 it is obtained:

$$f_{ge}(P_u) = \frac{1}{240\sqrt{P_0 P_u}} e^{-(P_u/P_0)^{1/10}}, \quad P_u \geq 0\,, \quad P_0 = u_0^2\,. \tag{3.5}$$

Note that for the purpose of power modelling, this density has been modified to be non-symmetrical. It should also be mentioned that unlike the impulse amplitudes, the power density is no longer of generalised exponential type. If variate transformation is applied on the Weibull form of the voltage distribution in Equation 3.2, the power density becomes:

$$f_{wb}(P_u) = \frac{\alpha}{2} b P_u^{\frac{\alpha}{2}-1} e^{-bP_u^{\alpha/2}}, \quad P_u \geq 0. \tag{3.6}$$

I.e., if we assume that the impulse amplitudes are Weibull distributed, the impulse powers are also Weibull distributed but with a modified shape parameter $\alpha/2$. Figure 3.2 shows the power densities derived from the voltage densities in Figure 3.1.

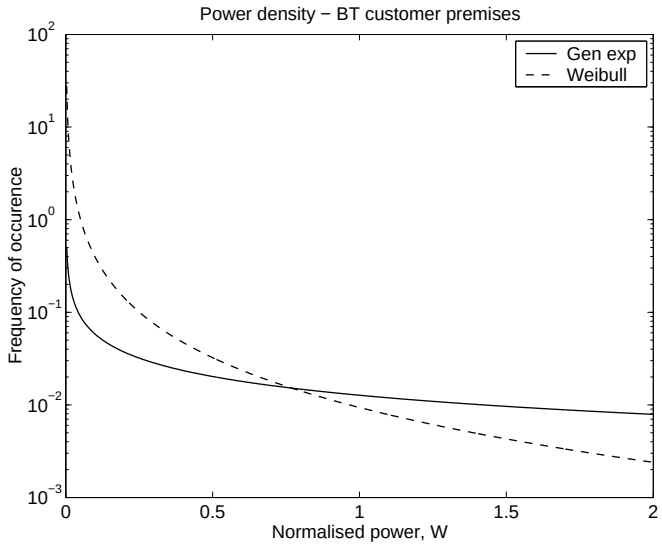

Figure 3.2: *Power densities derived from generalised exponential and Weibull approximations of voltage density measured at customer premises by BT.*

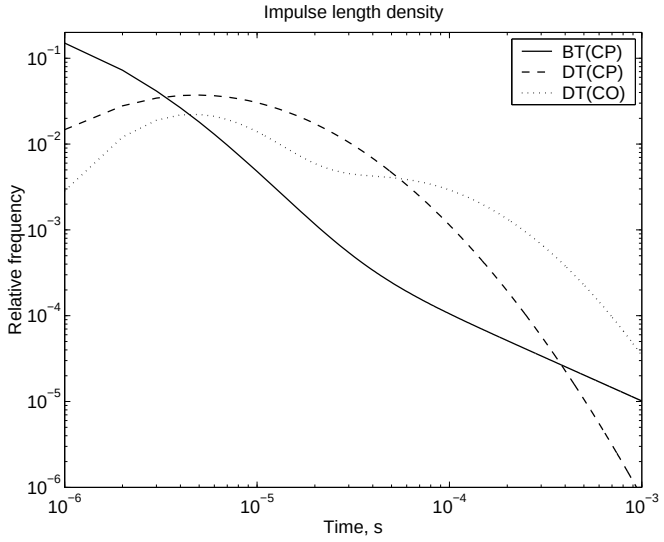

Figure 3.3: *Two-component log-normal approximation of impulse length densities from BT and DT measurements.*

Impulse lengths

The impulse lengths τ are modelled as proposed in [82, 83] with a mixture distribution of two log-normal components:

$$f_l(\tau) = B\frac{1}{\sqrt{2\pi}s_1\tau}e^{-(1/2s_1^2)\ln^2(\tau/\tau_1)} + (1-B)\frac{1}{\sqrt{2\pi}s_2\tau}e^{-(1/2s_2^2)\ln^2(\tau/\tau_2)}, \qquad (3.7)$$

where B, s_1, τ_1, s_2, and τ_2 are parameters. Obviously for $B = 1$, Equation 3.7 reduces to a single log-normal density. The model agrees well with the findings in [85] that the length distribution is heavy-tailed. Typical values of the distribution parameters for BT and DT measurements [3] are given in Table 3.2, and the respective densities are plotted in Figure 3.3.

	B	s_1	τ_1	s_2	τ_2
BT(CP)	0.45	1.25	1.3 μs	21.5	129 μs
DT(CP)	1	1.15	18 μs	-	-
DT(CO)	0.25	0.75	8 μs	1.0	125 μs

Table 3.2: *Model parameters for the impulse length densities from BT and DT measurements (after [3]).*

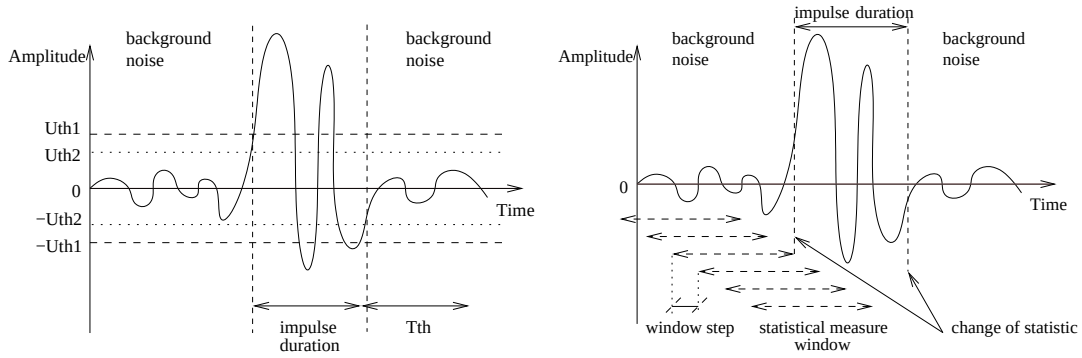

(a) Amplitude threshold detection method

(b) Statistical impulse detection method

Figure 3.4: *Impulse detection techniques.*

Impulse detection techniques

As with all studies of stochastic processes, impulse noise studies rely heavily on data from measurements to derive empirical distributions or verify the correctness of proposed models. A practical issue in impulse noise measurements is the need to detect impulse events and identify correctly their temporal boundaries in a stream of noise signal samples that also contains non-impulsive background noise. An appropriate impulse definition is required in order to produce credible statistics of the impulse noise. It is therefore important to comment on the impulse detection algorithms.

Amplitude threshold detection. A widely used impulse detection method is the hard amplitude threshold detection (Figure 3.4(a)), which was first proposed by Kaenel et al. [99]. An impulse is considered to have commenced when the noise amplitude exceeds the absolute value of a specified voltage threshold[1] U_{th1} and ends when the noise level falls under another threshold U_{th2} for a sufficiently long period of time T_{th}. The drawback of this method it that the definition of impulse length and the detection of an impulse altogether is threshold dependent. If the threshold values are not set appropriately, there may be a number of unwanted scenarios. For example, background noise with large peak-to-peak amplitude may trigger the impulse detection algorithm. Also, impulse events which should be classified as one impulse of long duration may actually be detected as multiple short impulses.

[1]The original proposal by Kaenel et al. [99] was to assume the impulse spans for the whole time it is above the lower level U_{th2}. Nevertheless, the definition given here is also widely in use.

Statistical impulse detection. To avoid the deficiencies of the hard amplitude threshold detection, a statistical method for impulse localisation has been developed by Mann, McLaughlin, and Levey [87]. In this technique, a statistical measure of the background noise before an impulse event is calculated and then compared through a sliding window with subsequent overlapping sections of the signal (Figure 3.4(b)). A significant deviation in the measure would indicate an impulse. There are several possible statistical measures that could be used for impulse detection. The approach used in [87] is to calculate amplitude histograms and compare them with a chi-squared test, which is defined as:

$$\chi^2 = \sum_{i=0}^{N-1} \frac{(X_i - x_i)^2}{x_i}, \tag{3.8}$$

where N is the number of histogram bins, X_i is the value of the i-th observed bin, and x_i is the value of the i-th expected bin. If a window is marked as containing an impulse by the chi-square check, an additional check is performed whether significant amplitudes are present in the window and only if this is true is the window declared to contain an impulse. A potential difficulty in this method is setting appropriately the values of the chi-squared threshold, the window length and the window step. Disadvantages of the technique are the time resolution smearing introduced by the step movement of the window, as well as the relatively high computational complexity.

Comparison. By comparing impulse statistics of the same data set obtained with both impulse detection methods, it was found in [87] that impulse lengths detected with the statistical method exhibit a more heavy-tailed distribution than if detected with the hard threshold technique. This is an indication that some impulse events detected statistically as long impulses, were identified with the hard threshold as a series of shorter impulses. Therefore, the statistical impulse detection method is preferable if accurate statistics of impulse noise are to be obtained.

3.2.4 Impulse spectral modelling

It was proposed in [3] to model statistically the impulse spectral characteristics by means of the auto-correlation function (ACF). It is well known (see e.g. [100]) that the ACF of a signal holds its spectral properties and is related to its power spectral density (PSD) via the Fourier transform:

$$S_{xx}(f) = \mathcal{F}[R_{xx}(\tau)] = \int_{-\infty}^{\infty} R_{xx}(\tau) e^{-j2\pi f \tau} d\tau, \tag{3.9}$$

where $R_{xx}(\tau)$ is the ACF[2], and $S_{xx}(f)$ - the PSD. The normalised ACF of an impulse can be represented as a sum of cosine-modulated decaying exponential functions:

$$\widehat{R}_{xx}(\tau) = \sum_{i=1}^{m} cos(2\pi\alpha_i\tau)e^{-\beta_i|\tau|}, \tag{3.10}$$

where $\widehat{R}_{xx}(\tau)$ is the approximated impulse autocorrelation function and the time delay τ would be replaced in the discrete case by samples. Parameters in this model are α_i and β_i, $i = 1, 2, \ldots, m$, of which α_i define the frequencies of the cosines, and β_i represent the decay of the exponential functions. The value of m, i.e. the number of necessary cosine-modulated exponentials depends on the required precision, as well as on the particular data set that needs to be modelled. The latter is related to the differences between the set up of DT and BT impulse measurements, the results of which were used as a base of this model. The DT equipment recorded impulses at a sampling rate of 10.24 MHz in a 400 μs recording window, of which 200 μs are pre-trigger samples [81–83]. The BT equipment used a 16 ms recording window at a sampling rate of 30 MHz [84, 85]. Another important difference is that the BT equipment was connected to the telephone line through the high-pass side of splitters (see Section 2.5, p. 13). As a result the DT data, which was recorded without the use of splitters, has significantly more energy at low frequencies than the BT data. This leads to differences in the spectral modelling and parameter estimation for the BT and DT data sets.

Autocorrelation function model for the BT data

In the case of the BT data, it was found that the ACF could be modelled well with only one cosine-modulated exponential [3]. An estimation of the model parameters, $\hat{\alpha}$ and $\hat{\beta}$, can be obtained from respectively the normalised zero crossings rate and the decay rate of each impulse ACF.

Zero crossings rate. The empirically obtained zero crossing histograms for BT data are complex in structure and therefore are approximated with a finite mixture model (see e.g. [102]) of three

[2]The autocorrelation R_{xx} is defined as a function only of the time lag τ because the ACF here describes individual impulses. It does *not* imply that the impulse noise is wide-sense stationary (see e.g. [101]) - a train of impulse events is indeed a non-stationary random process.

Gaussian probability density functions (pdfs) [3]:

$$f(\alpha) = \sum_{i=1}^{3} \frac{p_i}{\sqrt{2\pi}\sigma_i} e^{-(\alpha - m_i)^2 / 2\sigma_i^2}, \tag{3.11}$$

where m_i and σ_i are the mean and the standard deviation, and p_i is the weight of each Gaussian component. The zero crossings rate for BT data was found to be line dependent [3] and therefore [4] defines a default set of parameters plus several alternatives derived from various lines. The default parameter values are presented in Table 3.3 and a histogram of the zero crossing rate generated from the default mixture model is shown in Figure 3.5.

Mixing proportions	Mean m_i	Std.dev. σ_i
2.396284e-01	1.151241e-01	2.543812e-02
5.613619e-01	4.864239e-01	1.786954e-01
1.990133e-01	6.403411e-01	9.304163e-03

Table 3.3: *Default model parameters of the Gaussian mixture model for ACF zero crossing rate α (after [4]).*

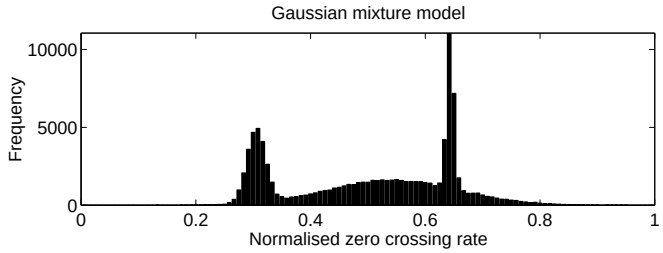

Figure 3.5: *Histogram of ACF zero crossing rate α generated with the Gaussian mixture model.*

Decay rate. The analysis showed that the decay rate β for the BT data does not depend on the studied telephone line but is dependent on the impulse length. To reflect the latter the impulse duration was divided in ranges and decay rate histograms were constructed for each range. It was found that for the BT data these histograms were well approximated using a standard Gaussian pdf[3] [3]. A summary of the impulse length ranges and the corresponding Gaussian distribution parameters are shown in Table 3.4.

ACF generation algorithm. With the statistical models for cosine frequencies α and decay rates

[3]Note that the decay rate can only take positive values. Mathematically the Gaussian pdf is capable of generating negative values, but negative decay rates are physically meaningless in the presented ACF model.

	Event length (μs)	Events in range (%)	Mean (μs)	Variance (μs^2)
shortest	0 - 1	1.9	3.832230e-02	4.112868e-05
short	1 - 3	62.6	2.666544e-02	6.296414e-05
medium	3 - 10	25.8	1.073394e-02	1.346540e-05
long	> 10	9.7	3.073201e-02	2.652703e-06

Table 3.4: *Impulse length ranges and default Gaussian model parameters for ACF decay rate β (after [3] and [4]).*

β, it is possible to generate impulse autocorrelation functions. Firstly, an impulse duration is generated from the length distribution defined in Equation 3.7. Depending on the range in which the length falls, the appropriate Gaussian pdf is evaluated to give the exponential decay rate $\hat{\beta}$. The zero crossing Gaussian mixture (3.11) with parameters corresponding to the line in consideration is evaluated to produce the estimate $\hat{\alpha}$. Finally, a synthetic autocorrelation function is generated by substituting the values of $\hat{\alpha}$ and $\hat{\beta}$ in (3.10). Each ACF generated in this way will be different and will provide a statistically correct representation of the spectral characteristics of the impulse, since the ACF parameters were drawn from statistical distributions based on measured data.

Statistical analysis of the autocorrelation functions for DT data

Due to the high energy level in the low end of the impulse spectra, the autocorrelation functions of the DT data require a model different from that for the BT data. It is evident from the cumulative distribution of the number of peaks in the impulse spectra (Figure 3.6), that less than 50% of the DT impulses have only one significant peak in their spectrum and their autocorrelation functions can be approximated with the ACF model for BT data. However, modelling the ACF for DT data with three cosine-modulated exponentials would cover 80% of the cases and offers a good trade-off between accuracy and model complexity. This means that the ACF model for DT data requires the estimation of six parameters. The cosine frequencies α_1, α_2, and α_3 can be obtained from the distributions of the frequencies of each of the three peaks. The decay rates β_1, β_2, and β_3 can be related to the bandwidth of each of the three peaks through the Fourier transform theory [3].

Figure 3.7[4] shows results from novel analysis of the three highest peaks and their respective

[4]These graphs have also been published in [3].

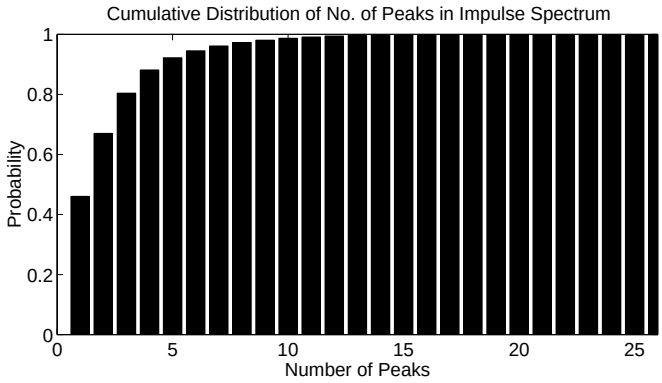

Figure 3.6: *Cumulative distribution of number of peaks in power spectral density for DT data.*

bandwidth distributions for DT data[5].

Spectral peaks. All three highest peaks have histograms similar in shape to that of the zero crossing distribution in Figure 3.5, so one possibility is to be modelled with a Gaussian mixture as in the case of BT data. It is also evident that the highest peak is concentrated at low frequencies, whereas the second and third highest peaks show clear signs of concentration in two distinct spectral regions. This leads to a second possibility to model each frequency α_1, α_2, and α_3 with a single Gaussian distribution. However, the suitability of this approach can be evaluated only after further analysis of the correlation between the peak heights and their frequency distribution. No comment can be made on whether the frequency distributions for DT data are telephone line dependent since line information was not present in the data set used in this study.

Peak bandwidths. The distribution of the peak bandwidths of the three highest peaks have similar shapes which can be modelled with a single distribution, as in the case of BT data. The dependence of the bandwidth statistics on impulse length is subject to further investigation.

The presented results provide foundation on which the statistical models of the parameters α_1, α_2, α_3, β_1, β_2, and β_3 can be defined and quantified and it is hoped that this analysis will stimulate further research in the field.

[5]Thanks to W. Henkel, currently with Telecommunications Research Centre, Vienna, Austria, and Th. Kessler, currently with T-Systems Nova GmbH., Darmstadt, Germany for providing data from DT measurements.

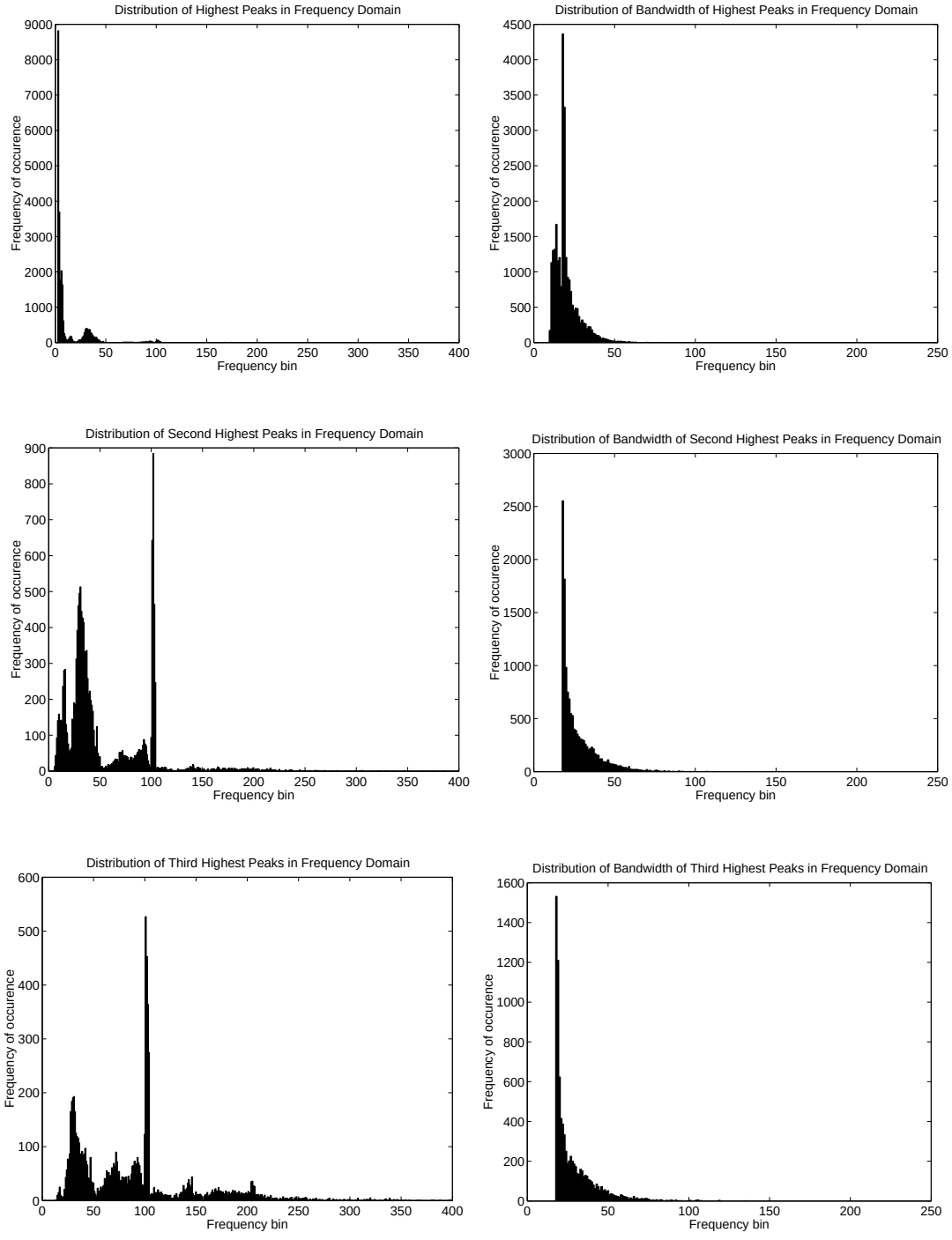

Figure 3.7: *Distribution of three highest peaks and their bandwidths in frequency domain for DT data.*

Spectral peak detection

As with the impulse detection in the time domain, correct peak detection in the frequency domain is an essential issue for producing appropriate spectral statistics of impulse noise and will be discussed in more detail.

Hill climbing algorithm. The peak detection technique used for the analysis above is based on the hill climbing algorithm, which is widely used in the areas of optimisation, data bases and artificial intelligence in general (see e.g. [103]). The hill climbing technique is good at finding local maxima and this is essentially what is needed for peak detection. In order to seek out only the significant peaks in the spectrum, two threshold values have been introduced (Figure 3.8). The "uphill" threshold S_{th+} from the nearest local minimum is used to indicate whether the local maximum is large enough to be of interest. The "downhill" threshold S_{th-} from the already detected local maximum marks the beginning of a local minimum and a search for new maximum starts.

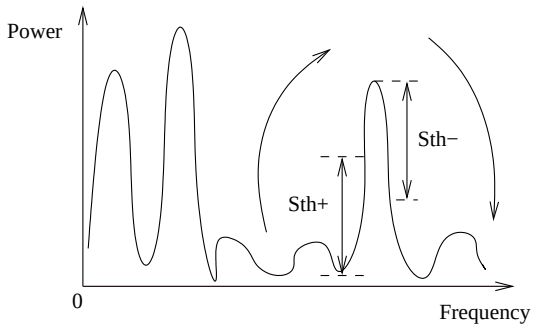

Figure 3.8: *Peak detection in impulse power spectra with hill climbing algorithm.*

Algorithm modifications. Unfortunately, the power spectral densities of real impulses (Figure 3.9) are by far not so smooth as in the ideal case. The presence of ripples with deep minima in the spectrum is a major hindrance for the hill climbing algorithm. In addition, as with all threshold algorithms, there is an inherent difficulty in determining appropriate values for the thresholds. Several measures have been taken to ensure correct spectral peak detection:

- spectral curve filtering, which in practice was implemented as averaging over a sliding window. A trade-off has to be found between the requirements for large window to smooth better the curve, and small window, so that not to distort important information about the peak amplitude and bandwidth. The sliding window was set manually after

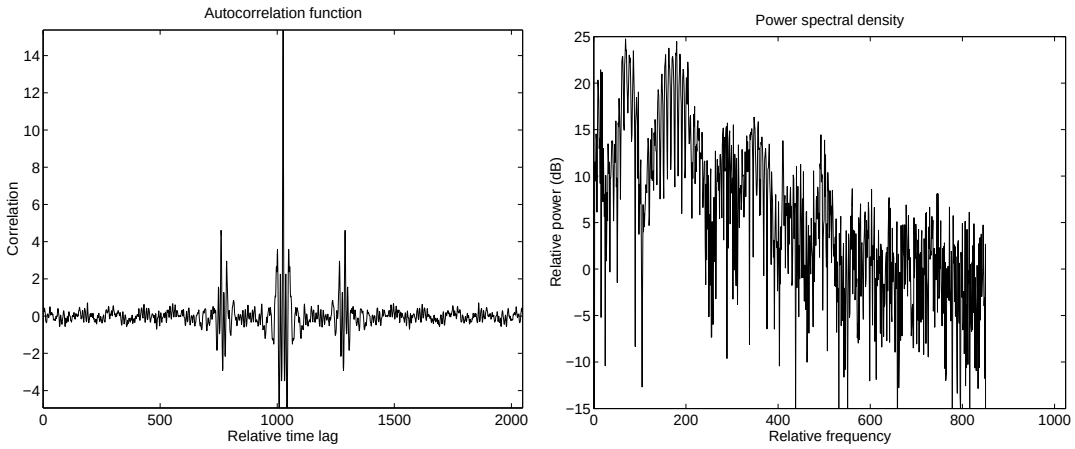

(a) Autocorrelation function

(b) Power spectral density

Figure 3.9: *Autocorrelation function and power spectral density of an impulse from DT measurements.*

examination of large number of impulse spectra;

- spectrum specific threshold values. The thresholds S_{th+} and S_{th-} are set separately for each spectral density as a proportion of the maximum observed value in the spectrum. This ensures that all significant peaks for each spectrum will be detected;

Figure 3.10(a) demonstrates the peaks detected in the spectrum of the impulse from Figure 3.9 with hill climbing and the above two modifications. A visual inspection of the results shows that several local maxima were detected on what should be regarded as a single peak. To prevent this, additional improvements were brought in:

- adaptive negative threshold. The threshold S_{th-} is set independently for each peak to be the maximum of a reference threshold value S_{refth-}, and some proportion of the value of the local maximum S_{locmax}/n; n = 2 $\Leftrightarrow$ 3 dB was found to give good results;
- double pass. The peak search is performed in both directions starting with lowest and highest frequency respectively. After comparison of the results the peaks that were detected only in one direction of the peak searches are discarded.

Performance. The additional modifications allow the hill climbing algorithm to detect correctly peaks with ripples as can be seen from Figure 3.10(b). Further improvements to this algorithm

or other peak detection methods can certainly be implemented, but this technique performed sufficiently well to produce the peak statistics results presented in the previous section.

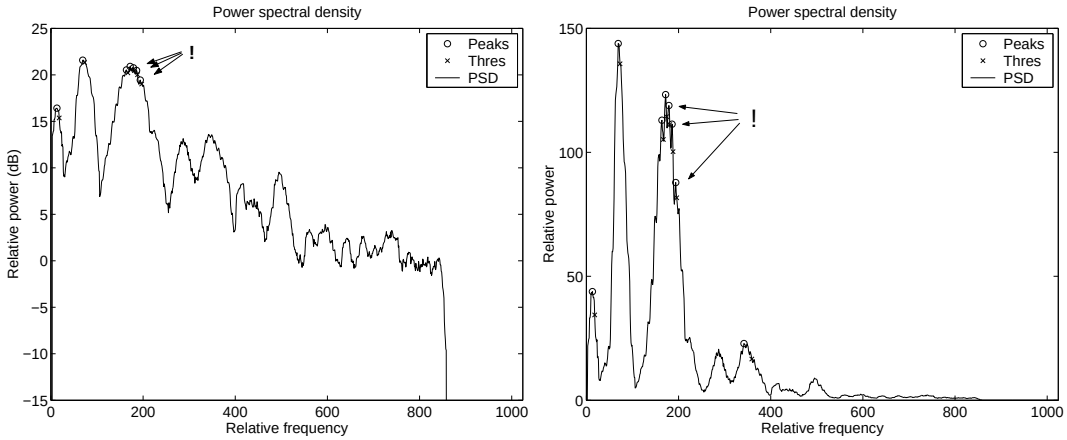

(a) Spectrum-specific thresholds, single pass

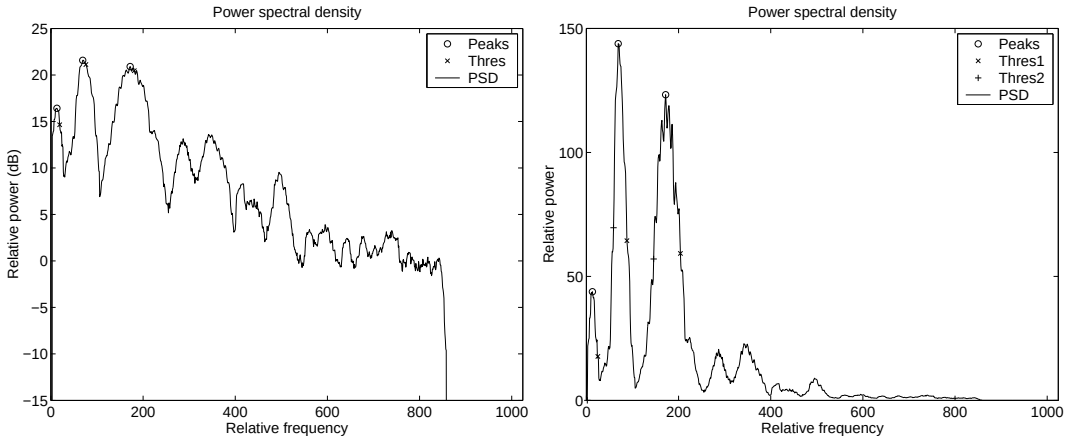

(b) Peak-adaptive negative threshold, double pass

Figure 3.10: *False peak detection (a) and correct peak detection (b) after additional hill climbing algorithm modifications, plotted in logarithmic (left) and linear (right) scales.*

3.2.5 Impulse generation with appropriate temporal and spectral characteristics

Combining the spectral and time domain properties of a stochastic signal is not a trivial task, since any filtering to obtain desired frequency characteristics would modify the time domain characteristics and vice versa. It is possible, however, to generate stochastic processes with pre-

defined distribution and correlation properties using a technique developed by Tough and Ward [90]. The correlation properties can in turn be related to the spectrum as shown before, therefore such an approach provides a solution to the problem. The Tough-Ward method employs a memoryless nonlinear transform (MNLT) to map between a zero-mean, unit-variance Gaussian pdf and the desired pdf, which in the general case could be arbitrary. The MNLT is used to calculate the relationship between the correlation coefficients of the two stochastic processes. The impulse generation would then consist in imposing a correlation on a Gaussian sequence, which after MNLT would produce an output sequence with both the required pdf and correlation structure.

Theoretical analysis

The MNLT is obtained by equating the cumulative distribution functions (cdf)[6] of the zero-mean unit variance Gaussian process and the required process. This is where the Weibull distribution for impulse amplitudes has advantage over the generalised exponential, because it allows easier analytical handling of the MNLT equation. For the double Weibull distribution defined in (3.3), the MNLT is given by:

$$\int_y^\infty \frac{1}{2}\alpha b|y'|^{\alpha-1}e^{-b|y'|^\alpha}dy' = \frac{1}{\sqrt{2\pi}}\int_x^\infty e^{-x'^2/2}dx'. \tag{3.12}$$

The solution to Equation 3.12 would yield [3][7]:

$$y = \begin{cases} \left(\frac{1}{b}\ln\left(\frac{1}{\mathrm{erfc}(x/\sqrt{2})}\right)\right)^{1/\alpha}, & x \geq 0, \quad y \geq 0 \\ -\left(\frac{1}{b}\ln\left(\frac{1}{2-\mathrm{erfc}(x/\sqrt{2})}\right)\right)^{1/\alpha}, & x < 0, \quad y < 0 \end{cases}. \tag{3.13}$$

An example of the relationship between x and y has been plotted in Figure 3.11(a). Using the results in [90], it can be shown that the relationship between the input Gaussian correlation coefficients, R_G, and the desired output Weibull correlation coefficients, $\langle y(0)y(t)\rangle$, is given by:

$$\langle y(0)y(t)\rangle = \frac{1}{2\pi}\sum_{n=0}^{\infty}\frac{R_G(t)^n}{2^n n!}\left[\int_{-\infty}^{\infty} e^{-x^2/2}H_n\left(\frac{x}{\sqrt{2}}\right)y\,dx\right]^2, \tag{3.14}$$

[6]The proposed MNLT actually equates the complementary cumulative distribution functions (ccdf), defined in the general case as $\bar{F}(z) = Pr(Z > z)$, but the term "cdf" was used in the original work of Tough and Ward [90] and is left unchanged in this discussion.

[7]Note that there is an error in [3]: the solution of the Gaussian-to-double-Weibull MNLT equation for $y < 0$ should be with a negative sign.

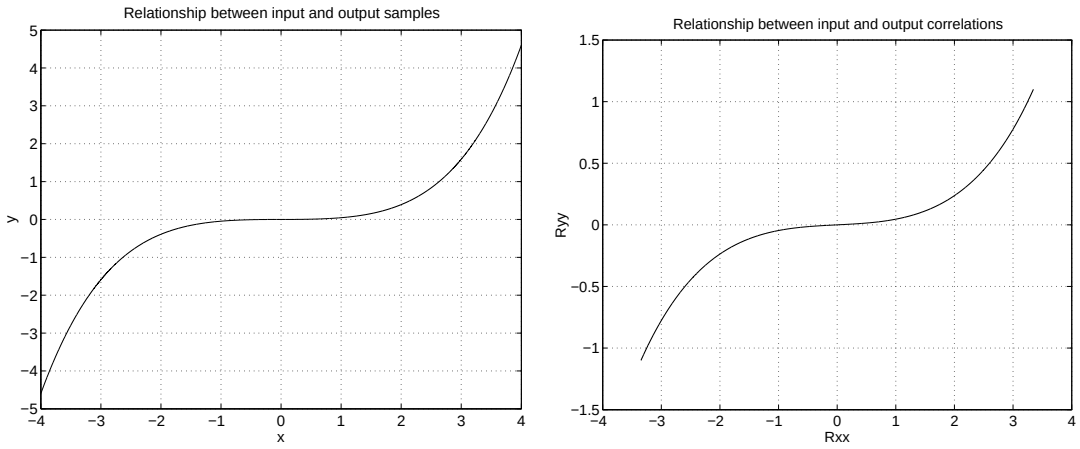

(a) MNLT **(b)** Correlations

Figure 3.11: *Graphical representation of a Gaussian-to-Weibull (a) MNLT and (b) correlations for double Weibull density with* $\alpha = 0.463$ *and* $b = 4.77$.

where y is given in (3.13) and H_n are Hermite polynomials of n-th degree defined as:

$$H_n(z) = (-1)^n \exp(z^2) \frac{d^n}{dz^n} \exp(-z^2). \tag{3.15}$$

The integral in (3.14) can be evaluated numerically and the resulting polynomial is used to generate a look-up table which gives the relation between the input and output correlation coefficients. The computational complexity of this process is relatively high but it should be noted that it has to be performed only once. An example of relationship between correlations is shown in Figure 3.11(b). Note also that it is possible to evaluate numerically the MNLT and the relationship between correlations for the generalised exponential distribution, which was the original proposal for impulse amplitude modelling (see section 3.2.3, p. 37).

Impulse generation algorithm

After the initial analysis and calculations, the actual impulse generation is carried out using the following algorithm [3]:

- Evaluate the impulse length pdf to obtain impulse duration.
- Generate a synthetic autocorrelation function using the length, the exponential decay, and

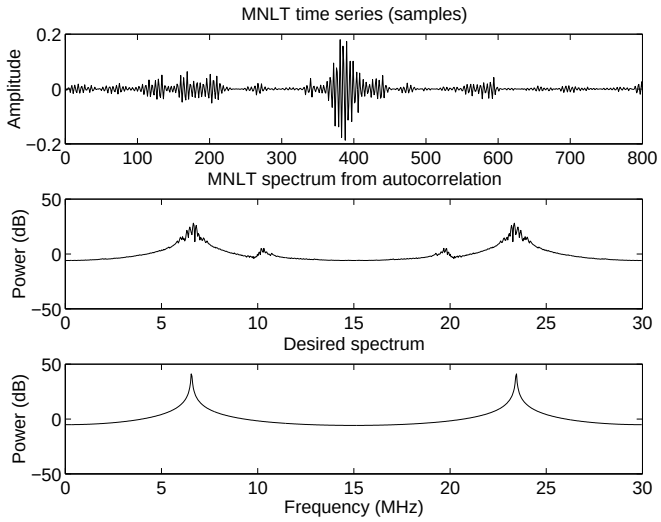

Figure 3.12: *Example of Tough-Ward impulse generation for an impulse of length 26.7 μs.*

the zero-crossing pdfs.

- Map the required output correlation to the input correlation in the Tough-Ward look-up table.
- Design a FIR filter with spectrum corresponding to the input correlation.
- Filter a Gaussian sequence of the required length with the FIR filter, thus imposing the required input correlation structure
- Apply MNLT on the filtered Gaussian sequence to obtain an impulse with the desired amplitude and spectral characteristics.

The algorithm is repeated for each required impulse and the computational complexity in the algorithm is dominated by the need to design a new a FIR filter for each iteration.

Performance of the impulse generator

The performance of the impulse generating algorithm is demonstrated in Figure 3.12. The generated impulse is shown in both the time and frequency domain, and the desired spectrum calculated from the synthesised autocorrelation function is plotted in the lowest graph. The results demonstrate that this impulse generation method achieves realistic impulse properties both in the time and frequency domain.

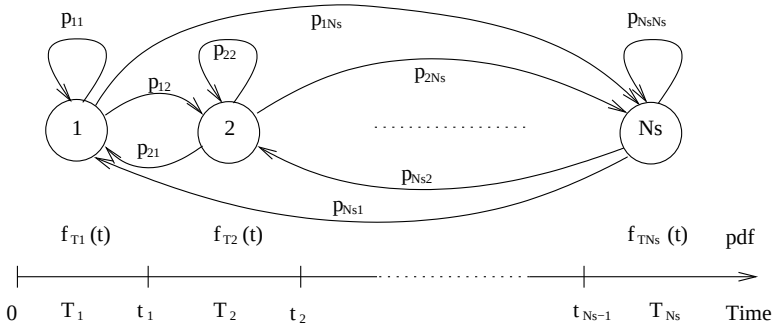

Figure 3.13: *Markov renewal model of impulse noise inter-arrival times.*

3.2.6 Inter-arrival times

The train of noise impulses can be regarded as a renewal process, i.e. series of random events in which the intervals between events are independent and identically distributed. Inter-arrival times between impulses exhibit a complex statistical behaviour. Their range is extremely large - various studies point out values from $\sim 10^{-5}$ to $\sim 10^{5}$ s. Also, the probability of small inter-arrival intervals is very high, and the tail of the distribution is very long and irregular. Finally, inter-arrival times evince a significant degree of clustering, i.e. consecutive intervals tend to be of comparable range. It was shown by Levey and McLaughlin that the statistical characteristics of inter-arrival times can be modelled successfully with a Markov renewal process [5, 84, 86].

Markov renewal model of inter-arrival times

This section will present only features of the Markov processes which will be used for subsequent analysis in this work. The theory of Markov models is well established and the reader can find a thorough background on the subject in e.g. [91, 104, 105].

For the purpose of modelling, the inter-arrival times are divided into ranges T_i, such that $T_i \equiv [t_{i-1}, t_i)$, $i = 1, 2, \ldots, N_S$; $\quad 0 = t_0 < t_1 < \cdots < t_{N_S} \rightarrow \infty$. Each Markov state corresponds to a time range, and the specific time within each range is drawn from an appropriate distribution with density function $f_{Ti}(t)$, $i = 1, \ldots, N_S$, $t \in T_i$, which in the general case can be arbitrary. The inter-arrival times model has been summarised graphically in Figure 3.13.

A Markov chain is described by its transition probability matrix P_{mar} defined as:

$$P_{mar} = \{p_{ij}\} = \begin{bmatrix} p_{11} & p_{12} & \cdots & p_{1N_S} \\ p_{21} & p_{22} & \cdots & p_{2N_S} \\ \vdots & & & \\ p_{N_S1} & p_{N_S2} & \cdots & p_{N_SN_S} \end{bmatrix}. \tag{3.16}$$

Here p_{ij} are the probabilities of transition from state i to state j, which must satisfy the requirements $p_{ij} \geq 0$ and $\sum_{j=1}^{N_S} p_{ij} = 1$ for $i, j = 1, \ldots, N_S$.

The introduction of density functions $f_{Ti}(t)$ to describe inter-arrival times statistics in each state is equivalent to generalising the Markov chain to a semi-Markov process, also called Markov renewal process (MRP) [91, 106]. In order to specify fully the MRP for impulse noise, it is necessary to determine the number of Markov states, the time range each state corresponds to, and the distribution within each time range.

Number of states. Intuitively it can be assumed that a larger number of states, N_S, in the Markov chain would lead to higher accuracy in the inter-arrival times modelling. In the extreme case each separate inter-arrival time can be deemed to be a Markov state but such a model would certainly be excessively complex. The number of states is therefore a trade-off between accuracy and complexity. It was pointed out in [5] that the Markov model need not be complex in order to benefit from its potential. A practical model of inter-arrival times can be constructed with only two states and a very powerful model can be achieved with as few as four states.

Time ranges. The ranges of inter-arrival times assigned to each state are determined by examination of the independence of times within each state and of the dependence of times between states. A method to test inter-state dependence was proposed in [107] where the observed number of transitions is compared with the expected number of transitions by means of a chi-squared type of test. This test can both demonstrate the existence of clustering in inter-arrival times and help introduce the correct level of clustering in the MRP via the transition probabilities. For full details about analysis of clustering of impulse noise see [5].

Density functions. The choice of density functions depends on the partitioning of inter-arrival times range and the data set that is to be modelled. It was pointed out in [5, 84, 86] that different inter-arrival time ranges from the same model may have to be approximated with different

distributions in order to achieve best fit to empirical data. The Pareto and exponential[8] distributions were proposed as possible options.

The Pareto, or hyperbolic distribution, is a good model for random variables with a slowly decaying density tail. The general form of the Pareto density function is given by (see e.g. [108]):

$$f_{par}(t) = \frac{\theta t_0^{\theta}}{t^{\theta+1}},\ t \geq t_0,\ t_0 > 0,\ \theta > 0, \tag{3.17}$$

where t_0 is a scale, and θ is a shape parameter.

The Poisson process is widely used for modelling random series of events. The inter-arrival times between events in the Poisson process have an exponential pdf defined as (see e.g. [106]):

$$f_{exp}(t) = \lambda e^{-\lambda t},\ t \geq 0, \tag{3.18}$$

where λ is a shape parameter.

Four-state Markov renewal model of impulse noise

It was proposed in [5, 84, 86] to partition the time for a four-state MRP model to ranges $[0, 1)$, $[1, 10)$, $[10, 100)$, and $[100, \infty)$ seconds. Data sets from several telephone lines were used to derive this model and in all cases the Pareto distribution was a good fit for the highest state, i.e. the longest times that form the tail of the distribution. However, in lower states, the exponential distribution appeared to be a better fit for some data sets. Therefore, two different models were proposed [5] - Model 1, in which all time ranges are approximated with Pareto distribution, and Model 2, in which some time ranges are Pareto, and others exponentially distributed. The parameters for both models are given in Table 3.5.

The empirical Markov transition probabilities were also found to be line specific [5]. Nevertheless, the statistical characteristics of most data sets had a reasonable level of consistency and

[8]The exponential distribution is sometimes referred to as Poisson distribution because it can fully specify a Poisson process. Strictly speaking, however, the Poisson distribution is defined as $Pr(N_t = r) = \frac{(\lambda t)^r e^{-\lambda t}}{r!},\ r = 0, 1, \ldots$ and gives the probability that r number of events will occur within a time period t.

State	1	2	3	4
Range	$t < 1$ s	$1 \leq t < 10$ s	$10 \leq t < 100$ s	$100 \leq t$
Model 1	Pareto			
	$\theta_1 = 0.874$	$\theta_2 = 1.539$	$\theta_3 = 1.531$	$\theta_4 = 2.513$
Model 2	Exponential	Pareto	Exponential	Pareto
	$\lambda_1 = 2.042$	$\theta_2 = 1.539$	$\lambda_3 = 0.0170$	$\theta_4 = 2.513$

Table 3.5: *Parameter values for a four-state Markov renewal model of inter-arrival times (after [5]).*

this allowed to derive transition probability estimates averaged over several studied lines:

$$P_{4st} = \begin{bmatrix} 0.801 & 0.038 & 0.061 & 0.100 \\ 0.470 & 0.123 & 0.221 & 0.186 \\ 0.375 & 0.068 & 0.281 & 0.276 \\ 0.350 & 0.045 & 0.217 & 0.388 \end{bmatrix}. \tag{3.19}$$

This transition probability matrix is valid for both models specified in Table 3.5.

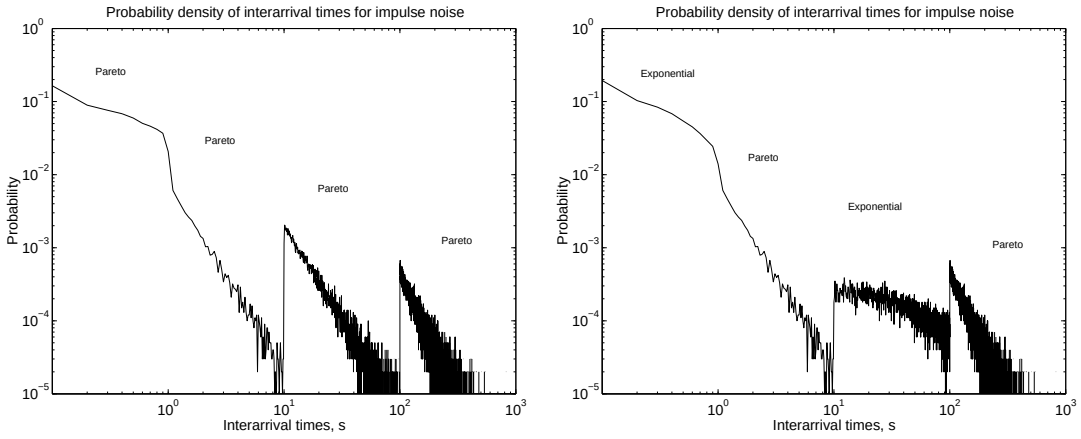

(a) Model 1 **(b)** Model 2

Figure 3.14: *Probability density of inter-arrival times generated with a four-state Markov renewal model.*

Log-log plots of the histograms of inter-arrival times generated from both models are shown in Figure 3.14. The graphs seem somewhat erratic with abrupt jumps especially in the tails, but this resembles the actual behaviour observed in empirical results. Histograms of intervals generated with Model 2 are plotted on linear axes in Figure 3.15(a) and zoom on the tail is

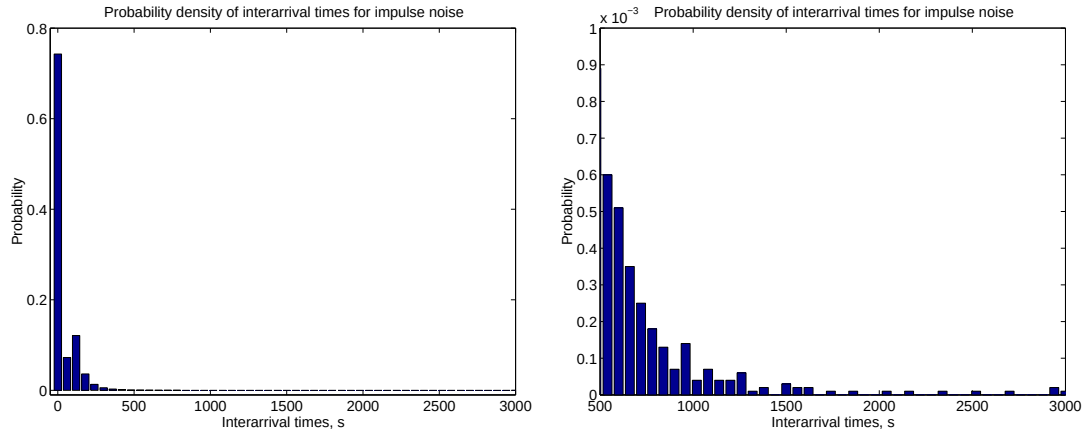

(a) Probability density

(b) Zoom in on the density tail

Figure 3.15: *Probability density of inter-arrival times generated with a four-state Markov renewal process - Model 2.*

shown in Figure 3.15(b). As in the empirical histograms (see e.g. Figures 1 and 2 in [5]), the vast majority of inter-arrival times are concentrated in the shortest range, and the tail is very long and with complex behaviour that differs significantly from the rest of the distribution.

Two-state Markov renewal model of impulse noise

The four-state MRP described in the previous section does provide accurate inter-arrival times modelling. However, a two-state MRP has also been proposed and standardised by ETSI [4] for xDSL testing and simulation purposes. The latter model concentrates on inter-arrival times of up to 1 s, which is sufficient to test the modem recovery times. It should also be noted that although the range of 1 s is small in comparison with the whole range of observed inter-arrival times (up to 10^5 s [5]), a large proportion of the inter-arrival time occurrences fall within this 1 s range (50% to 90% [5]). It was shown in [3] that a two-state MRP is adequate for modelling inter-arrival times of up to 1 s and no significant advantage is to be gained by adopting a more complex model.

The two-state MRP model specified in [4] divides the inter-arrival times in ranges of less and more than 1 ms. The lower state (shorter times) is modelled with exponential, and the higher state - with Pareto distribution. The values of the distribution parameters are given in Table 3.6.

State / Distribution	1	Exponential	2	Pareto
Range/Parameter	$t < 1$ ms	$\lambda = 0.16$	$t \geq 1$ ms	$\theta = 1.5$

Note that λ and θ are computed such that t is in ms.

Table 3.6: *Parameter values for a two-state Markov renewal model of inter-arrival times (after [4]).*

The transition probabilities matrix is defined as:

$$P_{2st} = \begin{bmatrix} 0.8 & 0.2 \\ 0.4 & 0.6 \end{bmatrix}. \tag{3.20}$$

The histogram of inter-arrival times generated from this model and a zoom of the density tail are shown in Figure 3.16. The results resemble closely the empirical histograms shown in Figures 4 and 5 in [3].

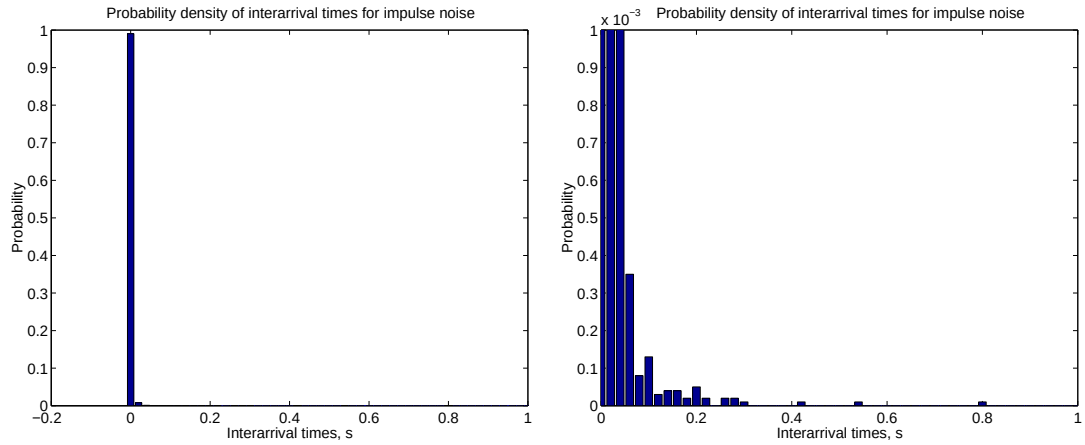

(a) Probability density

(b) Zoom in on the density tail

Figure 3.16: *Probability density of inter-arrival times generated with a two-state Markov renewal process.*

3.3 Crosstalk

Crosstalk between pairs in a multi-pair cable is another significant impairment for DSL systems alongside impulse noise. The cause of crosstalk is the electro-magnetic coupling between the

wires in a cable, or rather the imbalances in this coupling. As a result signals transmitted over one pair induce currents in the other pairs of the same cable, thus causing interference. The induced signals travel in both directions in the disturbed pairs. Those that continue in the same direction as the interfering signal add up to form far-end crosstalk (FEXT), and those that come back towards the source of the interferer add up to form the near-end crosstalk (NEXT). This is summarised graphically in Figure 3.17, where the thickness of the lines showing crosstalk gives a rough indication of the relative level of interference.

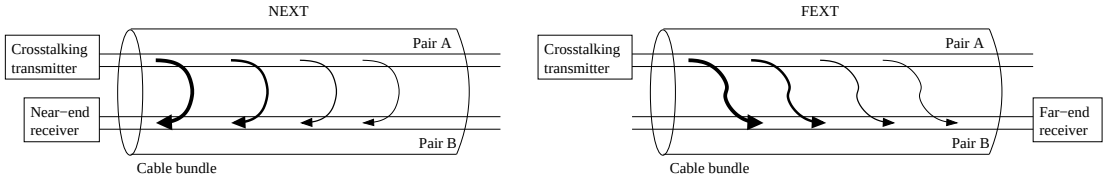

Figure 3.17: *Definition of near- and far-end crosstalk (NEXT and FEXT).*

3.3.1 Sources of crosstalk

With the rise in popularity of DSL services, it is increasingly possible that several pairs in a telephone cable will be used for DSL transmission. The DSL signals in one cable may be of the same DSL variety, but in the general case may be any combination of ISDN, HDSL, ADSL, SHDSL, VDSL, and perhaps non-standard equipment (Figure 3.18). The only DSL unlikely to be present in the same bundle is T1/E1, because their power spectrum is so aggressive to other transmission systems that they are normally (but not always) segregated in dedicated binder groups [6].

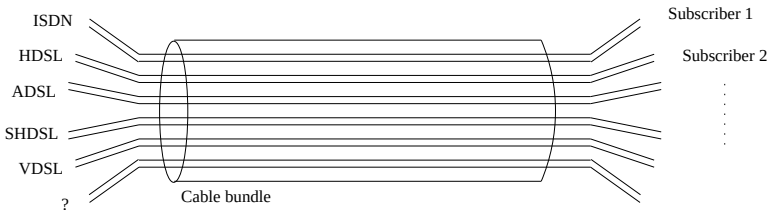

Figure 3.18: *Possible sources of crosstalk.*

Since the spectra of all DSL services overlap at least partially (see Section 3.3.4), any crosstalk from one DSL pair would represent interference to the DSL signal in the disturbed pair. If the

crosstalk to one DSL signal is caused by DSL of the same variety, it will be referred to in this work as *kindred* crosstalk, otherwise will be called *alien* crosstalk.

3.3.2 Crosstalk noise in the time domain

The majority of studies on crosstalk concentrate on its spectral features, since crosstalk interference lends itself better to characterisation in the frequency domain. This is because the underlying induction process is frequency dependent, and the power spectral densities (PSDs), or at least PSD masks, of the source signals of crosstalk interference, are readily available. Therefore, the studies of crosstalk in the time domain are relatively scarce.

A study by Kerpez [109] argued that both NEXT and FEXT are approximately Gaussian distributed at the receiver. Due to the frequency-dependent nature of crosstalk this assumption is clearly not true for crosstalk from a single source. However, when different contributors from different lines are added up, the central limit theorem (see e.g. [101]) loosely applies, and the distribution of the sum tends to be Gaussian. It is claimed in [109] that this holds for cases of practical interest. However, it is pointed out in [6] that while the deviation between the Gaussian and the real distribution may not be large, the difference is important in some cases such as development of crosstalk mitigation techniques.

The issue of crosstalk stationarity was considered by Pederson and Falconer [110], who found that crosstalk may not be stationary unless sampled at exactly the same rate as the crosstalk source signal. As a result DSL systems with higher sampling rates will see periodicity in the crosstalk from lines with lower sampling rate. If two DSL systems are synchronised to the same central office clock, the overall crosstalk will be cyclostationary (see e.g. [101]) with period equal to the least common multiple of the sampling periods of the two DSLs.

3.3.3 Crosstalk spectral modelling

The level of crosstalk is greatly affected by the specific loop topology and implementation. Important factors are for example the length and location of the overlap between the interfering and interfered loops, the specific pairs of the bundle and the wire cross-section used in each segment of the line, the length of the segments and connections between them, the presence of bridge taps. For specifications of test loop topologies see e.g. [1, 11].

Nevertheless, without loss of generality it can be assumed in crosstalk modelling that the interfering and interfered loops are of equal length. If these lengths differ, as shown in Figure 3.19, attenuated NEXT and unequal-level FEXT are observed. Extending a crosstalk model to take into account different loop lengths is trivial and details on this can be found in e.g. [32]. All other loop topology factors are taken into account by means of the statistical distribution of the crosstalk coupling coefficients as discussed later.

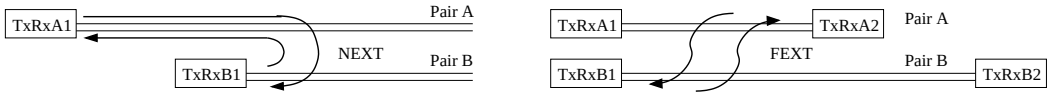

Figure 3.19: *NEXT and FEXT with different lengths of interfering and interfered loops.*

Crosstalk is modelled in the frequency domain by means of the crosstalk power transfer function $|H_{xt}(f,l)|^2$, which relates the power spectral density of the crosstalk interference $S_{xt}(f)$ to the spectral density of the disturbing signal $S_{src}(f)$:

$$S_{xt}(f) = |H_{xt}(f,l)|^2 \cdot S_{src}(f). \tag{3.21}$$

The crosstalk transfer function depends on the electro-magnetic coupling and the attenuation in the line, which in turn are functions of both the signal frequency f and the line length l, hence the functional dependence on these variables.

Crosstalk power transfer functions

Analytical expressions for the NEXT and FEXT transfer functions can be obtained by integrating the elementary contributions of induced signal along the line. Detailed analysis of capacitive and inductive coupling and imbalances, and derivations of the crosstalk transfer function can be found in e.g. [6, 32, 33]. Only the final results of this analysis will be presented here.

The NEXT power transfer function is given by [32, 33]:

$$|H_{next}(f,l)|^2 \approx k_{next}\, f^{1.5}(1 - e^{-4\alpha\sqrt{f}\,l}) \approx k_{next}\, f^{1.5}, \tag{3.22}$$

where k_{next} is a coupling coefficient between the two pairs in consideration, and α is a line attenuation coefficient. For the frequencies and loop lengths of practical interest for most DSL

systems, the term $e^{-4\alpha\sqrt{f}\,l}$ tends to zero [32]. This is not true for SHDSL, however, because its frequency band extends to very low frequencies. Nevertheless, substituting the term with zero in all cases is widely accepted since it only leads to a more conservative estimate.

The FEXT power transfer function has the form [6, 32, 33]:

$$|H_{fext}(f,l)|^2 = k_{fext}\,|H_{line}(f,l)|^2\,l\,f^2, \tag{3.23}$$

where $|H_{line}(f,l)|$ is the line transfer function, and k_{fext} is again a coupling coefficient between the disturbing and disturbed pairs.

The coupling coefficients k_{next} and k_{fext} depend on the electrical parameters of the cable, the cable structure, the relative position of the pairs involved, and are also influenced by aging and imperfections in the cable, bridge taps, wire connections and other factors. Therefore these coefficients are different for any pair of pairs and for any cable and can be considered random variables.

Statistical models of coupling coefficients

The statistical models of the crosstalk transfer functions are usually defined for some percentile of the worst case. Such a definition ensures that data rates and coverage of digital transmission systems are guaranteed for the majority of crosstalk conditions. For DSL services, the accepted norm is the 1% worst-case values of the crosstalk transfer function.

There have been a variety of empirical studies of crosstalk in the literature. Some interesting studies include that of Lin [111], Pollakowski [112], and Valenti [113], all of whom reported numerous measurement results. Unger proposed in [114] an expression for the 1% worst-case NEXT transfer function, where k_{next} is a function of the number of interfering pairs in the bundle. However, Huang and Werner [115] argued that with a binder group full of interferers, the 1% worst-case crosstalk level is independent of the number of pairs. Nevertheless, for the time being the accepted models use the Unger approach. For a 50-pair binder group the 1% worst-case coupling constants are defined as [6][9]:

$$k_{next} = 10^{-13} \cdot \left(\frac{n}{49}\right)^{0.6}, \tag{3.24}$$

[9] ANSI T1.413 [11] specifies slightly lower values for the coupling constants, namely $k_{next} = 0.8818 \times 10^{-13} \cdot (n/49)^{0.6}$ and $k_{fext} = 8 \times 10^{-20} \cdot (n/49)^{0.6}$.

$$k_{fext} = 9 \times 10^{-20} \cdot \left(\frac{n}{49}\right)^{0.6}, \tag{3.25}$$

where n is the number of disturbing pairs in the binder group. These values have been found to be valid for frequencies to 30 MHz [113].

Line transfer function

Unlike NEXT, the FEXT power transfer function depends substantially on the attenuation on the line, and therefore knowledge of the line transfer function $|H_{line}(f,l)|$ is required in order to estimate FEXT. It can be shown that [6]:

$$H_{line}(f,l) = \frac{Z_0 \cdot \operatorname{sech}(\gamma l)}{Z_S \cdot \left[\frac{Z_0}{Z_L} + \tanh(\gamma l)\right] + Z_0 \cdot \left[1 + \frac{Z_0}{Z_L} \cdot \tanh(\gamma l)\right]}, \tag{3.26}$$

where Z_S and Z_L are the source and load impedances, and tanh and sech are the hyperbolical tangent and secant functions respectively. The characteristic impedance Z_0 and the propagation constant γ of the twisted pair can be expressed as:

$$\gamma = \sqrt{(R + j\omega L) \cdot (G + j\omega C)} = \sqrt{Z \cdot Y} \qquad Z_0 = \sqrt{\frac{R + j\omega L}{G + j\omega C}} = \sqrt{\frac{Z}{Y}}, \tag{3.27}$$

where $\omega = 2\pi f$. The impedance Z and the admittance Y of the line per unit length depend on the resistance R, inductance L, capacitance C, and conductance G, which in turn can be determined from measurements using the following expressions [6]:

$$\begin{aligned} R(f) &= \sqrt[4]{r_{0C}^4 + a_C \cdot f^2} & L(f) &= \tfrac{l_0 + l_\infty (f/f_m)^b}{1 + (f/f_m)^b} \\ C(f) &= c_\infty + c_0 \cdot f^{-c_e} & G(f) &= g_0 \cdot f^{g_e} \end{aligned} \tag{3.28}$$

where r_{0C} is the copper DC resistance, a_C is a constant characterising the so-called "skin effect", l_0 and l_∞ are the low- and high-frequency inductance, f_m and b are a cut-off frequency and a parameter characterising the transition between low and high frequencies in the measured inductance, c_∞ is the so-called "contact" capacitance, and c_0, c_e, g_0, and g_e are constants chosen to fit the measurements.

3.3.4 Modelling crosstalk from xDSL systems

If the transmit power spectral density of the interfering signal is known, it is possible to evaluate NEXT and FEXT at the receivers of the disturbed signal by using the appropriate crosstalk transfer function in Equation 3.21. Definitions of the nominal transmit PSDs for the most common versions of ISDN, HDSL, ADSL, and SHDSL are given in Appendix A:

- *ISDN*. The nominal transmit PSD of 2B1Q-modulated ISDN signal is defined in Equation A.1. Details about the PSDs of 4B3T-modulated ISDN (mostly used in Germany) and ISDN with synchronised TDD (used in Japan) can be found in e.g. [15].
- *HDSL*. The HDSL power spectral density specified by Equation A.2 refers to 2B1Q-modulated HDSL with symbol rate 392 kbaud, i.e. bit rate 786 kbps over one pair. This means 1.544/2.048 Mbps over HDSL are achieved with two/three pairs respectively. For details about the PSDs of less common HDSL versions, e.g. 2B1Q-modulated HDSL with symbol rates 584 kbaud and 1160 kbaud, or CAP-modulated HDSL, see e.g. [22].
- *ADSL*. The ADSL power spectral densities given in Appendix A refer to the "full" (as opposed to "light" - see Section 2.5.5, p. 24) version of DMT-modulated ADSL. Because of the asymmetry in the bit rates, the ADSL signals have different PSDs depending on whether they are transmitted in the upstream (Equation A.4) or downstream (Equation A.3) direction. It is assumed that ADSL uses all available subcarriers in each direction and the total transmit power is set such that the PSD would not exceed the maximum allowed PSD. Note, however, that unlike ISDN and HDSL, ADSL allows variable bit rate and in the general case may not use all subcarriers, changing the transmit PSDs accordingly.
- *SHDSL*. SHDSL is, like ADSL, a multi-rate transmission technology. The bit rate affects significantly the symbol rate, and hence the nominal transmit PSD (Equation A.5) of the 16-PAM SHDSL signal. Note also that (A.5) specifies a symmetric PSD mask. Details about asymmetric PSD masks (optional in North America for 1.536 Mbps and 1.544 Mbps payload) can be found in [2].

The 1% worst-case NEXT power spectral densities from the DSL systems discussed above are plotted in Figure 3.20. Note it is assumed that the ADSL upstream is a source of NEXT, i.e. the

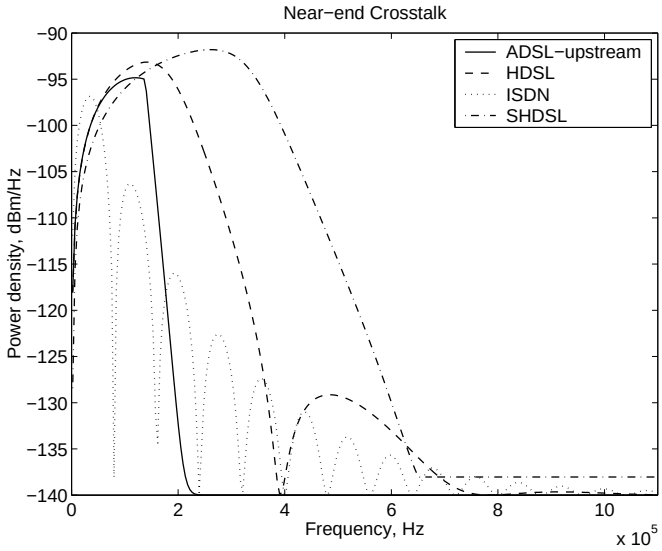

Figure 3.20: *1% worst-case level of near-end crosstalk at the customer premises from various DSL systems.*

graph shows NEXT at the customer premises[10]. Note also it has been intrinsically assumed that the sources of NEXT are in the immediate vicinity of the sink. In practice, however, there may be a significant physical separation between the customer premises of different DSL links, in which case attenuated NEXT will be observed. Nevertheless, this attenuation is insignificant, since for most loop plants the variation of loop length within one binder group is less than 20% of the total loop length. As a result the average NEXT is usually about 1 dB less than the modelled worst-case scenario [32].

3.3.5 Summing crosstalk in a mixed-signal environment

The crosstalk spectral model presented in Section 3.3.3 intrinsically assumes that all crosstalk interferers in the bundle are of the same type, i.e. have the same PSD. However, the co-existence of different versions of DSL on the same cable is becoming increasingly common because of the proliferation of DSL, the emergence of new DSL types, and the process of *unbundling*, i.e. simultaneous usage of the loop plant by various operators. Several summation methods for crosstalk from mixed sources are known in the literature. For the purpose of brevity only

[10] Sometimes ADSL is used in reverse mode, i.e. the downstream signal is transmitted upstream and vice versa. Such an arrangement is needed for e.g. web hosting or service providers, who require larger upstream than downstream bandwidth. It is much less common than the “orthodox” ADSL use and will therefore not be considered.

examples for NEXT summation will be given, applying the same summation methods to FEXT is trivial.

Direct summation method

The most straightforward mixing method is to sum the 1% worst-case crosstalk power contributions of each type of interferer. In the case of NEXT interference from m different systems, the total crosstalk PSD is given as:

$$S_{next}^{(dir)}(f, n_1, \ldots, n_m) = \left[\sum_{i=1}^{m} S_{src_i}(f) n_i^{0.6}\right] k'_{next} f^{1.5}, \tag{3.29}$$

where n_i is the number of systems with PSD $S_{src_i}(f),\ i = 1, \ldots, m$, and $k'_{next} = 10^{-13}/49^{0.6}$ for a cable bundle of 50 pairs.

However, the direct summation method is fundamentally incorrect [32, 116], since it assumes that all sources of crosstalk use simultaneously the worst pairs in a binder. From a purely mathematical point of view, if all interferers are considered to be of the same type, i.e. $S_{src_i}(f) = S_{src}(f),\ i = 1, \ldots, m$, then Equation 3.29 would transform into:

$$S_{next}^{(dir)}(f, n_1, \ldots, n_m) = S_{src_i}(f) k'_{next} f^{1.5} \sum_{i=1}^{m} n_i^{0.6}, \tag{3.30}$$

whereas the original single-type crosstalk model from (3.21), (3.22), and (3.24) would have predicted:

$$S_{next}(f, n_1 + \ldots + n_m) = S_{src_i}(f) k'_{next} f^{1.5} \left(\sum_{i=1}^{m} n_i\right)^{0.6}. \tag{3.31}$$

Since $\sum_{i=1}^{m} n_i^{0.6} \geq \left(\sum_{i=1}^{m} n_i\right)^{0.6}$, it is clear that the direct summation leads to overly pessimistic level of interference.

Mean PSD summation method

This method was originally proposed in [116] and consists of mixing the interferers at PSD level. The equivalent PSD is an arithmetic mean of the PSDs of the interfering signals and the

total NEXT PSD is given as:

$$S_{next}^{(meanPSD)}(f, n_1, \ldots, n_m) = \left[\sum_{i=1}^{m} S_{src_i}(f)\frac{n_i}{\sum_{j=1}^{m} n_j}\right] k'_{next} f^{1.5} \left(\sum_{i=1}^{m} n_i\right)^{0.6}. \quad (3.32)$$

The disadvantage of this method is that it can be overly optimistic, and although it achieves relatively low average error, its maximum prediction error is large, which is dangerous as it can lead to failures in the field [117]. A variation of this method is to define the equivalent PSD as a geometric mean of the various PSDs. The drawback of this definition is that it predicts zero interference if at least one of the disturbing PSDs is zero.

Annulus summation method

This method, first proposed in [118], requires a system of priority of interferers depending on how "bad" their crosstalk is. The n_1 interferers from the worst type 1 are given weighting as if they were causing the crosstalk alone. The second worst n_2 interferers are assigned weighting that would have been assigned by the single-type crosstalk model for disturbers $n_1 + 1$ to $n_1 + n_2$, etc. For two disturbers, this method defines NEXT as:

$$S_{next}^{(Annulus)}(f, n_1, n_2) = S_{src_1}(f) k'_{next} f^{1.5} n_1^{0.6} + S_{src_1}(f) k'_{next} f^{1.5} \left((n_1 + n_2)^{0.6} - n_1^{0.6}\right). \quad (3.33)$$

The drawback of the annulus crosstalk summation is that the hierarchy of interferers can be defined arbitrarily and this would affect the crosstalk levels predicted by the model.

FSAN summation method

This method, named after the Full Service Access Network (FSAN) consortium, was first proposed by Persico and Magnone of CSELT. The NEXT sum is defined here as [119]:

$$S_{next}^{(FSAN)}(f, n_1, \ldots, n_m) = \left\{\sum_{i=1}^{m} [S_{src_i}(f) n_i^{0.6}]^{1/0.6}\right\}^{0.6} k'_{next} f^{1.5}. \quad (3.34)$$

This method gives good estimates of the mixed-signal crosstalk [117, 120], is widely accepted and has become the ANSI standard [121] for summing crosstalk from mixed sources.

Generalised FSAN or Minkowski-bound summation method

A generalisation of the FSAN method was proposed by Galli and Kerpez [122]. It is based on exploiting the Minkowski inequality to derive a lower bound of the pessimistic direct summation method and has the form [123]:

$$S_{next}^{(Minkowski)}(f,\lambda,n_1,\ldots,n_m)=\left\{\sum_{i=1}^{m}[S_{src_i}(f)n_i^{0.6}]^{1/\lambda}\right\}^{\lambda}k'_{next}f^{1.5},\ 0<\lambda<1. \quad (3.35)$$

Here λ defines the degree of pessimism. For $\lambda \to 1$, the model is the most pessimistic and coincides with the direct summation method in (3.29), and for $\lambda = 0.6$ this model takes the FSAN form (3.34).

Hölder-bound method

Galli and Kerpez went on to derive another summation method from the direct summation model based on the Hölder inequality [123]:

$$S_{next}^{(\text{Hölder})}(f,\lambda,n_1,\ldots,n_m)=m^{-(1-\lambda)/\lambda}\left\{\sum_{i=1}^{m}[S_{src_i}(f)n_i^{0.6}]^{\lambda}\right\}^{1/\lambda}k'_{next}f^{1.5},\ 0<\lambda<1. \quad (3.36)$$

Again λ determines how pessimistic the model is. For $\lambda \to 1$, the model tends asymptotically to the direct summation method in (3.29), and for small λ the model is more optimistic.

The disadvantage of the Minkowski- and Hölder-bound methods is that they do not converge to the single-type crosstalk model as the spectra of the different disturbers become identical, although the error has been reported to be small [123].

A comparison between direct summation and the FSAN summation method for two mixed crosstalk scenarios is shown in Figure 3.21. The direct summation method is on average more pessimistic by about 1-2 dB than the FSAN method (the graphs have been plotted on linear scales in order that the difference is more visible).

3.3.6 xDSL spectral compatibility measures

In order to ensure acceptable levels of crosstalk for DSL systems, and thus their stable performance, the DSL transmit power must be kept under power spectral density masks defined in

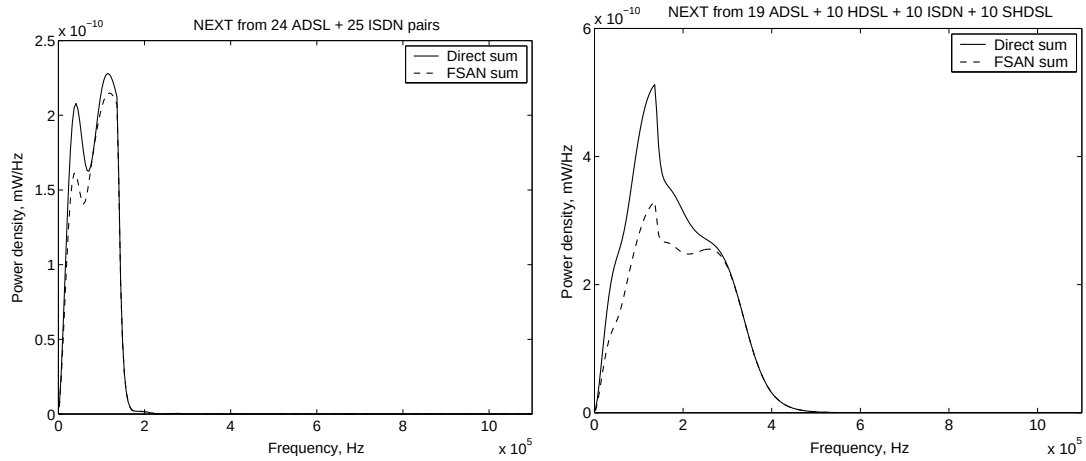

(a) NEXT from 24 ADSL + 25 ISDN

(b) NEXT from 19 ADSL + 10 ISDN + 10 HDSL + 10 SHDSL

Figure 3.21: *Sum of crosstalk from mixed sources using direct summation and the FSAN method.*

the respective standards. For example, the PSD mask for ADSL over POTS was shown in 2.7, p.22. These masks are usually selected such that a DSL system is crosstalk compatible both with systems of its own kind, and with other DSL types. However, the large variety of standard and non-standard DSL technologies, and the development of new DSL systems, makes it increasingly difficult to manage the spectrum in the local loop. Spectral compatibility is a particularly acute problem in an unbundled access network, where there can be little control over the technology different operators use. Therefore, the UK Office of Telecommunications (Oftel) introduced an access network frequency plan (ANFP). This plan specifies PSD masks for long, medium and short loops upstream and is applicable to all transmission systems used on the BT twisted-pair access network. In this way, the crosstalk interference in the access network is efficiently controlled. Full information about ANFP can be found in [124].

3.4 Radio frequency interference

Since the twisted pairs that make up the local loop are unshielded and the twisting cannot provide perfect balance in the electro-magnetic coupling, telephone lines also function as long aerials. Therefore they can both receive (ingress) and emit (egress) radio frequency interference

(RFI). It is usually considered that egress radiated from most DSL systems is insignificant except that from VDSL, which will be tackled via the PSD mask [6, 32]. Therefore, this section will concentrate mainly on ingress interference.

There are two easily identifiable potential sources of ingress RFI that use frequencies within the spectra of DSL systems - AM radio and amateur radio.

AM radio.

The AM radio occupies frequencies from 0.55 to 1.6 MHz, which overlap both the ADSL and VSDL spectra.

It is considered that AM radio does not represent a big impairment to ADSL, because close proximity to AM transmitter is unlikely (maximum differential-mode interference -70 dBm) and the balance of the twisted pair is relatively good (60 dB) at the ADSL frequencies [6, 32]. Besides, AM transmission is stable in time, has relatively narrow band (5 kHz) and may be accounted for during initialisation of the DMT modems, or in the case of single carrier modulation can be cancelled without serious deterioration of the wideband single carrier signal.

For VDSL frequencies, however, 60 dB line balance is too optimistic, and the interference levels may go as high as +30 dBm for common and -30 dBm for differential mode. Therefore, it is expected that tests for AM radio ingress will be included in the final version of VDSL standards.

Amateur radio (ham).

Ham radios operate in several frequency bands placed between 1.8 MHz and 29 MHz, and use single sideband modulation with bandwidth of usually around 2.5 kHz. Ham radio signals are much more bursty than AM radio, firstly because the ham operators tend to change the carrier frequency relatively often, and also the ham transmitter is silent when no information needs to be transmitted. Also, at ham frequencies the line balances are lower (around 30 dB [6]). The ham transmitters are usually low power (starting from around 50 W), but 1.5 kW ham radios are also possible. The worst case common mode from ham ingress is predicted as +30 dBm, and the worst-case differential mode - as 0 dBm [32]. Therefore, ham radio may be a significant impairment to VDSL systems and provisions will be incorporated in the VDSL standards.

3.5 Conclusion

This chapter has introduced the various sources of noise in telephone lines, with discussion on the noise statistics and models. Earlier statistical models of impulse noise have been shown to have a number of short-comings and a recently proposed impulse noise model has been chosen as the most accurate and complete alternative. The fact that this model allows for statistical description and generation of noise impulses with appropriate both time domain and spectral characteristics implies that it will represent accurately impulse noise when used for DSL studies. Some new work has demonstrated that a distribution of the impulse power in the time domain can be analytically derived from this model, which lays the basis for theoretical analysis of the impact of impulse noise on DSL. This impulse noise model can be extended further to reproduce impulses with more complex spectral contents, and the work on this may be aided by a new investigation of the impulse spectral features from empirical data that has been presented here.

It is evident from the discussion on crosstalk that due to variations in the modulations, different DSL systems generate interference with significantly different spectra. If the crosstalk originates from mixed signal sources, the use of special summation models is required, of which the FSAN method seems to combine desirable features with good performance. Finally, it has been shown that radio frequency interference represents a significant impairment only to VDSL.

Chapter 4
Simulation of ADSL system in the presence of impulse noise and crosstalk

4.1 Introduction

The main objective of this work - evaluating the impact of impulse noise and crosstalk on protocols and services transmitted over digital subscriber lines, is examined in this chapter. ADSL is of particular interest, since it is the most common DSL technology, but there are still open questions about its use for reliable delivery of high-bit rate services, other than simple Internet access, with different quality of service (QoS) requirements to a larger proportion of the loop plant. Moreover, the results from the analysis of ADSL could also be applied to DMT-based VDSL systems with framing similar to that in ADSL.

Simulation is a convenient approach to studying communications systems with complex structure, such as ADSL. The appropriate consolidation of ADSL, impulse noise and crosstalk models in a single simulation is described, and then the performance of ADSL according to the above aim is discussed. The performance metrics used in this study are DMT frame and ATM cell error rates and inter-error intervals (assuming that ATM cells are carried over an ADSL link), since it is frame and cell errors that are likely to impact services provided over DSL. The subjective perceived quality of MPEG2 video streamed over ADSL has also been analysed. It is shown that different framing parameter settings adversely affect the performance of ADSL in impulse noise. This performance has also been found to worsen in the presence of alien crosstalk in comparison with the case of only kindred crosstalk.

4.2 General considerations

The main objective of this simulation is to study the impact of impulse noise on protocols and applications transmitted over ADSL (Figure 4.1). There are, however, many possible data formats, various criteria to evaluate the transmission performance, and a number of parameters

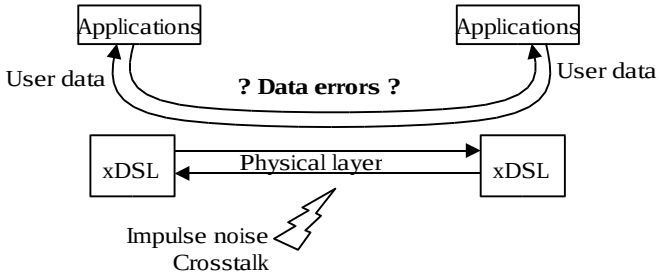

Figure 4.1: *Scope of work.*

which can influence that performance. It is therefore important to set specific simulation targets.

4.2.1 Data formats

There are numerous possible protocol stack configurations over DSL (see Section 2.4, p. 11). Several specific data types will be considered in this study.

ATM cells

Asynchronous transfer mode (ATM) is often quoted as one of the preferred protocols for transmission over DSL. Impulse noise introduces significant errors in the DSL system. ATM, however, has been primarily designed for a near error-free transmission medium. Moreover, different applications have different performance requirements towards lower protocol layers. Voice, for example, requires low latency and tolerable error rate, whereas data requires lossless transfers where errors can only be overcome by retransmission. If ATM is used as a link protocol, it is important to have information about the cell errors caused by impulse noise. Studying these errors and how they are influenced by different ADSL configurations is one of the primary targets in the presented simulations.

ADSL mux data frames

In some ADSL configurations user data may be transmitted over ADSL as a bit stream without an intermediate protocol. The performance of ADSL when carrying user information in such a mode can be evaluated by means of the ADSL mux data frame (reference point A in Figure 4.2). Therefore, this work also considers the mux data frame errors due to impulse noise.

MPEG-2 video stream

An MPEG-2 video stream has been chosen as a specific example of an application using ADSL as a transmission medium. The impact of impulse noise on the visual quality of a test video sequence carried directly over ADSL as a bit stream has been evaluated in this study.

4.2.2 Performance metrics

Due to the influence of data formatting at different layers of the protocol stack and the complex statistical nature of impulse noise, simple bit or byte error rates are insufficient to characterise fully the impact of impulse noise on protocols and services carried over ADSL.

Error rates

If ATM is used as an intermediate protocol over ADSL, cell errors are more likely to impact services carried on top as a single byte error may deem a whole cell unusable. Therefore, the ATM cell error rate has been used as one of the performance metrics in this study.

The ADSL frame error rate has also been analysed in the simulations, since frame errors are relevant to the performance of user bit streams carried over ADSL. Also, depending on the type of data they carry, entire ADSL frames may be made useless only by single or few byte errors.

Note that an ATM cell or an ADSL frame is considered damaged if at least one byte in it is errored after error correction at the receiver.

Error free seconds

The highly non-stationary nature of impulse noise has lead to the introduction of error free seconds as a performance indicator in DSL systems. An errored second is a second in which one or more errors occur [6]. Error free seconds are then defined as the time interval between two consecutive errored seconds. The one-second window, however, introduces time smearing which may mask certain peculiarities in the statistics of the error free intervals. Therefore, in this work error free seconds have been calculated between errored intervals of duration less than one second - typically several times the duration of a DMT symbol. Note that reducing the time resolution to one second is trivial. The error-free intervals between errored ATM cells

and ADSL frames have been analysed, since these are the errors of interest for services and applications.

Subjective image quality

It has long been known that objective quality measures, such as error rates or SNR, are not always a good indicator of the perceptive quality of encoded visual or audio data with low level of information redundancy. A bit-level error can cause artifacts with a different degree of visual or aural discomfort depending on the coding scheme and the data formatting. Therefore, a subjective test on the image quality of an MPEG-2 video stream has been carried out as part of this study.

4.2.3 Simulation parameters

There are several parameters which affect significantly the ADSL frame structure and its resilience to noise (see the description of the ADSL system architecture presented in Chapter 2):

- data rate required by the user, which is directly related to the size of the ADSL frames;
- strength of the Reed-Solomon FEC, i.e. the number of redundancy bytes;
- interleaving depth;
- number of ADSL mux frames per FEC codeword;
- DMT bit allocation scheme.
- impulse noise and crosstalk levels

The simulation results presented later in this chapter will evaluate the pre-defined performance criteria for the data types discussed earlier when changing one or more of the above parameters.

4.3 ADSL simulation design

This ADSL study considers only downstream transmission (from network to subscriber), which is more important from user perspective since ADSL has been designed to deliver higher bit

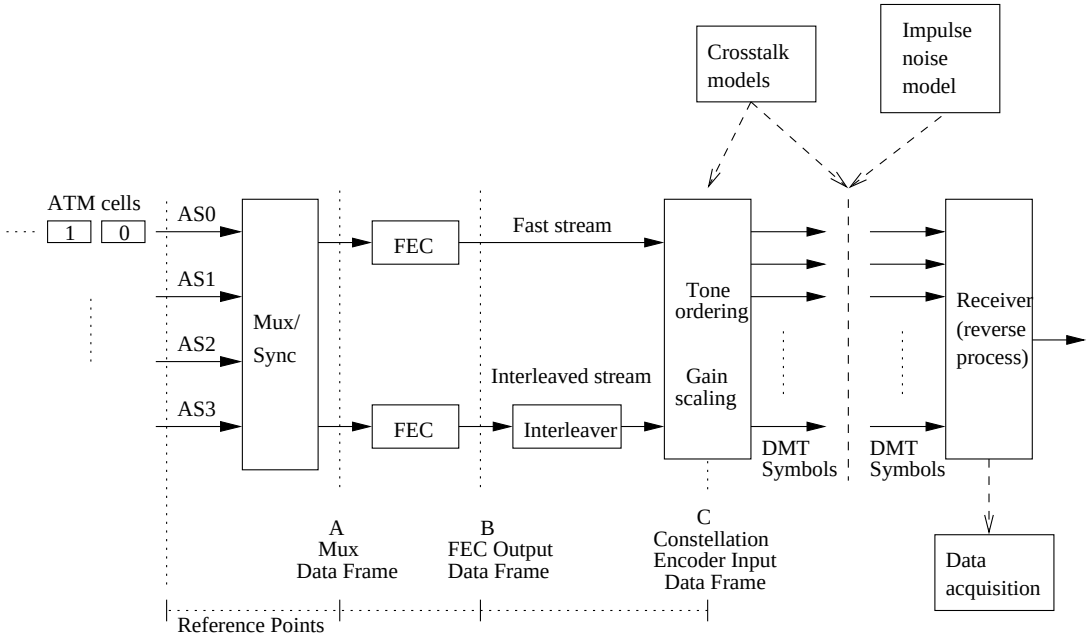

Figure 4.2: *Block diagram of ADSL downstream simulation in impulse noise and crosstalk (generic ADSL modem after [1] except signalling, CRC and scramblers).*

rates in downstream than in upstream direction. The downstream is also more susceptible to noise as it has a larger bandwidth and is placed in a higher frequency range than the upstream.

4.3.1 Simulation architecture

The structure of the ADSL downstream simulation (Figure 4.2) follows closely a generic ADSL modem (Figure 2.3, p. 15) as specified in [1, 11], with the following exceptions:

Signalling channels are not taken into account as this study is interested in the ADSL performance in stationary state, i.e. after completion of handshaking and synchronisation procedures between the transceivers at both ends of the line. Loss of synchronisation is considered unlikely.

Cyclic redundancy check (CRC) is not implemented since in the simulation both the transmitted and received messages are known and the CRC mechanism for remote error detection is unnecessary.

Scramblers are not implemented because their main function is to facilitate the receiver's digital signal processing algorithms, which are not the subject of this study and are considered to be optimal. The ADSL scramblers are self-synchronising and triple the bit errors [32]. How-

ever, the error correction and interleaving in ADSL is done at byte level, and a small error multiplication at bit level will not have a significant impact on the overall error performance of ADSL.

The number of available data channels is four (AS0-AS3) in the simulation as opposed to seven (AS0-AS3 and LS0-LS2) in the generic modem. The simultaneous usage of all seven channels specified in [1, 11] is highly unlikely in actual ADSL deployments and four channels are sufficient to exhaust numerous combinations of possible downstream bandwidth subdivisions.

Further comments

Data channels. Each of the four available data channels can be set independently at a specific bit rate and assigned either to the fast or the interleaved path. The user data can be either ATM or bit stream carrying arbitrary services.

Framing. The framing format complies fully with the specifications [1, 11] (see Section 2.5.2, p. 15), with the remark that bytes carrying data from non-implemented functions, such as signalling or CRC, have been replaced with dummy bytes.

Coding techniques. The Reed-Solomon FEC, interleaving and trellis coding have been implemented as specified in [1, 11] (See Section 2.5.3, p. 17, and Section 2.5.4, p. 19). The trellis decoder is based on the Viterbi algorithm.

Transmission line model. The characterisation of the transmission line is based on an empirical $RLCG$ model, a short description of which is provided in Section 3.3.3, p 64. Further information about $RLCG$ modelling, as well as specific values of the resistance R, inductance L, capacitance C, and conductance G per unit length of the transmission line can be found in e.g. [6, 32].

Impulse noise and crosstalk models. The latest and most accurate impulse noise and crosstalk models as described in Chapter 3 have been utilised in this simulation. The impact of impulse noise and crosstalk on data transmission is reflected in the simulation at DMT level. The symbols from the DMT subchannels are damaged with certain probability depending on the signal-to-noise ratio (SNR). The noise power needed for the SNR is in turn evaluated using the impulse noise and crosstalk models discussed in Chapter 3. Since crosstalk from digital subscriber lines is mostly time-invariant, the spectral shaping of the telephone channel due to

DSL crosstalk is taken into account in the bit loading algorithm.

Simulation data acquisition. The errors due to noise in the ADSL system are evaluated by comparing the transmitted and the received data. The statistics collected during simulation are related to ADSL mux data frame (reference point A on the receiver side, see Figure 4.2) and ATM cell errors, since these are the errors of interest.

4.3.2 Software implementation

The simulation software is based on the Matlab R12.1 software environment, which was chosen because of its high functionality and flexibility. The Matlab Signal Processing and Communications toolboxes are also required in order to run the simulation. Most simulation routines have been written in the Matlab programming language. However, several functions which are executed excessively slowly by the native Matlab interpreter have been implemented in C and compiled as Matlab executable files. These involve mainly functions performing intensive bit level computations, such as tone ordering or Reed-Solomon coding/decoding. The Matlab interpreter has not been optimised for bit operations, and implementing those in C leads to a significant reduction in the simulation time. However, the C routines require a considerable amount of additional code to interface the Matlab interpreter. Note also that the C code should be compiled into Matlab executables specifically for each hardware platform and operating system. The simulation software has been tested successfully on Ultra-Sparc Sun Solaris 5.8 and PC Redhat Linux 7.0.

4.3.3 Loading algorithm

The bit and energy allocation scheme in DMT modulation has a direct impact on the error rate of the transmitted data. In this simulation, the bit loading aims for a minimum error rate at a defined data rate (for background see Section 2.5.4, p. 21). A very efficient, albeit suboptimal loading algorithm was proposed in [44] by Chow, Cioffi, and Bingham. The algorithm's suboptimality only makes the bit allocation more realistic, since in actual ADSL deployments bit loading is usually not optimal anyway due to imperfect channel knowledge and varying conditions. The algorithm presented in [44] has been chosen as the basis on which a new, dedicated ADSL loading algorithm has been developed.

Basic loading algorithm

In this section, the bit loading algorithm proposed by Chow, Cioffi, and Bingham is described in some detail, since it forms the basis of an ADSL loading algorithm to be discussed later. A complete description is to be found in [6, 44].

The algorithm consists of three main stages. Firstly, in steps 1 to 7 it tries to find the optimal system performance margin γ_m. If the algorithm does not converge after $MaxCount$ number of iterations, then a suboptimal loop is executed in steps 8 and 9 to guarantee convergence. Finally, the energy distribution is adjusted for each subchannel in steps 10 and 11 to assure equal and optimal system performance margin over all used subchannels at the specified bit error rate (BER). The distinct steps of this process are described below.

1. Compute the signal-to-noise ratio for each subchannel, $SNR(i),\ \forall i$, assuming that all subchannels have a normalised energy level $\mathcal{E}(i) = 1,\ \forall i$.

2. Let the current system performance margin $\gamma_m = 0(dB)$, the iteration count $Iteration = 0$, and the number of used carriers $UsedCarriers = N_{total}$, i.e. the maximum number of available subchannels.

3. For $i = 1$ to N, calculate the number of bits $b(i)$, the rounded number of bits $\hat{b}(i)$, the bit difference $diff(i)$, and $UsedCarriers$ as follows:

$$b(i) = \log_2\left(1 + \frac{SNR(i)}{\Gamma + \gamma_m(dB)}\right), \tag{4.1}$$

$$\hat{b}(i) = round[b(i)], \tag{4.2}$$

$$diff(i) = b(i) - \hat{b}(i), \tag{4.3}$$

$$\text{If } \hat{b}(i) = 0,\ UsedCarriers = UsedCarriers - 1, \tag{4.4}$$

   where Γ in Equation 4.1 is the SNR gap (see Section 2.5.4, p. 21). For an uncoded, zero-margin system with a BER of 10^{-7}, $\Gamma \approx 9.8$ dB.

4. Let the total number of used bits $b_{total} = \sum_{i=1}^{N} \hat{b}(i)$. If $b_{total} = 0$, stop and declare bad channel.

5. Compute a new system performance margin γ_m using:

$$\gamma_m = \gamma_m + 10\log_{10}(2^{\frac{b_{total} - b_{target}}{UsedCarriers}}), \tag{4.5}$$

where b_{target} is the desired number of bits per DMT symbol.

6. Let $Iteration = Iteration + 1$.

7. If $b_{total} \neq b_{target}$ and $Iteration < MaxCount$, let $UsedCarriers = N_{used}$ and go back to step 3, else continue to step 8.

8. If $b_{total} > b_{target}$, then subtract one bit at a time from $\hat{b}(i)$ on the carrier that has the smallest $diff(i)$, adjust $diff(i)$ for that particular carrier, and repeat until $b_{total} = b_{target}$.

9. If $b_{total} < b_{target}$, then add one bit at a time to $\hat{b}(i)$ on the carrier that has the largest $diff(i)$, adjust $diff(i)$ for that particular carrier, and repeat until $b_{total} = b_{target}$.

10. Adjust the input energy so that the error probability for each subchannel $P_s(i), \forall i$ equals the target error probability $P_{s,target}$, given the bit allocation $\hat{b}(i)$.

11. Scale the final energy for all used carriers with a common scaling factor so that the total energy $\mathcal{E}_{total}$ equals the target energy $\mathcal{E}_{target}$.

The number of iterations needed for the algorithm to converge in actual system implementations was found to be [44] no more than 10.

ADSL bit loading requirements

The basic loading algorithm described in the previous section does not take into account two important ADSL requirements [1, 11]:

- The number of coded bits per carrier can be between 2 and 15. Single-bit constellations are not allowed in ADSL since they can be replaced by 2-bit constellations with the same average energy. Therefore an additional restriction on the number of bits per tone has to be included in the basic algorithm.

- If trellis coding is implemented (see Section 2.5.4, p. 20), there is a constellation expansion of 1 bit per four dimensions plus four extra bits to force the encoder back to zero. The number of required extra bits depends on the number of used carriers and therefore cannot be predefined at the start of the algorithm, but has to be set adaptively during algorithm execution.

The straightforward implementation of both these requirements can lead to instability, as their combination causes algorithm oscillation and even divergence from the targets in many realistic scenarios. A novel modification of the algorithm has been developed to allow for convergence while fulfilling both loading requirements simultaneously.

Modified loading algorithm

The basic loading algorithm has been modified in three main areas. Firstly, the target bit rate b_{target} is recalculated at each iteration to reflect the changing number of trellis redundancy bits and the single-bit constellations. Secondly, the maximum number of bits is restricted to a maximum of 15 bits. And finally, after the algorithm converges the subchannels with single-bit constellations are declared as unused, i.e. loaded with 0 bits. These modifications can be summarised as follows:

- The target number of bits b_{target} is calculated for each iteration of the basic algorithm at steps 5, 8, and 9 according to the expression:

$$b_{target} = b_{DSLframe} + b_{trellis} + b_{bias}, \tag{4.6}$$

  where $b_{DSLframe}$ is the number of bits in the DSL frame originally supplied to the tone ordering for transmission. The additional terms $b_{trellis}$ and b_{bias} are respectively the number of required trellis redundancy bits, and the number of bits in single-bit constellations, and can be calculated from:

$$\begin{aligned} b_{trellis} &= \begin{cases} round\left(\frac{1}{2}\sum_i 1\right) + 4, \ \forall i \text{ such that } \hat{b}(i) \geq 2, & \text{if trellis coding is on} \\ 0, & \text{if trellis coding is off} \end{cases} \\ b_{bias} &= \sum_i 1, \ \forall i \text{ such that } \hat{b}(i) = 1, \end{aligned}$$

- Step no. 9 changes to: Restrict the maximum number of bits in a constellation to 15. If $b_{total} < b_{target}$, then add one bit at a time to $\hat{b}(i)$ on the carrier with the largest $diff(i)$ that has less than 15 bits, adjust $diff(i)$ for that particular carrier, and repeat until $b_{total} = b_{target}$.

- A new step 9a is introduced between steps 9 and 10 to set to zero bits the single-bit constellations, i.e. let $\hat{b}(i) = 0, \forall i$, such that $\hat{b}(i) = 1$.

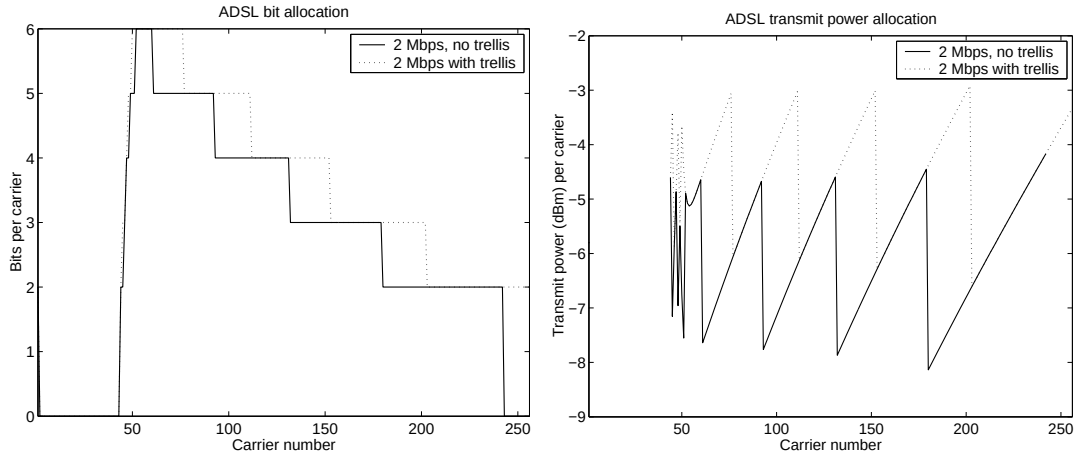

(a) Bit allocation

(b) Transmit power allocation

Figure 4.3: *Bit and transmit power allocation in ADSL with crosstalk from 49 ADSL disturbers over a 4 km loop with 0.4 mm wires.*

Since b_{target} has been biased by b_{bias}, the removal of the bits from single-bit constellations will leave the total number of bits exactly equal to $b_{DSLframe} + b_{trellis}$, using only constellations of 2 bits or more, but up to a maximum of 15, which was the ultimate goal.

Algorithm application

While no study of the general conditions for algorithm convergence will be presented here, extensive testing by simulation showed that the modified algorithm is stable and converges for all cases of practical interest. Note also that because of the variations in b_{target} at each iteration, the modified algorithm converges at a comparable, if slightly slower rate than the basic algorithm.

Figure 4.3 shows an example of bit and transmit power allocation in ADSL with and without trellis coding for 2 Mbps user data and 16 RS bytes over a 4 km line with 0.4 mm wires in the presence of crosstalk from 49 ADSL disturbers in a 50-pair bundle.

ADSL crosstalk. The carriers in the lower frequency spectrum are not loaded because of the high level of NEXT interference from the ADSL upstream at low frequencies (see Figure 3.20, p. 66). At higher frequencies (above approximately 400 kHz in this particular example), FEXT from the ADSL downstream dominates and exerts a larger influence on bit allocation than

NEXT.

Trellis coding. The constellation expansion carried out by the trellis coding increases significantly the required number of bits in the DMT symbol (in this example from 672 to 783 bits). Due to the high level of NEXT at low frequencies, the algorithm tends to load the extra bits in higher-frequency carriers, which has implications about the error probability in these subchannels.

Transmit power. The transmit power allocation is saw-tooth shaped with a peak-to-peak span of approximately 3 dB due to the integer bit constellation constraint. If trellis coding is activated, the allocated power is generally higher than in the case of no trellis coding. In this way the larger trellis-coded constellations achieve the same bit error rate as the non-trellis coded ones. Note also that the transmit power can be scaled upwards as long as it complies with the total energy or the power spectral mask requirements. Here this has not been done to allow for comparison between the trellis and non-trellis case.

4.3.4 Error probability at the physical layer

In order to analyse the errors at higher protocol levels, it is essential to have an appropriate estimate of the symbol errors at the physical layer of the ADSL system. Therefore, the symbol error probability will be discussed in detail in this section.

Exact expression for symbol error probability

As mentioned earlier (see Section 2.5.4, p. 19), each DMT subchannel uses quadrature amplitude modulation (QAM). The ADSL standard [1, 11] specifies that M-ary QAM constellations with an even number of bits b are rectangular, i.e. their $M = 2^b$ points fall on a rectangular grid. Such constellations are equivalent to two PAM signals on quadrature carriers, each having $\sqrt{M} = 2^{b/2}$ signal points. Therefore, the probability of a symbol error for the M-ary QAM system is [125]:

$$P_M = 1 - \left(1 - P_{\sqrt{M}}\right)^2, \tag{4.7}$$

where $P_{\sqrt{M}}$ is the probability of error of a $\sqrt{M}$-ary PAM with half the average power of the equivalent QAM system in each quadrature signal. $P_{\sqrt{M}}$ can be calculated from [125]:

$$P_{\sqrt{M}} = 2\left(1 - \frac{1}{\sqrt{M}}\right) \mathcal{Q}\left(\sqrt{\frac{3}{M-1}\frac{\mathcal{E}_{av}}{\sigma^2}}\right), \tag{4.8}$$

where $\mathcal{E}_{av}$ is the average symbol energy, σ^2 is the noise power, and $\mathcal{Q}(x)$ is the $\mathcal{Q}$-function defined in Equation 2.5, p. 21.

Upper bound of the symbol error probability

The result for symbol error probability in Equation 4.7 is exact only for an even number of bits b per constellation. If b is odd, there is no equivalent $\sqrt{M}$-ary PAM system. It can be shown, however, that the symbol error probability has a tight upper bound defined as [125]:

$$P_M \leq 4\mathcal{Q}\left(\sqrt{\frac{3}{M-1}\frac{\mathcal{E}_{av}}{\sigma^2}}\right). \tag{4.9}$$

While some authors argue that the upper bound is an acceptable approximation for any $b \geq 1$ [125], others claim that constellations with $b \leq 4$ must be treated separately if higher precision is required [32].

Comments

Figure 4.4 shows a comparison between the symbol error probability estimates calculated using the exact expression (4.7) and the upper bound (4.9) for two different sizes of the symbol constellation: $M = 4 \leftrightarrow b = 2$ and $M = 64 \leftrightarrow b = 6$. The signal-to-noise ratio per symbol is defined as SNR $= \mathcal{E}_{av}/\sigma^2$.

It can be seen that for low SNR the upper bound approximation yields overly pessimistic estimates of the symbol error probability, that numerically may even exceed the value 1. The low precision at low SNR is a significant drawback of the upper bound approximation when evaluating the impact of impulse noise, since the noise impulses are characterised with high energy levels and the SNR of symbols affected by impulse noise is typically very low. Therefore the exact expression (4.7) will be used in this study for both even and odd b, and the symbol error probability calculated in this way has been represented graphically in Figure 4.5.

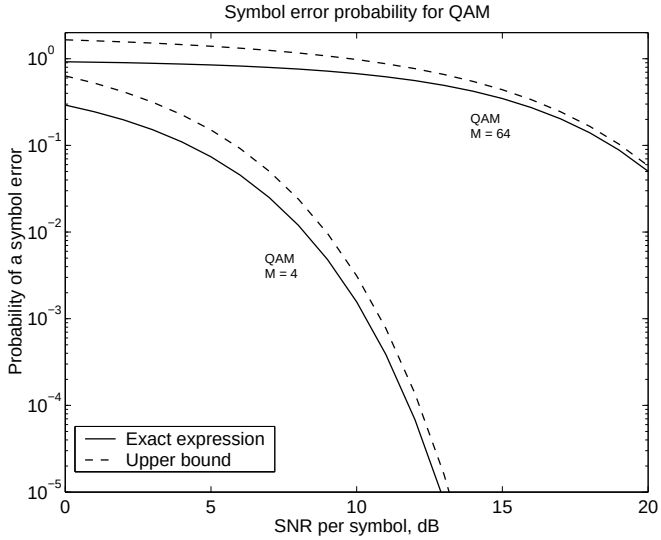

Figure 4.4: *Comparison between exact expression (4.7) and upper bound (4.9) of the probability of a symbol error for QAM.*

It will be assumed in this study that if a QAM symbol is deemed corrupt after evaluation of the error probability, all bits in this symbol are damaged. Such an approach is acceptable [32] because the RS coding in ADSL is byte-organised, and symbol errors containing a few bit errors are corrected with the same efficiency as single bit errors.

4.3.5 Default physical layer parameters

Unless specified otherwise, the following physical layer characteristics are assumed in the ADSL simulations presented in subsequent sections:

Telephone line. A twisted pair with 0.4 mm wires and 4 km length is considered in this study. The values of the relevant physical parameters, needed to calculate the line transfer function as described in Section 3.3.3, p. 64, can be found in e.g. [6].

Impulse noise. The impulse noise model used in this simulation (see Section 3.2, p. 32) requires numerous parameters characterising statistically the impulse amplitudes and spectral contents, impulse duration, and impulse inter-arrival times. The main references for specific parameter values are [3] and [5]. Note that the inter-arrival times will be modelled with a four-state Markov renewal model, since it characterises the whole range of inter-arrival times and provides a better accuracy than the two-state model. The latter has been defined to facilitate testing and crude simulation of xDSL systems and only accounts for the shortest (< 1 s) inter-arrival times.

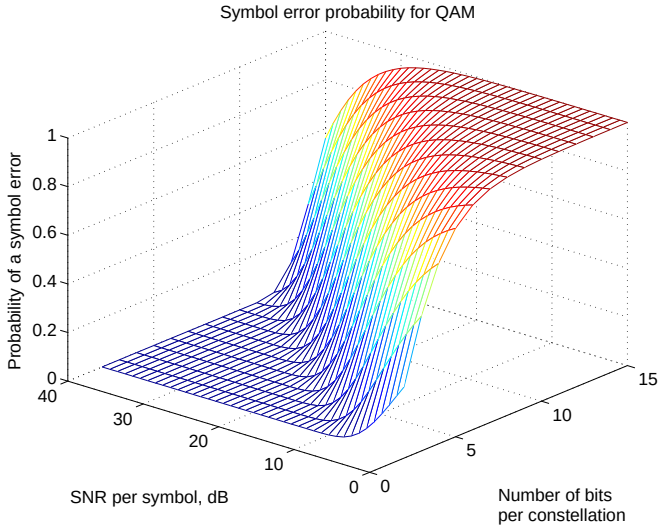

Figure 4.5: *Probability of a symbol error for QAM as a function of the SNR per symbol and the number of bits per constellation.*

Crosstalk. The simulated line is assumed to be subjected to crosstalk from 49 ADSL disturbers, i.e. is placed in a 50-pair binder where all lines carry ADSL. The relevant crosstalk power spectral density can be calculated as described in Section 3.3, p. 59. Other crosstalk configurations will be specified and considered later in Section 4.7.

4.4 ADSL frame and ATM cell error probability

This section presents the results of simulation of an ATM over ADSL system in the presence of impulse noise and crosstalk for different bit rates and interleaving depths, and with $R = 16$ RS redundancy bytes per codeword. The performance metrics used are ATM cell/header/payload error rate and ADSL frame error rate. Note that an ADSL mux frame carries a different number of ATM cells depending on the user data rate. For example, at 2 Mbps an ADSL mux frame contains 64 bytes or approximately 1.2 ATM cells of 53 bytes each, at 4 Mbps - 128 bytes or 2.4 cells, and at 6 Mbps - 192 bytes or 3.6 cells on average.

4.4.1 Impact of interleaving

Figure 4.6 shows the mux frame and ATM cell error probability as a function of the interleaving depth for different data rates. The frame and ATM cell error rates increase initially with the rise of the interleaving depth. This behaviour is due to the fact that as a result of the interleaving

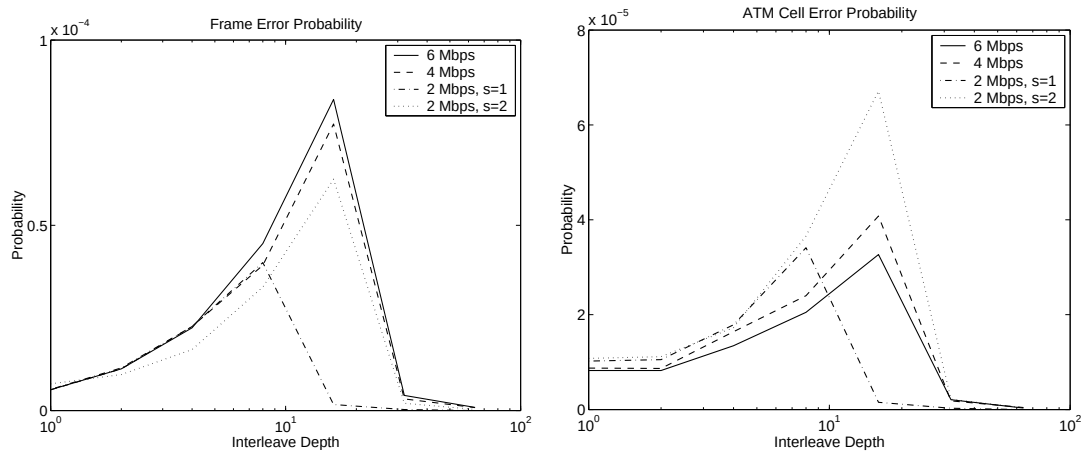

(a) Mux data frame error rate

(b) ATM cell error rate

Figure 4.6: *Mux data frame and ATM cell error probability, for R=16 RS bytes.*

errors are spread over more than one FEC codewords. If the error spreading is insufficient, the number of errors in a codeword is still larger than the error correction capabilities of the code. Therefore error correction is impossible to perform. However, the errors have been spread over multiple codewords and as a result they affect more frames and cells. Above a "cut-off" value of the interleaving depth, the error spreading is sufficient to allow for the FEC code to correct the errors. As a consequence the frame and cell error rates fall abruptly. Similar results for the impact of the interleaving depth, but on the TCP/IP over ATM over ADSL end-to-end performance, have been reported in [126].

It is clear that interleaving makes sense only for depths large enough for the error correction code to cope. Intermediate values of the interleaving depth only worsen the mux frame and ATM cell error rates. Therefore services requiring low latency, such as voice or video-conferencing, should use no interleaving, whereas for services tolerant to some delay, e.g. video on demand, it will be feasible to use large interleaving depths. This conclusion has been summarised graphically in Figure 4.7.

4.4.2 DSL frame vs. ATM cell error rates

Performance in terms of ATM cells differs from that of DSL multiplexed data frames (after deinterleaving if applicable and FEC). At the considered bit data rates (2 Mbps to 6 Mbps)

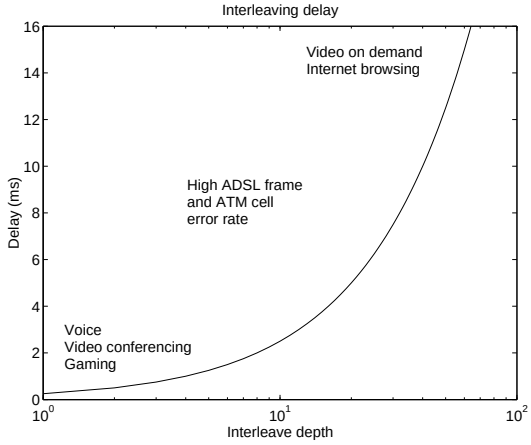

Figure 4.7: *Delay due to interleaving in ADSL systems.*

DSL mux frames are larger and there is a higher probability that they will be damaged than ATM cells. If the performance of a DSL system is evaluated solely on the basis of errored DSL mux frames, the performance estimation will be inaccurate and pessimistic.

Note also that for interleaving depths below the cut-off value, higher bit rates exhibit better cell error performance than lower bit rates. The opposite is true for ADSL mux frames, i.e. higher bit rates have a worse frame error probability. The higher the bit rate, the more ATM cells there are in an ADSL frame, and the more likely it is that whole cells from the ATM stream will remain undamaged, especially if there is interleaving.

4.4.3 ATM cell header and payload error rates

Due to the smaller size of the ATM headers their error probability is lower than the ATM payload error probability for equal framing parameters (Figure 4.8). Moreover, errors in headers are much less affected by changes in the interleaving depth than the payload. At the critical interleaving depth (with largest cell error rates) the discrepancy between header and payload error rates is largest. If a header is errored the ATM cell is discarded. A significant proportion of the cells, however, have valid headers but damaged payloads. Therefore, the ATM error detection mechanism cannot be relied upon to identify unerrored cells. Most protocols both at lower and at higher layers have their own mechanisms for error detection and/or correction in order to avoid protocol and application confusions due to undiscovered errors. At lower layers, ADSL itself has an error detection mechanism for the mux data frames. It applies, however, to the entire ADSL frame and in this way “good” ATM cells may be discarded alongside dam-

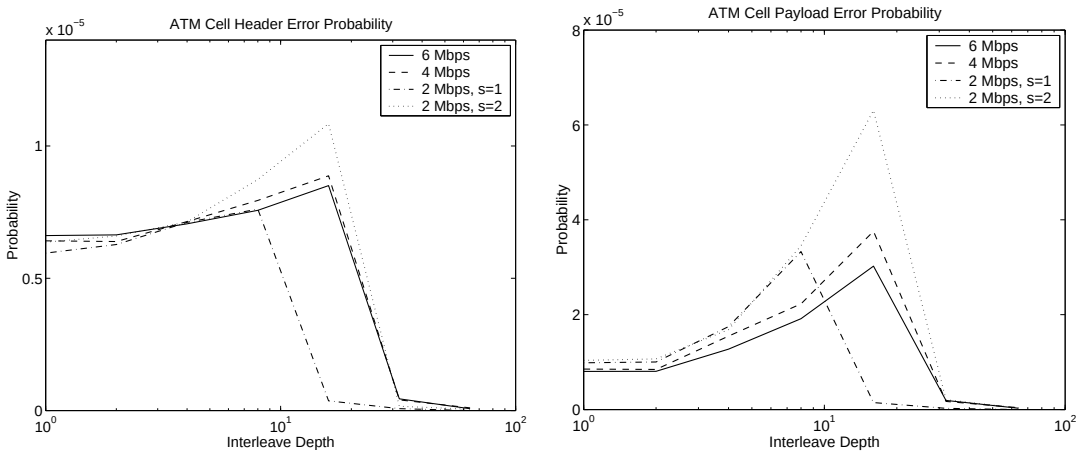

(a) ATM header error rate

(b) ATM payload error rate

Figure 4.8: *ATM header and payload error probability for R=16 RS bytes.*

aged ones. Similarly, the ATM adaptation layers (AAL) also have error detection mechanisms. However, again the contents of several ATM cells may be combined into one error detection codeword, such as in the case of AAL5. Therefore, an appropriate higher level protocol stack must be selected if such isolated unerrored cells are to be detected and used.

It should be pointed out that these results are for inter-cell interleaving. Some studies (see e.g. [127]) suggest that intra-cell interleaving may outperform substantially inter-cell interleaving in burst error environments. However, an intra-cell interleaving scheme is not allowed by the ADSL standards.

4.4.4 Impact of the strength of the Reed-Solomon code

The results in Figures 4.6 and 4.8 for 2 Mbps with one and two mux frames per RS codeword ($s = 1$ and $s = 2$) allow for comparison between different strengths of the error correction code, i.e. 16 as opposed to 8 FEC bytes per mux frame respectively. Both at cell and at frame level, the better error protection leads to lower ”cut-off” interleaving depth. There is therefore a scope to reduce the latency for applications that use interleaving by increasing the strength of the error protection.

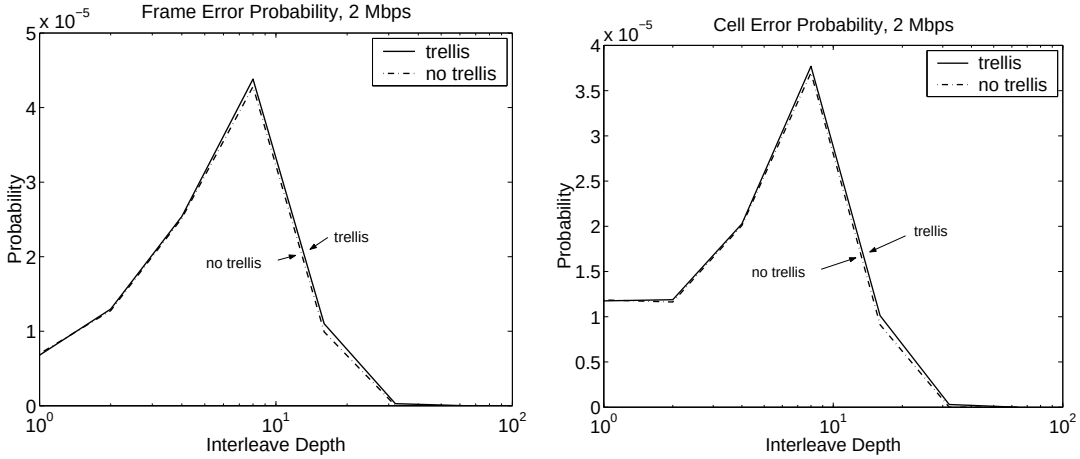

(a) ADSL frame error rate

(b) ATM cell error rate

Figure 4.9: *ADSL frame and ATM cell error rates for 2 Mbps interleaved channel with or without trellis coding.*

4.4.5 Impact of trellis coding

As can be seen in Figure 4.9, the error rates due to impulse noise of both ADSL frames and ATM cells remain virtually unchanged regardless of whether trellis coding has been used. This can be explained by the fact that the trellis encoding/decoding in ADSL is carried out across the subcarriers within one DMT symbol[1]. The use of trellis codes is based on the assumption that the noise is close to white, i.e. that the noise samples are uncorrelated from one subcarrier to the next [42]. Impulse events, however, damage bits in a significant number of the subcarriers in the DMT symbol, which is equivalent to a long burst of errors at the input of the trellis decoder. As a result the decoder is unable to correct the errors and may even cause error multiplication. The latter explains why the error rate is even slightly higher at high interleaving depths when trellis coding is used. The error spreading caused by interleaving is enhanced by error multiplication due to incorrect trellis decoding, which causes the overall error to exceed occasionally the correction capabilities of the Reed-Solomon code.

Note that in order to ensure fairness in the comparison between the non-trellis and trellis-coded case, in this particular simulation, only the four least significant, (potentially) trellis-coded bits

[1]The trellis coding in ADSL would be much more efficient against impulse noise if each subcarrier were coded separately over multiple DMT symbols. However, such a system would have a prohibitively high complexity and latency [40], and therefore the scheme proposed in [42] has been used for ADSL.

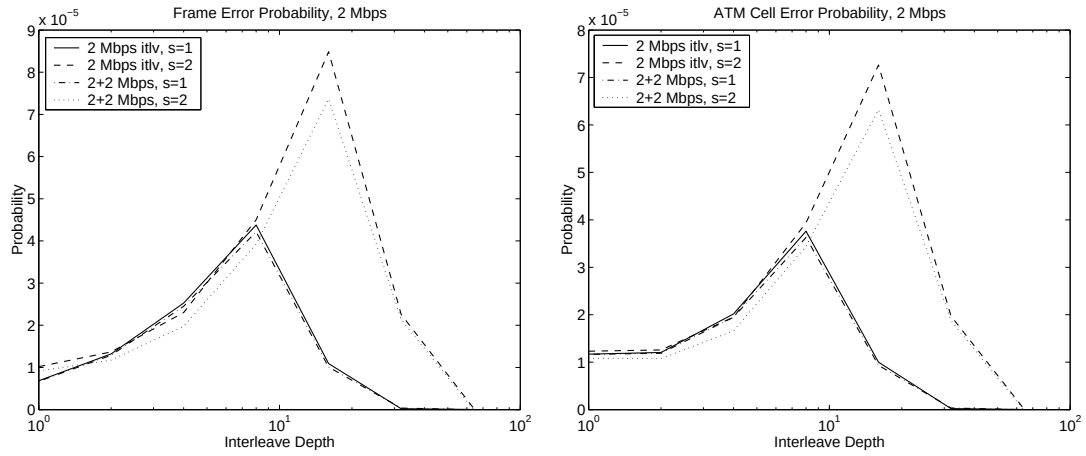

(a) ADSL frame error rate

(b) ATM cell error rate

Figure 4.10: *ADSL frame and ATM cell error rates for 2 Mbps interleaved channel, transmitted alone or alongside a 2 Mbps fast channel.*

have been corrupted if the respective constellation has been deemed damaged with a certain probability. Note also that all other simulation results in this chapter have been produced without trellis coding.

4.4.6 Dual latency mode

The ADSL standards allow for dual latency operation, i.e. simultaneous use of the fast and interleaved channels [1, 11]. Figure 4.10 shows a comparison between the ADSL frame and ATM cell error rates for a single latency 2 Mbps interleaved channel, and a 2 Mbps interleaved channel transmitted together with a 2 Mbps fast channel in an aggregate 4 Mbps dual latency configuration. It is interesting to note that both the ADSL frame and the cell error rates are slightly higher in the single than in the dual latency mode for equal channel data rate and strength of error protection. The small difference in the error rates can be traced back to the way the loading algorithm assigns energy to the subchannels. In comparison with the single latency mode, the dual latency mode in this particular simulation has a higher overall bit rate (4 Mbps), hence the number of bits that need to be loaded onto the DMT symbol is higher, and therefore the constellation size in each subchannel increases. In order to ensure the same symbol error rate at the required system performance margin (see Section 2.5.4, p. 21), the loading algorithm raises the transmit energy assigned to each subchannel. The impulse noise

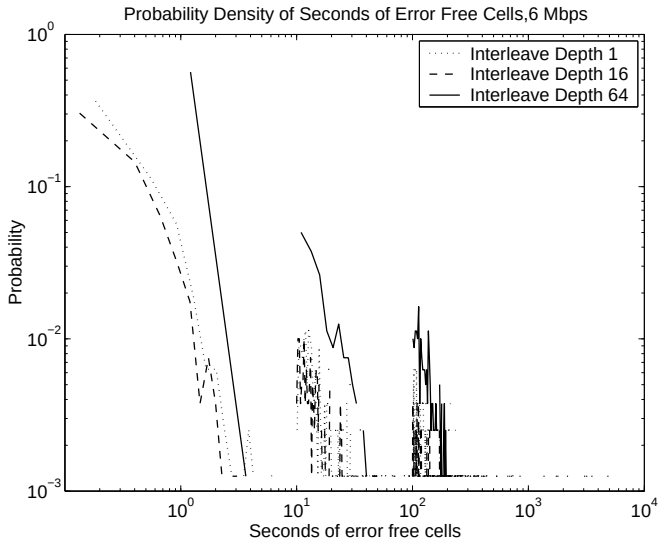

Figure 4.11: *Seconds of error free cells for user data rate 6 Mbps at various interleaving depths (minimum 5 unerrored cells).*

energy, however, remains with the same statistical characteristics and therefore the symbol error rate, and hence the ADSL frame and ATM cell error rates, decrease slightly. The effect is more visible if there is interleaving because the lower error rate at bit level allows for more frames to be corrected by the Reed-Solomon code after deinterleaving.

4.5 Error free intervals

Similarly to the previous section, the results presented here are based on simulation of an ATM over ADSL system in the presence of impulse noise and crosstalk for different bit rates and interleaving depths, and with $R = 16$ RS redundancy bytes per codeword. The performance metric used is statistics of inter-arrival times between errored cells and frames.

4.5.1 Seconds of error free cells

The probability densities of error free seconds for ATM cells for various interleaving depths are shown in Figure 4.11. The distribution of error free seconds for interleaving depth 16 does not differ significantly from that when there is no interleaving (interleaving depth 1). This is due to the fact that at interleaving depth 16, the error spreading is insufficient to allow for error correction, and the shortening of inter-error times in comparison with the non-interleaved case

due to error multiplication is insignificant. Interleaving depth 64, however, is above the "cut-off" interleave depth value, the error correction removes a large proportion of the errors and the graph shifts towards higher probability for larger number of error free cells. That is, the distribution of the seconds of error free cells depends on the RS codeword error correction rate, rather than on the cell error rate.

It is interesting to note that the clustering which is characteristic for impulse noise inter-arrival times, is also reflected in the distribution of inter-error intervals (compare Figure 4.11 to Figure 3.14 on p. 57). Note also that although the shape of that distribution may change because of error correction, clustering remains as a characteristic.

4.5.2 Seconds vs. number of error free cells

The statistics of error free seconds do not change significantly with various user data rates (Figure 4.12(a)) even though the mux frames carry a different number of ATM cells depending on the bit rate. The explanation for this is that if an impulse damages a mux frame, the errors would occur in the same temporal position in the stream of ATM cells regardless of the cell rate, therefore the distribution of intervals between cell errors would also be invariant.

This is not so, however, if the distribution of the number of error free cells is considered. This distribution depends on the data rate (Figure 4.12(b)), since for different bit rates one unit of time contains a different number of cells (Figure 4.12(c)). At higher data rates the distribution shifts towards larger number of consecutive error free cells.

The metric error free seconds is very much preferred in the DSL world. Higher protocol levels, however, are mostly interested in the error performance in terms of data units such as ATM cells, IP packets, or payload bits. It was shown above that the inter-error statistics due to impulse noise are different for number of unerrored cells and seconds of unerrored cells. Therefore, the error free data blocks may be a more representative metric of the system performance from the point of view of higher protocol layers than the error free seconds.

4.5.3 Minimum acceptable number of unerrored cells

Because of interleaving and the resulting error spreading, and especially at large interleaving depths, one impulse event may damage *non*-consecutive ATM cells, between which there is a

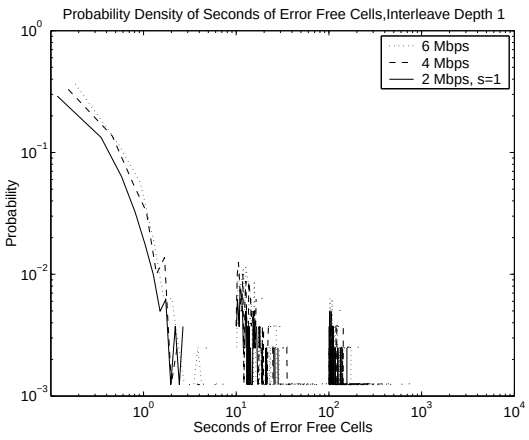

(a) Seconds of error free cells

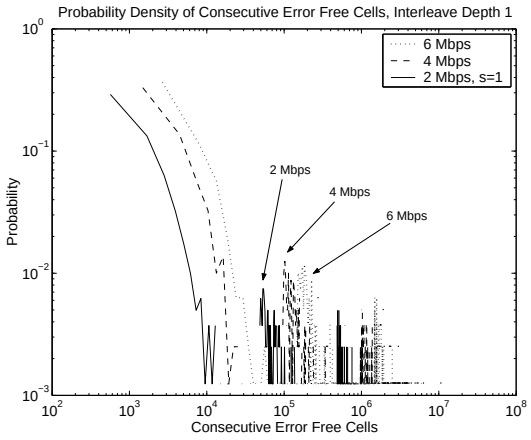

(b) Number of error free cells

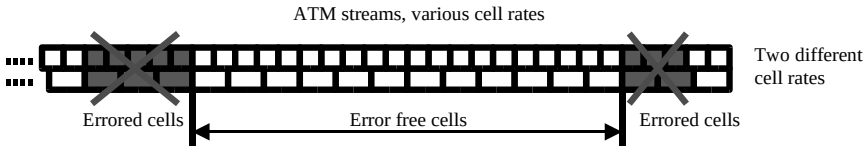

(c) Intervals between errored cells at different bit rates

Figure 4.12: *Seconds of error free cells vs. number of error free cells (minimum 5 unerrored cells).*

certain number of unerrored cells (Figure 4.13(b)).

It is up to the application running over ATM to utilise such unerrored cells. It is very unlikely that an IP packet can make use of them because it usually comprises the payload of several ATM cells. Other applications, however, such as voice based on AAL2, can benefit from such isolated unerrored cells. The statistics of seconds of error free cells change depending on the minimum acceptable number of unerrored cells. If this number is small, most error free periods concentrate around smaller values and the distribution at higher error free intervals is shifted downwards (Figure 4.13(a)).

Note that the error free seconds in Figures 4.11 and 4.12 are derived for a minimum acceptable number of five unerrored cells. This relatively large number has been chosen for the purpose of comparison and clearer analysis. For the given DSL framing and ATM cell size, any smaller minimum number of unerrored cells will lead to excessive change in the shape of the distribu-

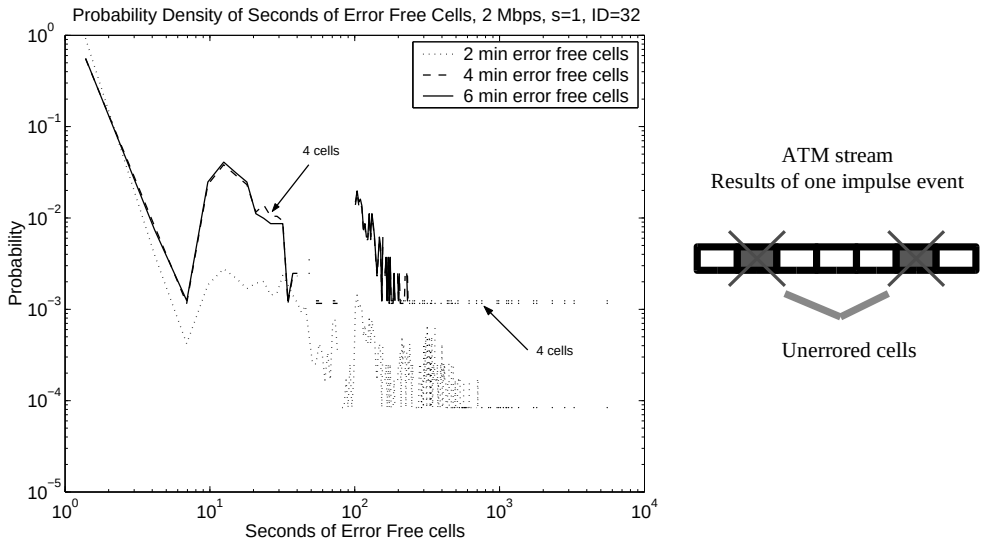

Figure 4.13: *Seconds of error free cells with different minimum number of unerrored cells.*

tions and will cover to some extent the impact of changes in other parameters.

4.6 Comparison between interleaving and multiple frames in RS codeword

Impulse noise is the primary cause of burst errors in xDSL transmission systems. Interleaving and coding several DMT symbols[2] into a single Reed-Solomon FEC codeword are two framing techniques in ADSL which can potentially mitigate the impact of burst errors. These techniques, however, increase the latency in the transmission tract. Moreover, their practical implementation requires additional hardware and software. Therefore the benefits of using them must be carefully evaluated. A comparison between these burst error mitigation techniques from the point of view of higher layers has been presented in this section. ADSL mux frame error rates and ATM cell error rates have been used as performance metrics.

[2]Although strictly speaking a DMT symbol is different from its corresponding ADSL mux frame, these two terms are widely used as interchangeable due to the straightforward mapping between the user data they refer to.

Bit rate	**Symbols per FEC codeword**				
	1	2	4	8	16
0.25 Mbps	o.k.	o.k.	o.k.	o.k.	o.k.
0.5 Mbps	o.k.	o.k.	o.k.	o.k.	n.a.
1 Mbps	o.k.	o.k.	o.k.	n.a.	n.a.
2 Mbps	o.k.	o.k.	n.a.	n.a.	n.a.
4 Mbps	o.k.	n.a.	n.a.	n.a.	n.a.
6 Mbps	o.k.	n.a.	n.a.	n.a.	n.a.

n.a. = not applicable

Table 4.1: *Possible number of DMT symbols in a single RS codeword in ADSL depending on the bit rate in the interleaved channel.*

4.6.1 Framing restrictions

The Forward Error Correction (FEC) utilised in ADSL is Reed-Solomon in Galois field GF(2^8) and therefore the maximum codeword size is 255 bytes (see Section 2.5.3, p. 17). The restriction on the codeword size limits the number of ADSL symbols that can be included in a single codeword depending on the bit rate and the number of redundancy bytes in the interleaved channel (Table 4.1). For large bit rates (4 and 6 Mbps) it is impossible to include multiple symbols in a FEC codeword. Up to 16 DMT symbols per FEC word are allowed in the interleaved channel of ADSL [1]. Also, up to 16 parity bytes are standardised for each channel (fast or interleaved).

4.6.2 Interleaving vs. multiple symbols per FEC codeword

The results presented in Figure 4.14 allow for comparison between interleaving and multiple symbols per FEC codeword. The two techniques have been compared for identical strengths of the error correction code, i.e. identical ratios between payload and redundancy bytes regardless of the number of symbols per codeword. That is, if the number of symbols per codeword increases, the number of redundancy bytes per codeword also rises accordingly.

The following notations have been used. Itlv is the interleaving depth (in the interleaving case), S is the number of DMT symbols per FEC frame (in the multiple symbols case), R is the number of parity bytes in a codeword, and R_{symb} is the number of parity bytes per DMT symbol.

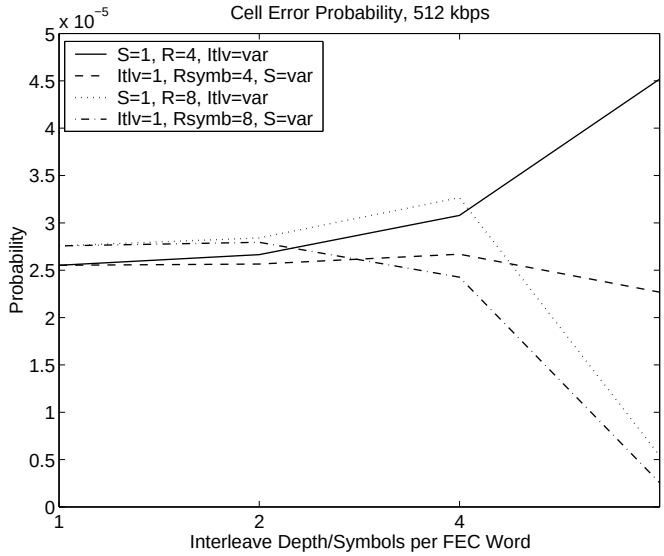

(a) ATM cell error probability

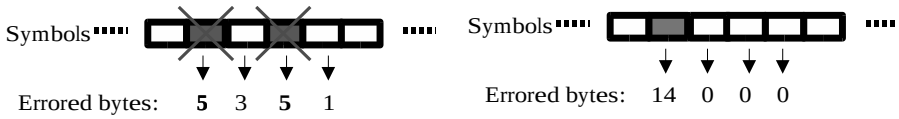

(b) Interleaving **(c)** Multiple symbols per FEC word

Figure 4.14: *Interleaving vs. multiple DMT symbols per codeword.*

ATM cell error rates as a function of interleaving

As the interleaving depth rises, the ATM cell error rate also increases (Figure 4.14(a), graphs for Itlv$= var$). If the interleaving depth exceeds a certain cut-off value, however, the cell error rate drops. The mechanism of this phenomenon was discussed in detail in Section 4.4.1. The error spreading over several symbols due to interleaving and the potentially non-uniform distribution of the number of errored bytes per symbol have been summarised graphically in Figure 4.14(b).

ATM cell error rates as a function of the number of symbols per FEC codeword

The ATM cell error rate remains almost flat initially as the number of symbols in a codeword increases (Figure 4.14(a), graphs for S $= var$). After a certain cut-off value in the number of symbols per codeword, the cell error rate decreases. This effect can be explained in the fol-

lowing way. At a low number of symbols in a FEC word, even one heavily corrupted symbol is sufficient for the whole codeword to be damaged beyond the error correction capabilities of the code. However, the errors remain clustered in the data stream as there is no error spreading (Figure 4.14(c)). Therefore the byte errors affect roughly the same number of packets (ATM cells), even as the size of the codeword increases. Above a certain cut-off value for the number of symbols per codeword, the cell error probability falls. This is due to the fact that the codeword becomes large enough and only a small proportion of the bytes within a codeword are errored. Note that 97% of the noise impulses are of a length such that they do not affect more than two DMT symbols [3]. The FEC code can then correct the errors caused by impulse noise and the cell error rate drops.

The cell error probability as a function of the number of symbols per codeword increases slightly in the initial "flat" region of the graph (Figure 4.14, graphs for S $= var$ with four redundancy bytes per symbol - $R_{symb} = 4$). The explanation for this effect is the following. If the size of the codeword is small (e.g. it contains two symbols), there is a more frequent switching between user data and redundancy bytes. Therefore it is more probable that the error bursts will span both user and redundancy bytes. If an error burst is not correctable, it is more likely that both the user data and the redundancy bytes will be affected. However, from the point of view of the higher-level protocol (in this case ATM), only the user data error rate matters. Therefore we observe a lower cell error rate. For larger number of symbols in a codeword, the redundancy bytes are concentrated at the end of the codeword. It is then less likely that an error burst would span over both user data and redundancy bytes. In this case impulse noise tends to affect longer sequences of user data bytes. As a result we observe a minor increase in the cell error probability as the codeword size increases before the cut-off number of symbols in a codeword.

Remarks

The results show that the performance of the interleaving technique is generally worse than multiple DMT symbols per FEC word. The cell error rate as a function of interleaving exhibits a peak before the cut-off interleaving depth, whereas the cell error rate as a function of the number of symbols in a codeword remains almost flat below the cut-off value of number of symbols. For interleaving depth and number of symbols per codeword above their cut-off values the two cell error rates converge.

Note, however, that multiple DMT symbols per FEC word offers significant benefits only at a large number of symbols per FEC word and at satisfactory FEC protection. The latter two are subject to restrictions as described in Section 4.6.1. In the particular case of 512 kbps data rate, the maximum allowed number of DMT symbols per FEC word is four with four parity bytes per symbol, or two when there are eight parity bytes. There is therefore a limit to the improvement obtained. Similar restrictions also limit the improvement for other bit rates - 256 kbps and 1 Mbps.

Note also that the cell error probability is slightly higher for a higher number of correction bytes (compare graphs for 8 and 4 parity bytes in Figure 4.14). This is due to the fact that the correction bytes add up to the size of the DMT symbols. Larger DMT symbols are more susceptible to noise and therefore the cell error rate is higher.

4.6.3 Burst error mitigation at different bit rates

The data rate influences considerably the restrictions imposed on the burst error mitigation techniques by the ADSL framing requirements, and therefore affects the performance of those techniques. Several ranges of data rates have been identified.

Low data rates (256 kbps)

Figure 4.15 presents the ADSL mux frame error rate and the ATM cell error rate as a function of the interleave depth at 256 kbps. Two scenarios with a different number of symbols in an FEC codeword have been considered. Broadly speaking, at such a data rate combining multiple symbols in a codeword improves the ADSL frame/ATM cell error rates.

However, consider the case when there is no interleaving (interleaving depth 1). The ADSL frame error rate is higher for larger number of symbols in a codeword (Figure 4.15(a)). This anomaly can be explained in the following way. When several symbols are combined into one FEC word, the payload bytes are ordered first, followed by the redundancy bytes at the end of the codeword. One DMT timeslot therefore carries payload bytes from two consecutive ADSL payload frames (except the last DMT timeslot of a codeword, which carries the redundancy bytes and possibly part of one ADSL mux frame). If a DMT symbol is severely corrupted and the errors cannot be corrected, these errors span over two consecutive ADSL frames. This causes error proliferation and increases the frame error rate.

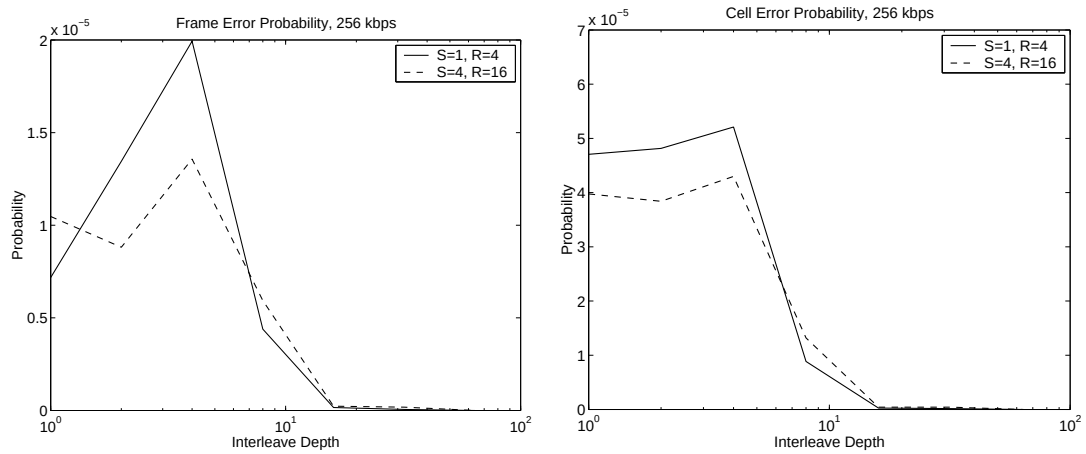

(a) Frame error rate

(b) Cell error rate

Figure 4.15: *ADSL mux frame and ATM cell error probability, 256 kbps, Rsymb = 4.*

Let us now consider the ATM cell error probability when there is no interleaving. In contrast to the frame error rate, the cell error rate declines when combining multiple symbols into one codeword. This effect is due to the following. At such low bit rates an ATM cell comprises several ADSL frames. For example, at 256 kbps an ADSL frame consists of 8 bytes, as opposed to 53 bytes for an ATM cell. That is why the error spread over the frames does not have a big impact on the cell error rate. However, some codewords are actually corrected due to the larger codeword size. Therefore the overall ATM cell error probability is lower.

Medium data rates (512 kbps and 1 Mbps)

The ATM cell error rate as a function of the interleave depth for 512 kbps and 1 Mbps is presented in Figure 4.16. Several scenarios with different numbers of symbols in a FEC codeword have been considered. The results show that combining multiple symbols in a codeword has adverse effects on the ATM cell error rates.

In Section 4.6.2, a mechanism was described by which the ATM cell error rate increases when the number of symbols in a codeword rises for equal interleave depth and number of FEC bytes per symbol (Figure 4.14). This effect is also visible in Figure 4.16. The cell error rate worsens more significantly at 1Mbps than at 512 kbps. This is due to the fact that at 1 Mbps the size of the ADSL frames is 32 bytes - comparable with the size of the ATM cells of 53 bytes. Therefore any increase in the ADSL frame error rate impacts to a large extent the ATM cell error rate.

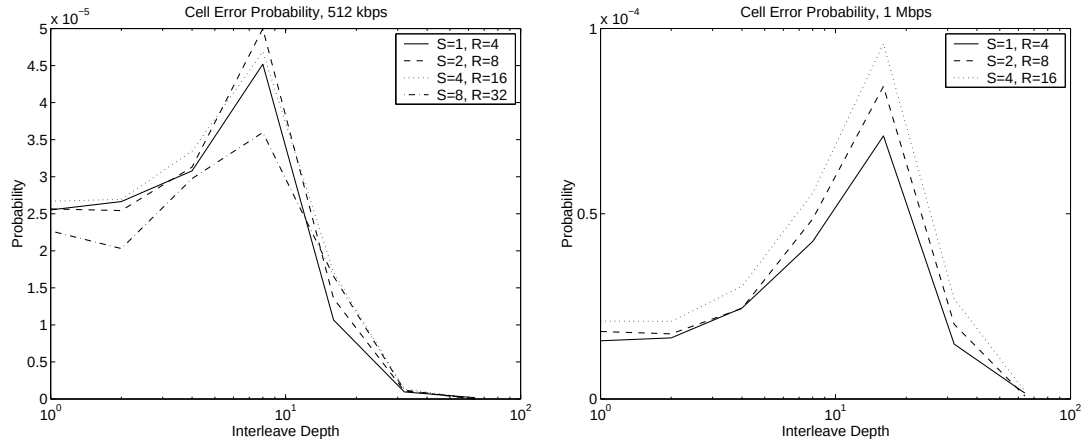

(a) 512 kbps **(b)** 1 Mbps

Figure 4.16: *ATM cell error probability, 512 kbps and 1 Mbps, Rsymb = 4.*

Only when the number of symbols per codeword is above its cut-off value (dash-dotted line in Figure 4.16(a)) the cell error rate declines. Note, however, that this threshold is reached with 32 parity bytes per codeword. All devices may not support such a large number of parity bytes, the standard has a minimum requirement up to only 16 parity bytes [1].

High data rates ($\geq$ 2 Mbps)

At 2 Mbps only a maximum of two symbols can be combined into a FEC word because of the codeword length restrictions. At such bit rate and maximum FEC capabilities (sixteen parity bytes), combining symbols in a FEC word worsens performance. At higher bit rates (e.g. 4 Mbps and 6 Mbps) it is impossible to fit more than one symbol in a single FEC codeword.

4.6.4 Interaction between interleaving and multiple symbols per FEC word

The combined action of interleaving and multiple symbols per FEC word has an adverse effect on the cell error probability in comparison to the cases when only one of the techniques has been used. In general the relationship between error probability and interleaving depth follows a typical pattern. The cell error probability initially rises when interleaving depths increase but exhibits a sharp drop after reaching a cut-off interleaving depth. However, at low and medium bit rates (256 kbps and 512 kbps) a slight drop of the cell error probability is observed at an interleaving depth of 2 when multiple symbols per codeword are also used (Figures 4.15

and 4.16(a)). A combination of small error spreading from interleaving and larger codewords turns out to be beneficial and leads to a reduction in the cell error rate. However, at higher interleaving depths (larger than 2 but lower than the cut-off value) the error proliferation because of interleaving dominates and worsens the performance. At large interleaving depths (32 or 64) the packet error rates for different numbers of symbols per codeword converge.

4.7 Impact of crosstalk in an unbundled environment on ADSL performance

Many countries are in the process of unbundling their access networks, i.e. granting different operators access to the incumbent's loop plant. This unbundling represents a risk for DSL deployment in that spectral control and management of the services deployed becomes more problematical. Crosstalk from services in neighbouring pairs is an important source of noise/interference on the line. Consequently, its impact must be taken into account in an unbundled environment.

This section presents results from a study of data transmission over ADSL impaired by impulse noise and crosstalk mixture from kindred (ADSL) interferers, and interferers alien to ADSL, such as HDSL and ISDN. Changing kindred crosstalk conditions have also been considered. The performance metrics used are ADSL mux frames and ATM cell/header error rates.

4.7.1 Crosstalk scenarios

It is assumed that the line under consideration is placed in a bundle of 50 pairs, where all 49 additional pairs carry a DSL service (i.e. the worst case). Five crosstalk scenarios have been considered:

- Kindred-only: 49 ADSL pairs;
- Mixture: 24 ADSL + 25 HDSL pairs;
- Mixture: 24 ADSL + 25 ISDN pairs;
- Mixture: 19 ADSL + 15 HDSL + 15 ISDN;

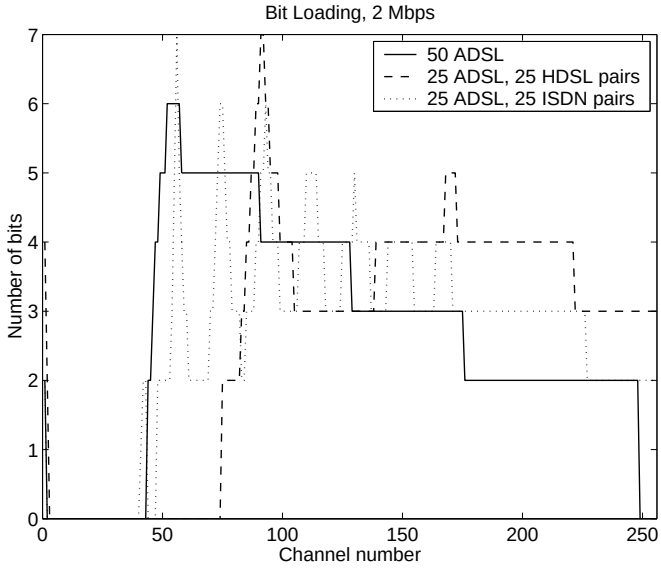

Figure 4.17: *Bit loading for 2 Mbps in different crosstalk conditions.*

- Changing kindred: 24 ADSL pairs during initialisation (bit loading), which consequently have increased to 49 ADSL pairs.

Note that the HDSL version considered here uses a 2B1Q-modulated signal at 392 kbaud (784 kbps) per pair, full duplex [20, 22, 23]. Similarly ISDN transmits a 2B1Q-modulated signal at 80 kbaud (160 kbps) [15–17]. A discussion of the crosstalk generated by various xDSL systems was presented in Section 3.3.4, p. 65.

The crosstalk interference from mixed sources has been summed using the FSAN method (see Section 3.3.5, p. 66), because it gives good estimates [117, 120] and has been accepted as a standard [121].

4.7.2 Bit loading in mixed crosstalk environment

The bit allocation scheme largely depends on the crosstalk spectrum (Figure 4.17). Alien crosstalk (HDSL and ISDN) overlaps larger frequency ranges in the ADSL downlink spectrum and deteriorates the SNR of more DMT subchannels than the kindred (ADSL) crosstalk. To compensate for the smaller number of usable subchannels in the presence of alien crosstalk, the bit allocation algorithm tends to load larger number of bits in subchannels with good SNR and in higher frequency ranges in comparison with the case of kindred-only crosstalk.

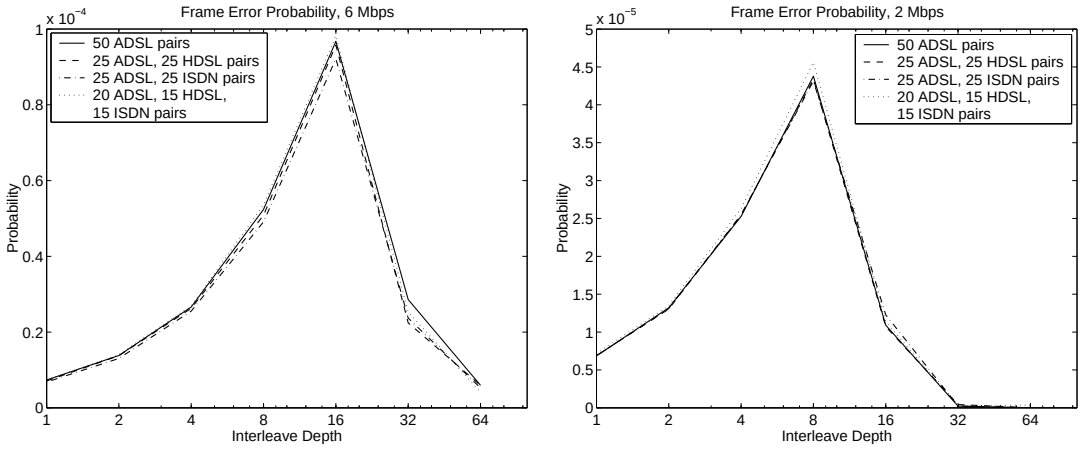

(a) 6 Mbps **(b)** 2 Mbps

Figure 4.18: *Frame error probability in different crosstalk scenarios.*

4.7.3 Results

Impact of alien crosstalk

At 2 Mbps alien crosstalk from HDSL and ISDN worsens the frame error rate (Figure 4.18(b)). The influence may not seem very significant, but is large enough to raise questions. In an unbundled market there can be little control over the services provided by competitors on the same bundle. Moreover, new DSL versions are constantly emerging and this may lead to further complications. The impact of HDSL or ISDN alone on ADSL does not seem to be very large. This is due to the use of DMT and noise-based loading algorithms in ADSL. However, combination of both HDSL and ISDN and with the added kindred ADSL have a noticeable effect on ADSL errors at higher levels. This is a result of the fact that the crosstalk mixture leaves few ”clean” DMT subchannels, i.e. most channels suffer from deteriorated SNR.

For lower bit error rates (2 Mbps) the influence of crosstalk on the ADSL mux frame error rate is more significant (Figure 4.18). This can be explained with the fact that for identical interfering spectra the number of bits in a subchannel is larger when higher bit rates are transmitted. Then DMT symbols are more susceptible to noise. For impulse noise with the same energy more DMT symbols will be damaged in comparison with lower bit rates. Thus the effects of the additional crosstalk noise are underminded.

Similar to the trends in frame error rates, HDSL and ISDN crosstalk raise the cell error rate

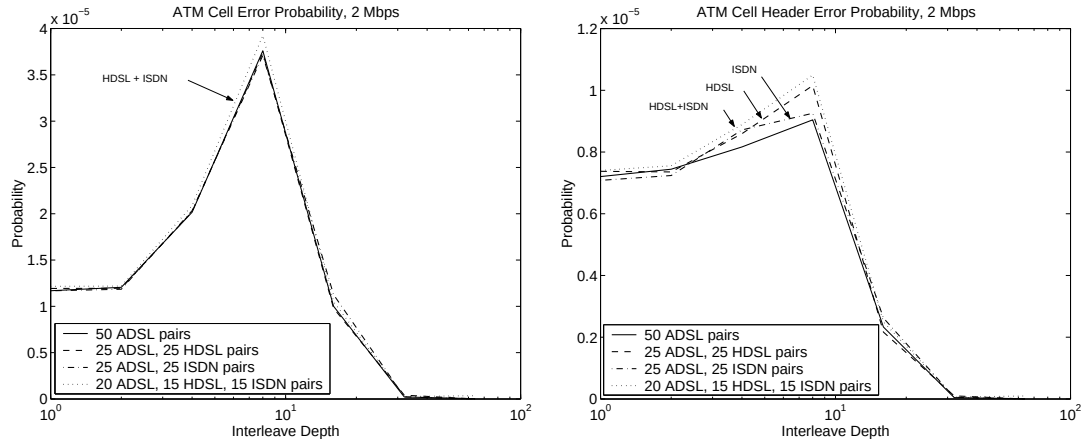

(a) ATM cells **(b)** ATM headers

Figure 4.19: *ATM cell/header error probability in different crosstalk scenarios.*

caused by impulse noise (Figure 4.19(a)). Due to the spectral incompatibility alien crosstalk tends to be more aggressive compared to kindred crosstalk. ATM cell header error rates (Figure 4.19(b)) are proportionally more affected by crosstalk than cell error rates. Headers are much smaller in size than ATM cells, which is a sign that the additional noise power from crosstalk leads to larger spread of errors on byte level (note that the interleaving implemented in the model is intercell [11]). This in turn means that some services, e.g. voice based on AAL2, would be more affected since it is based on small portions of information and does not count on retransmission. On the contrary, IP over ATM is unlikely to show a significant difference in performance because of the larger average size of an IP packet in comparison with an ATM cell.

Increased kindred crosstalk

In this scenario the ADSL modem has been initialised based on a fewer number of interferers, (24 ADSL pairs), but consequently the number of interfering services has been increased to 49 ADSL pairs. The results are shown in Figure 4.20. As can be expected, for both high and low bit rates the increase in crosstalk levels after initialisation leads to worse cell error rates. It is therefore recommended that ADSL modems re-adjust their bit loading scheme according to changing crosstalk conditions. Increase in the crosstalk level can be compensated for by increasing the transmit power. If the crosstalk interference drops, the transmit power can be

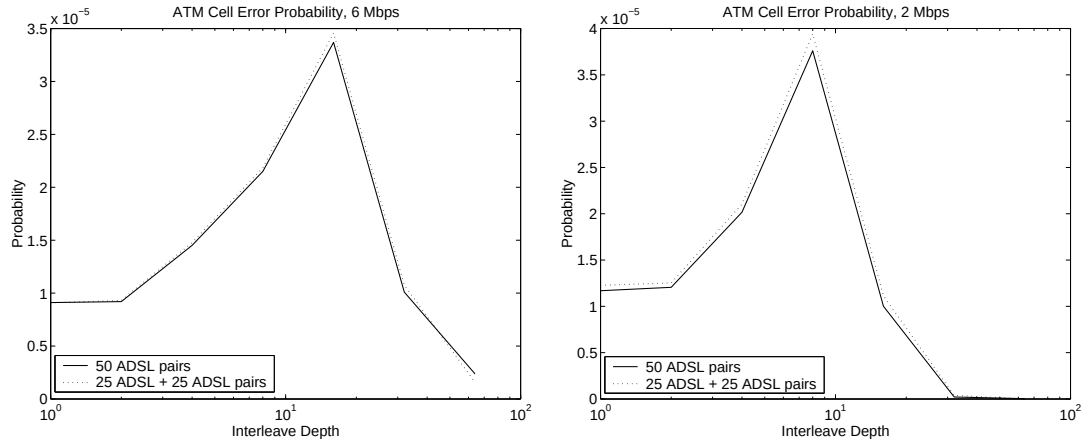

(a) 6 Mbps **(b)** 2 Mbps

Figure 4.20: *ATM cell error probability in changing crosstalk scenario.*

lowered for more efficient spectral management in the local loop. Changes in the crosstalk level can also be counterbalanced by bit re-allocation. There is, however, an issue with the overall link stability across all users of the bundle. If all DSL links in the cable start re-adjusting their bit loading schemes simultaneously, there is a danger of oscillations in the bit allocations or overall increase in the transmit power and hence the crosstalk levels, neither of which will achieve the final aim - to reduce the error rate. For further discussion of the problem of multiuser power control in DSL see e.g. [128].

4.8 MPEG-2 bit stream over ADSL subjected to impulse noise

MPEG-2 video stream has been used as an example of an end user application. The video transmission has been simulated as a direct bit stream over ADSL, without an intermediate protocol such as ATM or IP. Two bit rates have been considered - 1.5 Mbps and 4 Mbps. The impact of impulse noise and crosstalk on the subjective quality of MPEG-2 over ADSL system with different interleaving depths has been evaluated subjectively.

4.8.1 Simulation description

For the purpose of comparison the noise impulses have been scheduled to arrive at regular intervals of 2.7 s. However, the characteristics of individual impulses, such as amplitude and

duration, have still been drawn from the appropriate distributions.

The MPEG-2 videos used are test bitstreams available from Tektronix [129]. The sequences have been selected to include a still image, a human face, a slowly moving indoor image, and a moving landscape.

FEC has been set at the highest standardised strength, e.g. 16 bytes per codeword. Only one DMT symbol has been encoded in a codeword for the 1.5 Mbps video bitstreams.

4.8.2 Results

Comments about the video quality[3] will be presented separately for 4 Mbps and 1.5 Mbps video bitstreams.

4 Mbps MPEG-2 video bitstream

The following effects of impulse noise on video quality have been found noteworthy:

- 1 - no interleaving. The FEC cannot cope with the burst errors caused by impulse noise and as a result there are noticeable artifacts in the images at the arrival of noise impulses.
- 2, 4, 8, 16 - the size and duration of error artifacts rises gradually with the increase of the interleaving depth.
- 32 - this interleaving depth allows for certain errors to be corrected and introduces a much lower latency than interleaving depth 64 (8 ms interleaving delay at depth 32 compared to 16 ms interleaving delay at depth 64). However, there is still a notable number of outstanding uncorrected errors that prove crucial for the image quality. The error spreading due to interleaving causes long and unpleasant artifacts and can even force the MPEG-2 decoder out of synchronism.
- 64 - at this interleaving depth the error spreading is sufficient and virtually all errors are corrected by FEC. The received image is almost identical to the original before transmission.

[3]On encountering an error in the video bitstream, some video decoders jump to the next "good" video frame, rather than show images distorted by errors. In order to appreciate fully the impact of errors on the video quality, and the difference between this quality for different interleaving depths, you need to use a decoder which shows *all* video frames, including the errored ones. One such decoder has been suggested in Appendix D.

The results show that if enabled, interleaving should be set to the maximum possible depth (64) for 4 Mbps video transmission. Intermediate interleaving depths worsen the video image quality, even though the frame and cell error probabilities may exhibit improvement on the non-interleaved case.

1.5 Mbps MPEG-2 video bitstream

The perceived subjective quality of the 1.5 Mbps MPEG-2 video bitstream depends in a similar fashion on the interleaving depth as the 4 Mbps MPEG-2 video. Note, however, that the cut-off interleaving depth, at which the number of artifacts reduces significantly, is 16 (as opposed to depth 32 for 4 Mbps). This effect is a result of a lower symbol error probability and higher probability for RS error correction if the bit rate is lower. Identical results have been observed for ADSL frames and ATM cells as discussed in Section 4.4, p. 87 (see also Figure 4.6).

The simulation results show that in this particular example of 1.5 Mbps video transmission, it is acceptable to reduce the interleaving depth to 16 without compromising the image quality. Such a configuration would be useful for delay-sensitive applications, which cannot tolerate the time lag caused by interleaving with maximum depth.

Note that small differences in the frame and cell error rate correspond to large deviations in the perceptive quality of video images. Therefore the error rates for frames and cells presented in earlier sections were plotted on linear scale. In this way the graphs visualise better the potential effect of errors on user applications.

Both the 1.5 Mbps and 4 Mbps video bitstreams at all interleaving depths allowed by the ADSL standards [1, 11] are provided on CD, as described in Appendix D.

4.9 Conclusion

In this chapter the results of simulation of an ADSL system have been presented. The focus has been on evaluating the impact of impulse noise and crosstalk on higher protocol layers, such as ATM cells, ADSL frames, and MPEG-2 bit stream, for different ADSL framing parameters. The ATM cell and ADSL frame error rates and inter-error intervals, as well as subjective video quality have been used as performance metrics.

The ADSL simulation architecture mirrors closely a generic ADSL modem, and the latest and most accurate impulse noise and crosstalk models have been used. A novel extension of a loading algorithm has been developed to allow for stable bit allocation for DMT with restricted subtone constellation size and trellis coding.

The DSL framing has been found to have an adverse impact on services transmitted over ADSL. The interleaving depth should be set to its maximum value if the applications running over ADSL can tolerate latency, otherwise no interleaving should be used. Intermediate interleaving depths only deteriorate the performance at higher levels, such as ATM cells, ADSL frames, and MPEG-2 video.

If combining multiple symbols in one FEC codeword is considered as an alternative to interleaving, three data rate ranges can be distinguished. For low bit rates (256 kbps) it is justified to use multiple symbols per FEC word as an alternative to interleaving. At medium bit rates (512 kbps and 1 Mbps) usage of multiple symbols per FEC word may bring improvement in performance, but not with the parameter settings allowed in the current standards. At high bit rates (2 Mbps and above), there is no alternative to interleaving because of restrictions on the number of symbols that can be combined in a FEC word at such bit rates.

The strength of the FEC code influences considerably the error rate performance and should be set to the maximum allowed number of redundancy bytes. Trellis coding, on the other hand, has no significant impact on the errors due to impulse noise and cannot contribute to the impulse noise mitigation.

The distribution of error free intervals (seconds or data units) between error events exhibits a high degree of clustering, similar to the one shown by inter-arrival times of impulse noise. Error free cells, packets, or even data bytes take into account the bit rate at which the DSL system operates, and are therefore a more appropriate inter-error measure for higher protocol layers than the error free seconds. The effective distribution of error free intervals as seen from higher layers varies according to the degree an application can utilise unerrored cells that occur between error bursts. Detecting the unerrored cells, however, is impeded by the fact that error protected ATM cell headers are less affected by impulse noise than the unprotected cell payload.

Alien crosstalk from HDSL and ISDN services or increased kindred crosstalk in the same bundle leads to higher ADSL frame/ATM cell error rates caused primarily by impulse noise. The

crosstalk mixture from multiple alien DSL services leads to higher deterioration than when only one alien interferer is present. Although not very significant on cell level, this deterioration is pronounced at bit level and can affect certain services. Therefore spectral compatibility is an important issue in an unbundled environment.

Chapter 5
Theoretical analysis of errors in DSL systems in impulse noise environment

5.1 Introduction

The statistical model of impulse noise presented in Chapter 3 is used in this chapter to evaluate analytically the impact of impulse noise on xDSL systems. The impulse amplitude statistics serve as the basis for a new Bernoulli-Weibull model of impulse noise in the local loop. It is shown that earlier models that assume Gaussian distributed impulse amplitudes or Rayleigh distributed powers are not applicable to impulse noise in telephone lines. Using the Bernoulli-Weibull model, it is demonstrated that multicarrier QAM performs better than single carrier systems but only for low impulse power and low impulse probability.

The data errors in ADSL are then analysed using the Bernoulli-Weibull model and temporal impulse statistics, and the theoretical approach is shown to offer good approximation to the simulation results.

In the final part of the chapter, the Bernoulli-Weibull model is also used for the study of SHDSL systems. The analysis of the data errors in SHDSL shows that ADSL offers a significantly better impulse noise mitigation than SHDSL but only after using fully the interleaving and error correction techniques.

5.2 Impact of impulse noise on single and multi-carrier QAM in xDSL systems

Earlier works have analysed the effect of impulse noise on QAM modulation [12, 13, 130] but with impulse noise models that do not apply to the impulse noise in telephone lines. In [131], the performance of a binary signal in telephone lines has been studied using the impulse noise model from [82]. This model has been modified in later works [3, 4] and the results in this analysis are based on the latter, modified version, which was presented in Section 3.2, p. 32.

5.2.1 Bernoulli-Weibull impulse noise model

In order to evaluate theoretically the impact of impulse noise on DSL systems, a new local loop - oriented noise model at symbol level will be introduced. It was discussed in Section 3.2 that the original proposal [82] was to model the statistics of the impulse amplitudes u with a generalised exponential distribution $f_{ge}(u)$ (Equation 3.1, p. 37). However, the Weibull distribution $f_{wb}(u)$ (Equations 3.2 and 3.3) can be used as an alternative [3]. Since the latter distribution is analytically more tractable, it will also be used in the current analysis. Note also that background noise in the local loop can be approximated with a Gaussian distribution [82].

The received signal $r(m)$ in the symbol domain can be expressed as:

$$r(m) = a(m) + n(m), \tag{5.1}$$

where $a(m)$ is the transmitted complex symbol drawn from the QAM constellation under consideration. Let us assume that the combined complex noise $n(m)$ at the receiver is a sum of an impulse Bernoulli-Weibull component and a background Gaussian component, i.e.:

$$n(m) = bnl(m) \cdot w(m) + \overline{bnl}(m) \cdot g(m), \tag{5.2}$$

where w is a complex Weibull process with parameters α and b, g is a complex additive white Gaussian noise (AWGN) with mean zero and variance $2\sigma_g^2$, and bnl is a real Bernoulli process, i.e. an independent and identically distributed (i.i.d.) sequence of zeros and ones with probability $\Pr(bnl = 1) = p$. It is assumed that the process w refers to the combined effect of impulse noise and AWGN, because the distribution is derived from empirical data of this very combination.

5.2.2 Two-dimensional noise amplitude statistics

The noise amplitude statistical models need to be considered in two dimensions to facilitate the evaluation of the impact of noise on orthogonal signals. Therefore, a new extension of the Weibull amplitudes model to a bivariate form will be presented and used for error performance analysis. A more detailed consideration of the Weibull distribution can be found in Appendix B.

Bivariate Weibull noise statistics

If the impulse noise amplitude u is Weibull distributed, then the complex impulse noise with real and imaginary components u_R and u_I will have a bivariate Weibull complementary cumulative distribution function (ccdf) of the form:

$$\bar{F}_{wb,I}(u_R, u_I) = e^{-b'(u_R^2+u_I^2)^{\alpha/2}},\ u_R, u_I \geq 0,\ \alpha > 0,\ b' > 0, \tag{5.3}$$

where the parameter b has been scaled to $b' = 2^{\alpha/2}b$ to reflect the fact that both components of the complex impulse noise contribute to the noise power. The bivariate Weibull pdf, after expansion to four quadrants to allow for negative values of u_R and u_I, is defined as:

$$\begin{aligned} f_{wb,I}(u_R, u_I) &= \frac{1}{4} \cdot \alpha^2\ |u_R|\ |u_I|\ e^{-b'\ (u_R^2+u_I^2)^{\alpha/2}} \times \\ &\times \left[b'^2 \left(u_R^2 + u_I^2\right)^{\alpha-2} + b' \left(\frac{2}{\alpha} - 1\right) \left(u_R^2 + u_I^2\right)^{\frac{\alpha}{2}-2} \right]. \end{aligned} \tag{5.4}$$

This bivariate Weibull distribution has been used earlier in reliability studies, e.g. by Hougaard [132].

Bivariate Gaussian noise statistics

The complex background noise statistics can be described with a zero-mean bivariate Gaussian distribution f_g with independent variables u_R and u_I [13, 130]:

$$f_g(u_R, u_I) = \frac{1}{2\pi\sigma_g^2} e^{-(u_R^2+u_I^2)/(2\sigma_g^2)}, \tag{5.5}$$

where $2\sigma_g$ is the background noise power. The bivariate normal distribution is well studied and further information about its properties can be found in e.g. [101].

5.2.3 Performance of single-carrier QAM in impulse noise

Using the noise model presented in Section 5.2.1, it can be shown that the combined noise probability density would be:

$$f_{n,SC}(n_R, n_I) = p \cdot f_{wb,I}(n_R, n_I) + (1-p) f_g(n_R, n_I), \tag{5.6}$$

where p is the impulse probability, n_R and n_I are the real and imaginary noise components, and $f_{wb,I}(n_R, n_I)$ and $f_g(n_R, n_I)$ are the bivariate Weibull and bivariate Gaussian probability densities specified in the previous section.

Error probability for QAM signals

For a rectangular M-QAM constellation with M $= 2^k, k = 2, 4, 6, ...$ points at distance d apart, the exact expression for symbol error probability is [13]:

$$P_{s,QAM} = 1 - \frac{1}{2^{k-2}} \left[D_1 + (2^{\frac{k}{2}-1} - 1)^2 D_2 + (2^{\frac{k}{2}-1} - 1) D_3 + (2^{\frac{k}{2}-1} - 1) D_4 \right], \quad (5.7)$$

where D_1 is the probability of correct decision for the corner symbol points, D_2 for the inner square, and D_3 and D_4 for the horizontal and vertical edges less the corners:

$$\begin{aligned} D_1 &= \Pr\left(n_R \geq -\frac{d}{2} \quad \& \quad n_I \geq -\frac{d}{2} \right), \\ D_2 &= \Pr\left(|n_R| \leq \frac{d}{2} \quad \& \quad |n_I| \leq \frac{d}{2} \right), \\ D_3 &= \Pr\left(|n_R| \leq \frac{d}{2} \quad \& \quad n_I \geq -\frac{d}{2} \right), \\ D_4 &= \Pr\left(n_R \geq -\frac{d}{2} \quad \& \quad |n_I| \leq \frac{d}{2} \right). \end{aligned} \quad (5.8)$$

Note that the distance between constellation points d for 2^k-QAM is defined as [125]:

$$d = \sqrt{\frac{6}{2^k - 1} \mathcal{E}_s} = \sqrt{\frac{6}{2^k - 1} \tau_s \sigma_a^2}, \quad (5.9)$$

where $\mathcal{E}_s$, σ_a^2, and τ_s are respectively the symbol energy, power, and duration.

The probability of symbol error can be converted into an equivalent probability of a binary digit error. For M-ary orthogonal signals with symbol error probability $P_{s,M}$, the bit error probability P_b is given by [125]:

$$P_b = \frac{2^{k-1}}{2^k - 1} P_{s,M}, \quad M = 2^k. \quad (5.10)$$

QAM error probability in Bernoulli-Weibull impulse noise environment

By integrating the combined noise probability density $f_n(n_R, n_I)$ from Equation 5.6, in the appropriate limits as specified in Equations 5.8, it is obtained:

$$\begin{aligned}
D_1 &= p\left[1 - e^{-b'\left(\frac{d}{2}\right)^\alpha} + \tfrac{1}{4}e^{-b'\,2^{\alpha/2}\left(\frac{d}{2}\right)^\alpha}\right] + (1-p)\left[1 - \mathcal{Q}\left(\frac{d}{2\sigma_g}\right)\right]^2, \\
D_2 &= p\left[1 - 2e^{-b'\left(\frac{d}{2}\right)^\alpha} + e^{-b'\,2^{\alpha/2}\left(\frac{d}{2}\right)^\alpha}\right] + (1-p)\left[1 - 2\mathcal{Q}\left(\frac{d}{2\sigma_g}\right)\right]^2, \\
D_{3,4} &= p\left[1 - \tfrac{3}{2}e^{-b'\left(\frac{d}{2}\right)^\alpha} + \tfrac{1}{2}e^{-b'\,2^{\alpha/2}\left(\frac{d}{2}\right)^\alpha}\right] + (1-p)\left[1 - \mathcal{Q}\left(\frac{d}{2\sigma_g}\right)\right]\left[1 - 2\mathcal{Q}\left(\frac{d}{2\sigma_g}\right)\right],
\end{aligned} \tag{5.11}$$

where $\mathcal{Q}(x)$ denotes the $\mathcal{Q}$-function (see Equation 2.5, p. 21). The symbol error probability P_s and the bit error probability P_b can then be found using Equations 5.7 and 5.10 respectively.

Additional remarks

It can be shown that in the case of Weibull distributed impulse noise amplitudes, the impulse noise power $2\sigma_i^2$ can be obtained from (see Appendix B):

$$\sigma_i^2 = b'^{-2/\alpha}\Gamma\left(1 + \frac{2}{\alpha}\right), \tag{5.12}$$

where α and b' are the Weibull parameters, and $\Gamma(z) = \int_0^\infty t^{z-1}e^{-t}dt$ is the gamma function.

In all subsequent results the signal-to-background noise (SBR) ratio is defined as $\frac{\sigma_a^2}{2\sigma_g^2}$, and the signal-to-impulse noise ratio (SIR) - as $\frac{\sigma_a^2}{2\sigma_i^2}$.

5.2.4 Bernoulli-Weibull vs. Bernoulli-Gaussian noise model

It is interesting to compare the Bernoulli-Weibull model with the results obtained in [12–14] using Gaussian or Rayleigh impulse noise models. Figure 5.1 shows plots of the bit error rate (BER) performance in Bernoulli-Weibull and Bernoulli-Gaussian impulse noise. If the impulse amplitudes are Weibull distributed the performance of single carrier QAM remains poor for significantly higher signal-to-impulse noise ratios (SIR) than in the case of Gaussian impulse amplitudes. This is due to the fact that the Weibull distribution is more heavy-tailed than the Gaussian distribution, a demonstration of which can be seen in Figure 5.2. Therefore those

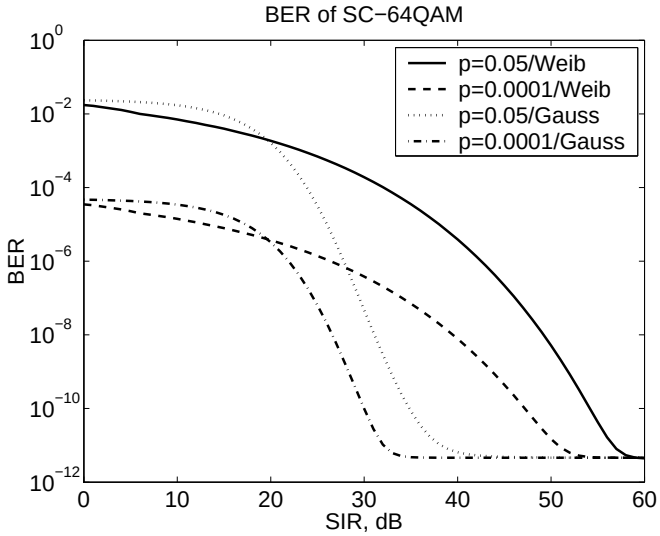

Figure 5.1: *Comparison between the performance of SC-64QAM for Bernoulli-Weibull and Bernoulli-Gaussian impulse noise model with SBR = 30 dB.*

models that assume Gaussian impulse amplitudes, which are also equivalent to Rayleigh power distributions [13], offer too optimistic results for the analysis of digital subscriber line systems.

5.2.5 Performance of multi-carrier QAM in impulse noise

This analysis will consider the most common multi-carrier QAM version, namely discrete multi-tone (DMT) modulation, which is employed in ADSL and is also likely to be standardised for VDSL.

DMT modulation

The DMT modulation is carried out by applying inverse discrete Fourier transform (IDFT) to the transmitted symbol. Assuming perfect synchronisation, timing, and an ideal channel, the received symbol $r(m)$ for N-carrier DMT modulation is given by [40]:

$$r(m) = \frac{1}{\sqrt{N}} \sum_{i=0}^{N-1} a(i) e^{j2\pi im/N} + n(m),\ m = 0, 1, \ldots, N-1, \tag{5.13}$$

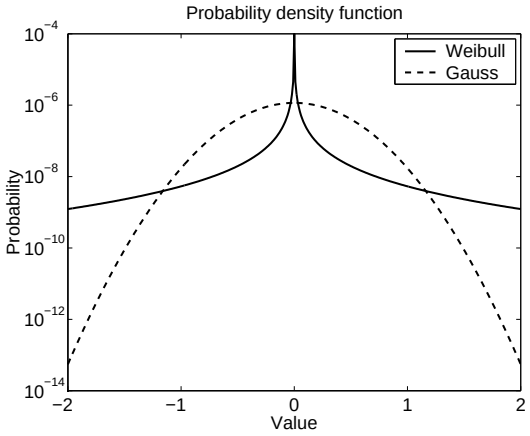

Figure 5.2: *Comparison between univariate double Weibull and zero-mean Gaussian distributions with identical variance* $\sigma^2 = 0.344$.

where again $a(m)$ is the transmitted QAM data symbol, and $n(m)$ is the combined complex noise defined in (5.2). Performing a discrete Fourier transform (DFT) on the received sequence $r(m)$ yields the recovered transmitted symbols $a(m)$ and a noise component $n_f(m)$:

$$a(m) + n_f(m) = \frac{1}{\sqrt{N}} \sum_{i=0}^{N-1} r(i) e^{-j2\pi im/N},\ m = 0, 1, 2...N-1, \tag{5.14}$$

where $n_f(m)$ is the DFT of the line noise:

$$n_f(m) = \frac{1}{\sqrt{N}} \sum_{i=0}^{N-1} n(i) e^{-j2\pi im/N},\ m = 0, 1, 2...N-1. \tag{5.15}$$

Noise pdf for DMT signals

Using Equation 5.15, it is possible to derive an expression for the characteristic function (cf) of the complex noise component $n_f(m)$, namely:

$$\Phi_{n_f}(\omega_1, \omega_2) = \sum_{i=0}^{N} \binom{N}{i} p^i (1-p)^{N-i} \Phi_{wb}^i(\omega_1, \omega_2) \Phi_g^{N-i}(\omega_1, \omega_2), \tag{5.16}$$

where $\Phi_{wb}(\omega_1, \omega_2)$ and $\Phi_g(\omega_1, \omega_2)$ are the characteristic functions of the bivariate Weibull and bivariate Gaussian distributions respectively.

In the general case the cf $\Phi(\omega_1, \omega_2)$ of a bivariate distribution with pdf $f(x_1, x_2)$ is defined as

(see e.g. [98]):

$$\Phi(\omega_1, \omega_2) = \int_{-\infty}^{\infty} \int_{-\infty}^{\infty} e^{j\omega_1 x_1 + j\omega_2 x_2} f(x_1, x_2) dx_1 dx_2. \tag{5.17}$$

Hence the cf $\Phi_g(\omega_1, \omega_2)$ of the bivariate Gaussian distribution with pdf (5.5) is:

$$\Phi_g(\omega_1, \omega_2) = e^{-\sigma_g^2(\omega_1^2+\omega_2^2)/2}. \tag{5.18}$$

Explicit expressions for the Weibull cf are not available in the general case and particularly if the shape parameter α is smaller than 1 (see Appendix B, [98, 133]). However, all studied impulse amplitude statistics in the local loop are approximated by Weibull distributions with $\alpha < 1$ (see Table 3.1, p. 38 and [3]). That is why a numerical approach has been developed to calculate the noise pdf for multi-carrier QAM.

It is known that multiplication of cfs corresponds to a convolution of pdfs (see e.g. [101]). The pdf of the combined noise in the case of N-carrier DMT modulation can therefore be expressed as:

$$f_{nI,MC}(n_R, n_I) = \sum_{i=0}^{N} \binom{N}{i} p^i (1-p)^{N-i} \cdot f_{wb,I}^{(*\,i)}(n_R, n_I) * \frac{1}{2\pi\sigma_{g,i}^2} e^{-(n_R^2+n_I^2)/(\sigma_{g,i}^2)}, \tag{5.19}$$

where $\sigma_{g,i}^2 = \frac{(N-i)\sigma_g^2}{N}$, and $f_{wb,I}^{(*\,i)}(n_R, n_I)$ denotes i-fold convolution of the function $f_{wb,I}(n_R, n_I)$. The two-dimensional convolution of two functions $f_1(x, y)$ and $f_2(x, y)$ is given in the general case by (see e.g. [134]):

$$f_1(x, y) * f_2(x, y) = \int_{-\infty}^{\infty} \int_{-\infty}^{\infty} f_1(v, w) f_2(x - v, y - w)\, dv\, dw. \tag{5.20}$$

Similarly to the Weibull characteristic function, no closed-form solution to the convolution of the Weibull probability densities can be found. It is possible, however, to evaluate this convolution numerically.

Alternative bivariate Weibull distribution

The numerical convolution of two-dimensional functions poses significant computational and memory requirements when high precision is required. Therefore, a bivariate Weibull distribu-

tion of an alternative form has been considered, which gives sufficiently accurate results for a significantly lower usage of computing resources.

Let us assume that the two orthogonal components of the complex impulse noise are independent and Weibull distributed with parameters α and b. The joint distribution of the two components is also Weibull of a form which will be referred to in this work as type II, and which has the following ccdf:

$$\bar{F}_{wb,II}(u_R, u_I) = e^{-b'(u_R^\alpha + u_I^\alpha)},\ u_R, u_I \geq 0, \tag{5.21}$$

The pdf of this distribution will simply be the product of the marginal pdfs, and after an expansion to four quadrants to allow for negative values of u_R and u_I has the form:

$$f_{wb,II}(u_R, u_I) = \frac{1}{4}\alpha^2 b'^2 |u_R|^{\alpha-1}|u_I|^{\alpha-1} e^{-b'(|u_R|^\alpha + |u_I|^\alpha)}. \tag{5.22}$$

Going back to the original bivariate Weibull distribution with ccdf (5.3), which will be referred to as type I, there is a certain degree of dependence between its variables. The correlation between the random variables $\log U_R$ and $\log U_I$ is given by [135]: $1 - \left(\frac{\alpha}{2}\right)^2$. It has been found, however, that the error rates calculated using the original Weibull distribution do not differ significantly from the error rates based on the alternative Weibull model introduced in the current section, the latter producing slightly more pessimistic estimates than the former (Figure 5.3). The type II distribution offers considerable computational advantages over type I, since the numerical convolution needs to be carried out only in one dimension. Therefore, the alternative bivariate Weibull distribution will be used for evaluating the performance of the multi-carrier QAM.

Weibull type II noise pdf for DMT signals

Using the alternative bivariate Weibull distribution of type II, the combined noise pdf for N-DMT modulation can be calculated from:

$$\begin{aligned} f_{nII,MC}(n_R, n_I) &= \sum_{i=0}^{N} \binom{N}{i} p^i (1-p)^{N-i} \cdot f_{wb}^{(*\,i)}(n_R) * \frac{1}{\sqrt{2\pi}\sigma_{g,i}} e^{-n_R^2/\sigma_{g,i}^2} \times \\ &\times\ f_{wb}^{(*\,i)}(n_I) * \frac{1}{\sqrt{2\pi}\sigma_{g,i}} e^{-n_I^2/\sigma_{g,i}^2}, \end{aligned} \tag{5.23}$$

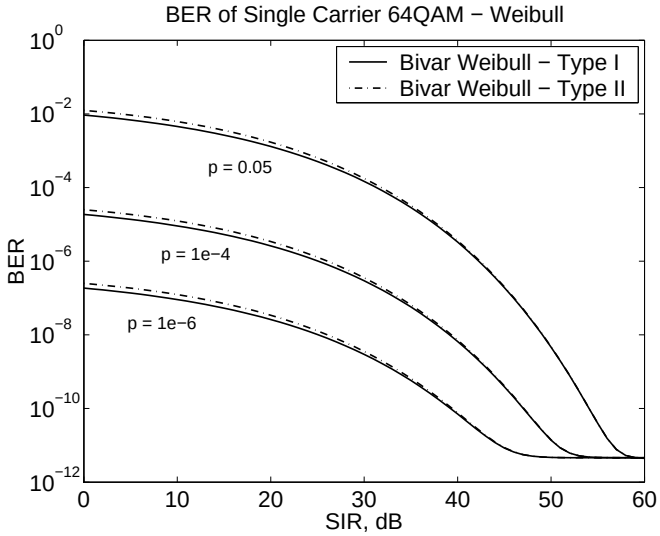

Figure 5.3: *Analytical performance of SC-64QAM with SBR = 30 dB and impulse noise amplitudes modelled with bivariate Weibull distribution type I (correlated) and type II (independent variables).*

where $\sigma_{g,i}^2 = \frac{(N-i)\sigma_g^2}{N}$, the function $f_{wb}(x) = \frac{1}{2}\alpha b'|x|^{\alpha-1}e^{-b'|x|^\alpha}$ is the marginal pdf of the bivariate type II - Weibull distribution, and $f_{wb}^{(*\,i)}(x)$ denotes i-fold convolution of the function $f_{wb}(x)$.

Note that Equation 5.23 specifies only one-dimensional convolution, which in the general case is defined as $f_1(x) * f_2(x) = \int_{-\infty}^{\infty} f_1(v) f_2(x-v)dv$. Therefore, this approach is computationally much less intensive than the one using the original type I - Weibull pdf.

After evaluating the noise pdf (5.23), it can be integrated numerically in the limits specified in (5.8), and then the probabilities of correct detection can be substituted in (5.7) to yield the symbol error probability.

5.2.6 Single-carrier vs. multi-carrier QAM in impulse noise

The analysis laid out in previous sections is used here to consider the bit error rate (BER) for single carrier 64QAM (Fig. 5.4), and for 256-carrier 64QAM (Fig. 5.5) for various values of the impulse probability p.

As it can be seen from the two figures, multi-carrier (MC) QAM outperforms single-carrier (SC) QAM for high values of SIR, because the DFT operation spreads the impulse over all N

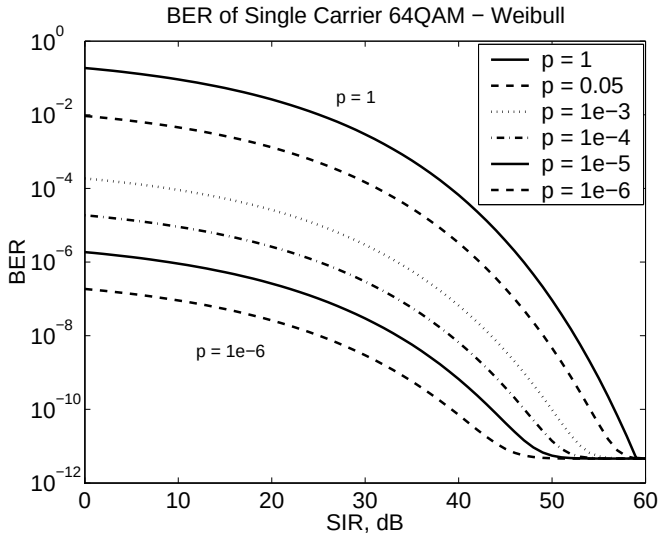

Figure 5.4: *Analytical performance of SC-64QAM in local loop impulse noise with SBR = 30 dB.*

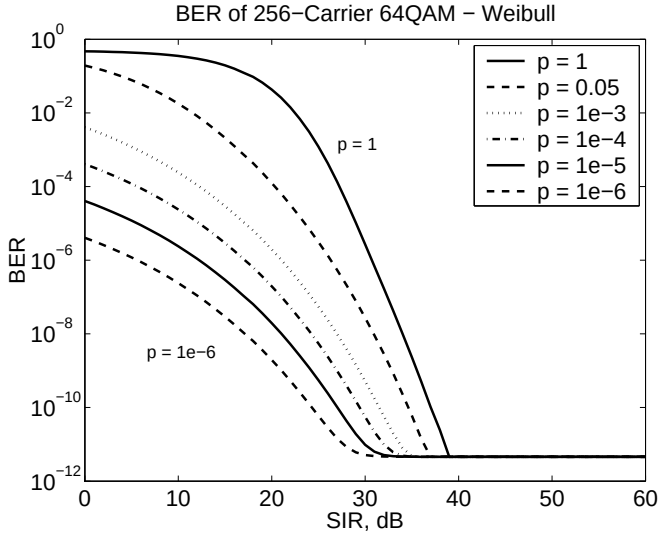

Figure 5.5: *Analytical performance of 256-carrier 64QAM in local loop impulse noise with SBR = 30 dB.*

data symbols and diminishes the noise impact. For low SIR, however, MC QAM has a higher error rate than the SC QAM due to the fact the the noise level is high and after the spreading it affects the majority of subchannels. Note that for very low values of SIR, the error rate of MC QAM still remains higher than that of SC QAM even if the impulse probability p is small. This is a result of the heavy tail of the Weibull distribution, which is related to the tendency of impulse amplitudes to exhibit occasionally very high amplitudes.

5.3 Impulse duration and inter-arrival time estimates

It was pointed out in Section 3.2.3, p. 36, that in addition to the impulse amplitudes, the statistical description of impulse noise in the time domain involves two more temporal characteristics, namely impulse duration and inter-arrival times [3]. The current section discusses the analytical approach to obtaining averaged estimates of these two characteristics.

Impulse duration

The impulse length τ can be modelled with a log-normal mixture distribution [82, 83], as discussed in Section 3.2.3, p. 40. The mean impulse duration $\bar{\tau}$ equals the first moment of the pdf $f_l(\tau)$ and can be found from the following expression:

$$\bar{\tau} = \int_{-\infty}^{\infty} \tau f_l(\tau) d\tau = B\ \tau_1\ e^{s_1^2/2} + (1-B)\ \tau_2\ e^{s_2^2/2}, \tag{5.24}$$

where B, s_1, τ_1, s_2, and τ_2 are the parameters from Equation 3.7. E.g. for $B = 1$, $s_1 = 1.15$, and $\tau_1 = 18\,\mu s$ (see Table 3.2), the mean duration $\bar{\tau} \approx 34.87\,\mu s$.

However, the estimate provided by the mean value is slightly biased upwards by the tail of the distribution. Therefore, it may be preferable to use the median impulse duration $\tau_{1/2}$, which can be found by solving the equation:

$$\int_{\tau_{1/2}}^{\infty} f_l(\tau) d\tau = \frac{1}{2} \;\Leftrightarrow\; B \cdot \mathrm{erf}\left(\frac{\ln(\tau_{1/2}/\tau_1)}{s_1\sqrt{2}}\right) + (1-B) \cdot \mathrm{erf}\left(\frac{\ln(\tau_{1/2}/\tau_2)}{s_2\sqrt{2}}\right) = 0. \tag{5.25}$$

For the same example of $B = 1$, $s_1 = 1.15$, and $\tau_1 = 18\,\mu s$, the median impulse duration is simply $\tau_{1/2} = \tau_1 = 18\,\mu s$.

Inter-arrival time

In Section 3.2.6, p. 54, an inter-arrival times model based on a Markov renewal process with N_S states was presented, where the time is divided into N_S non-overlapping time ranges T_i, and the inter-arrival time in each range is described by a pdf $f_{T_i}(t)$, $i = 1, \ldots, N_S$, $t \in T_i$ [5]. The mean inter-arrival time $\bar{t}$ can be represented as a weighted sum of the means for the different time ranges as follows:

$$\bar{t} = \sum_{i=1}^{N_S} \pi_i \bar{t}_{T_i} = \sum_{i=1}^{N_S} \pi_i \frac{\int_{T_i} t\, f_{T_i}(t)\, dt}{\int_{T_i} f_{T_i}(t)\, dt}, \tag{5.26}$$

where $\bar{t}_{T_i}$ denotes the mean inter-arrival time for the time range T_i, $i = 1, \ldots, N_S$. The probability π_i that a Markov process occupies state i, $i = 1, \ldots, N_S$, indicates the likelihood that the inter-arrival times belong to range T_i. The state probabilities must satisfy the requirement $\sum_{i=1}^{N_S} \pi_i = 1$ and their limiting values can be calculated using the expression [104]:

$$\pi = \pi P_{mar}\ , \tag{5.27}$$

where $\pi = [\pi_1, \pi_2, \ldots, \pi_{N_S}]$ is the steady-state probability vector formed by the N_S-state probabilities, and P_{mar} is the Markov transition probability matrix as defined in Equation 3.16.

If the four-state Markov model presented in Section 3.2.6, p. 56 is used as an example, with transition probabilities given in Equation 3.19, and pdfs specified by the all-Pareto model in Table 3.5, it is possible to calculate the steady-state probabilities, the range mean times, and the overall mean inter-arrival time as shown in Table 5.1.

State	1	2	3	4
Range	$t < 1$ s	$1 \leq t < 10$ s	$10 \leq t < 100$ s	$100 \leq t$
Steady-state probabilities	$\pi_1 = 0.653$	$\pi_2 = 0.047$	$\pi_3 = 0.123$	$\pi_4 = 0.177$
Range mean times, s	$\bar{t}_{T_1} = 0.673$	$\bar{t}_{T_2} = 2.090$	$\bar{t}_{T_3} = 20.96$	$\bar{t}_{T_4} = 166.1$
Overall mean time, s	$\bar{t} = 32.44$			

Table 5.1: *Mean inter-arrival times for a Markov model with transition probabilities as in Equation 3.19 and all-Pareto pdfs specified in Table 3.5.*

5.4 Data errors in ADSL

In Section 5.2, an impulse noise model at symbol level was introduced and applied to estimate analytically the impulse noise impact on multi-carrier QAM (DMT) in the general case. Building on that analysis, it will now be shown how estimates of the data errors at higher layers can be obtained in the particular case of ADSL framing.

5.4.1 General considerations

Analysis of impulse noise measurements conducted on the Deutsche Telekom (DT) network concluded that less than 1% of all impulses have a length of 200 μs or more [88]. The same conclusion was reached for impulses measured on British Telecom lines [85]. It was also discussed in Section 2.5.2, p. 15, that the length of a DMT symbol is 250 μs from a bit-level perspective, or approximately 246.4 μs after inserting an extra synchronisation symbol every 68 ADSL frames [1, 11]. It can therefore be concluded that no significant impulse events have a duration longer than that of a DMT symbol.

Furthermore, simulations using the platform described in Chapter 4 showed that less than 5% of all impulses span between two consecutive DMT symbols, and an even smaller proportion are capable of injecting a significant level of noise energy to both symbols. In other words, it can be accepted with a reasonable accuracy that an impulse event is likely to only affect one DMT symbol.

Impulse probability

The Bernoulli-Weibull model defined in Section 5.2.1 includes as a parameter the impulse probability p. The ratio between impulse length and ADSL symbol duration discussed above requires a special approach to deal with p in the case of ADSL. The impulse probability $P(IN)$ can be represented as:

$$P(IN) = \frac{\tau_{1/2}}{\bar{t}} = \frac{\tau_{adsl}}{\bar{t}} \cdot \frac{\tau_{1/2}}{\tau_{adsl}} = P(IE) \cdot P(IN|IE), \tag{5.28}$$

where $\tau_{1/2}$ is the median impulse duration, τ_{adsl} is the length of the DMT symbol in ADSL, and $\bar{t}$ is the mean impulse inter-arrival time. In order to facilitate the subsequent analysis of data errors in ADSL, the impulse probability $P(IN)$ has been split into the probability

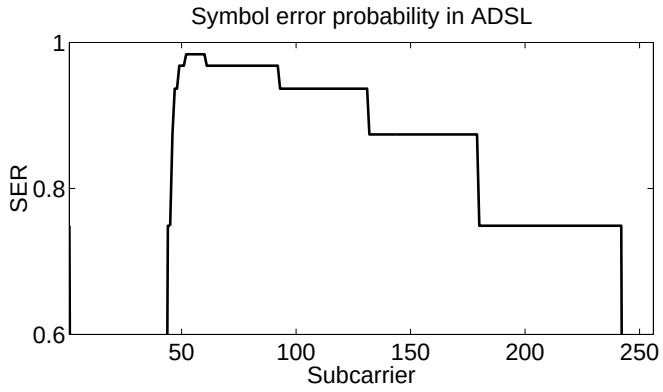

Figure 5.6: *Symbol error probability in the ADSL subcarriers during an impulse event, for conditional impulse probability $P(IN|IE) = 0.073$ and bit loading as in Figure 4.3 - no trellis coding.*

$P(IE) = \tau_{adsl}/\bar{t}$ that the DMT symbol will experience an impulse event, and a conditional probability of impulse noise $P(IN|IE) = \tau_{1/2}/\tau_{adsl}$, if the considered DMT symbol has been hit by an impulse event.

For example, for $\tau_{adsl} = 246.4\,\mu$s, and $\bar{t} = 32.44\,s$ and $\tau_{1/2} = 18\,\mu$s from the example in Section 5.3, the total impulse probability $P(IN) = 5.55 \cdot 10^{-7}$, the probability for impulse event $P(IE) = 0.76 \cdot 10^{-5}$, and the conditional impulse probability $P(IN|IE) = 0.073$.

5.4.2 ADSL subcarrier symbol error probability

Due to the adaptive bit loading in ADSL, the data symbols transmitted in each subcarrier have a different error probability depending on the constellation size, allocated energy, the line transfer function and the noise level in the subcarrier.

An example of the symbol error probability per carrier in ADSL during an impulse event has been plotted in Figure 5.6. The calculations have been carried out using the Bernoulli-Weibull noise model and the approach suggested in Section 5.2.5, with conditional impulse probability $P(IN|IE) = 0.073$. The bit loading is as shown in Figure 4.3 - non-trellis coded case, with 672 bits per DMT symbol, i.e. 2 Mbps user data and 640 kbps overhead including 16 FEC bytes per codeword, and default physical parameters as specified in Section 4.3.5. A comparison between Figures 4.3 and 5.6 shows clearly that for smaller constellations the symbol error probability is lower.

5.4.3 Byte error probability

The bytes in the ADSL frame are composed of bits which in the general case may be transmitted in different subcarriers and have different bit error rates. If the bits that constitute a byte have error probabilities $P_{b,i},\ i = 0 \ldots 7$, then the byte error probability $P_{B,adsl}$ will be:

$$P_{B,adsl} = 1 - \prod_{i=0}^{7}(1 - P_{b,i}). \tag{5.29}$$

Since the impulse noise has a high power relative to the received signal power, the bit error probability is close to its maximum. Therefore, in the particular example given in the previous section, the bit error probability varies very little - from $P_{b,2} = 0.4993$ for 2-bit constellations to $P_{b,6} = 0.4998$ for 6-bit constellations. Therefore, the byte error probability for all subcarriers can be calculated as $P_{B,adsl} = 0.9961$. This is obviously a rather high value and shows that if a DMT symbol is hit by an impulse, in this example it is likely that practically all bytes in the ADSL frame will be damaged.

5.4.4 ADSL frame error probability

The probability that a DMT symbol will be hit by an impulse event is simply $P(IE)$ defined earlier. Although the ADSL frame error probability depends on $P(IE)$, it is also influenced by several other factors, such as whether the DMT symbol will carry a user data frame (as opposed to a synchronisation frame), the error correction capabilities of the FEC code, and the interleaving depth. The frame error probability $P_{F,adsl}$ can in the general case be expressed as:

$$P_{F,adsl} = P(IE) \cdot P_{user} \cdot P_{fail}, \tag{5.30}$$

where $P_{user} = \frac{68}{69}$ is the probability that the affected frame contains user information (one of every 69 DMT symbols is a synchronisation symbol), and P_{fail} is a coefficient corresponding to the FEC correction failure.

Forward error correction

It was discussed in Section 2.5.3, p. 17 that the FEC implemented in ADSL is based on Reed-Solomon (RS) coding and executes in Galois Field GF(2^8) with a maximum codeword length of 255 bytes. If R denotes the number of redundancy bytes in the RS codeword, the code is

capable of correcting up to $R/2$ byte errors with random locations within the codeword. The probability of FEC correction failure is given by (see e.g. [125]):

$$P_{fail} = 1 - P_{cor} = 1 - \sum_{i=0}^{R/2} \binom{N_{cw}}{i} P_{B,adsl}^{i} (1 - P_{B,adsl})^{N_{cw}-i}, \tag{5.31}$$

where N_{cw} is the codeword size, P_{cor} is the probability of FEC error correction, and $P_{B,adsl}$ is the byte error probability in the codeword.

Interleaving

The process of interleaving has the effect of multiplying the error rate at frame level, but reducing the error probability at byte level. If the interleaving depth is D, the correction failure coefficient P_{fail} can be approximated by:

$$P_{fail} \approx \left[1 - \sum_{i=0}^{R/2} \binom{N_{cw}}{i} \left(\frac{P_{B,adsl}}{D} \right)^{i} \left(1 - \frac{P_{B,adsl}}{D} \right)^{N_{cw}-i} \right] \cdot D. \tag{5.32}$$

The coefficient P_{fail} is representative of the combined effect of FEC and interleaving on the errors at frame level, and may have a value larger than 1, which corresponds to an increase in the number of errored frames after interleaving and error correction.

5.4.5 Results

It is interesting to compare the analytical approach presented here with results obtained through simulation. Figure 5.7 shows a comparison between theoretical and simulation results of the ADSL frame error rate for two bit rates. Both the simulation and the calculations have been carried out under identical conditions, with physical parameters and ADSL bit loading as specified in the examples given earlier in this section.

The match between theoretical and simulation results is relatively good, which shows that the assumptions, distribution estimates, and expressions employed in the theoretical analysis reflect closely the physical reality.

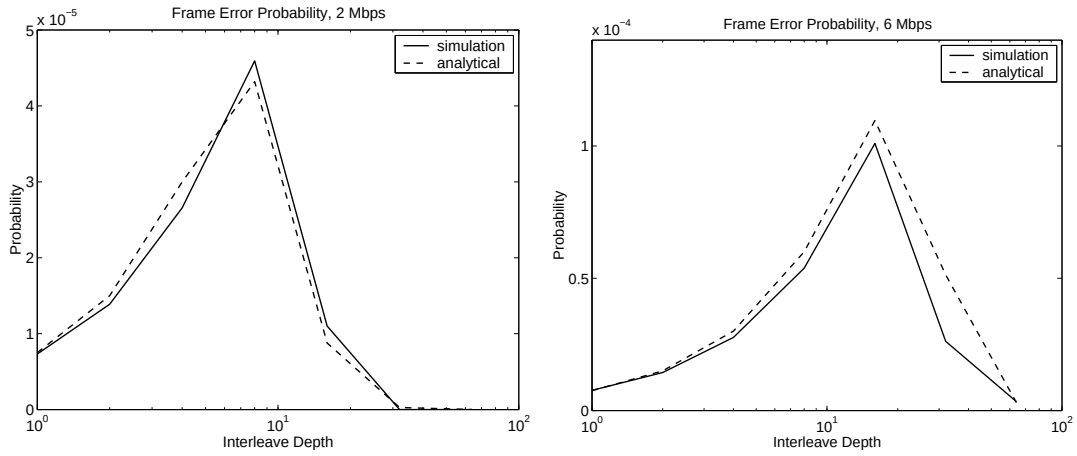

(a) 2 Mbps **(b)** 6 Mbps

Figure 5.7: *ADSL frame error rate for 2 and 6 Mbps interleaved channel with 16 RS redundancy bytes and no trellis coding - theoretical vs. simulation results.*

5.5 Data errors in SHDSL

SHDSL is a DSL service which caters for applications requiring symmetric network access and is expected to prove popular with business customers. While it offers bit rates comparable to those of ADSL, SHDSL has an entirely different framing format. A theoretical analysis of the data errors in SHDSL due to impulse noise will be presented in this section. No simulation analysis for SHDSL has been conducted, as SHDSL has a relatively simple modulation and framing and the theoretical results can be expected to lie close to the results obtained through simulation.

5.5.1 General considerations

Only features relevant to the SHDSL performance in impulse noise will be discussed here, whereas full information can be found in [2, 29].

For the current analysis, the SHDSL system (see Section 2.6, p. 25) is considered to be in a stationary state after the initial hand-shaking procedures. Scrambling, precoding and spectral shaping are not considered since their function is related to the digital signal processing algorithms at the receiver, which are outside the scope of this work and are assumed optimal.

5.5.2 Analysis of PAM in impulse noise

The Bernoulli-Weibull noise model presented in Section 5.2.1 can also be used for PAM, which is the modulation employed in SHDSL. Note, however, that since the PAM signal is only modulated in one dimension, the noise n will also be considered in one dimension only. The combined noise probability density then becomes:

$$f_{n,PAM}(n) = p \cdot f_{wb}(n) + (1-p) f_g(n), \tag{5.33}$$

where n is the combined noise, $f_{wb}(n) = \frac{1}{2}\alpha b |n|^{\alpha-1} e^{-b|n|^\alpha}$ is the univariate Weibull noise density, and $f_g(n) = \frac{1}{\sqrt{2\pi\sigma_g'}} e^{-(n^2)/(2\sigma_g'^2)}$, $\sigma_g' = \sqrt{2}\sigma_g$ is the univariate version of the Gaussian background noise density.

Error probability for PAM signals

The exact expression for symbol error probability for an M-PAM symbol with $M = 2^k$ points at distance d apart is:

$$P_{s,PAM} = 1 - \frac{1}{2^{k-1}} \left[D_A + (2^{k-1} - 1) D_B \right], \tag{5.34}$$

where D_A is the probability of correct decision for the outermost points, and D_B - for the inner points:

$$\begin{aligned} D_A &= \Pr\left(n \geq -\frac{d}{2} \right), \\ D_B &= \Pr\left(|n| \leq \frac{d}{2} \right), \end{aligned} \tag{5.35}$$

where the distance between constellation points d for 2^k-PAM is defined as [125]:

$$d = \sqrt{\frac{6}{2^{2k}-1} \mathcal{E}_s} = \sqrt{\frac{6}{2^{2k}-1} \tau_s \sigma_a^2}, \tag{5.36}$$

where $\mathcal{E}_s$, σ_a^2, and τ_s are respectively the symbol energy, power, and duration.

For M-ary PAM, $M = 2^k$, the symbol error probability $P_{s,PAM}$ can be transformed into bit

error probability $P_{b,PAM}$ simply from [125]:

$$P_{b,PAM} = \frac{P_{s,PAM}}{k}. \tag{5.37}$$

PAM error probability in Bernoulli-Weibull impulse noise environment

After integrating the combined noise probability density (5.33) in the limits specified by (5.35):

$$\begin{aligned} D_A = &\quad p\left[1 - \tfrac{1}{2}e^{-b\left(\frac{d}{2}\right)^{\alpha}}\right] &&+ (1-p)\left[1 - \mathcal{Q}\left(\frac{d}{2\sigma_g'}\right)\right], \\ D_B = &\quad p\left[1 - e^{-b\left(\frac{d}{2}\right)^{\alpha}}\right] &&+ (1-p)\left[1 - 2\mathcal{Q}\left(\frac{d}{2\sigma_g'}\right)\right]. \end{aligned} \tag{5.38}$$

where $\mathcal{Q}(x)$ denotes the $\mathcal{Q}$-function (see Equation 2.5, p. 21). The symbol error probability P_s and the bit error probability P_b can then be found using Equations 5.34 and 5.37 respectively.

5.5.3 Impulse length and SHDSL symbol duration

SHDSL uses a 16-level trellis-coded pulse amplitude modulation (TC-PAM) with a variable symbol duration depending on the data rate [2]. If the user data rate is $R = n \times 64 + i \times 8$ kbps, where $3 \leq n \leq 36$ and $0 \leq i \leq 7$, for $n = 36$, $i = 0, 1$, then the symbol duration $\tau_{shdsl} = \frac{3}{R+8}$ ms. The symbol durations for several typical data rates are shown in Table 5.2.

User data rate, R	1.024 Mbps	2.048 Mbps	2.312 Mbps
Symbol duration, τ_{shdsl}	2.91 μs	1.46 μs	1.29 μs
% impulses shorter than τ_{shdsl}	5.65%	1.45%	1.1%
% impulses longer than $3 \cdot \tau_{shdsl}$	73.5%	89.1%	91%

Table 5.2: *SHDSL symbol duration and percentage of impulses for various bit rates and impulse lengths model as in Section 3.2.3.*

It has been concluded in [3] that less than 2% of all impulses are of a duration 1 μs or less. If the lognormal distribution from Equation 3.7 with parameters $B = 1$, $s_1 = 1.15$, and $\tau_1 = 18\,\mu s$ (Table 3.2) is used again as an example, the percentage of impulses shorter than the symbol or much longer than the symbol can be calculated, and the results are presented in Table 5.2. Obviously the majority of impulse events have a length which is much larger than the duration of the SHDSL modulation symbol.

Impulse probability

An impulse probability as in the Bernoulli-Weibull model (Section 5.2.1) can also be defined for the case of SHDSL with the expression:

$$P(IN) = \frac{\tau_{1/2}}{\bar{t}} = \frac{\tau_{shdsl}}{\bar{t}} \cdot \frac{\tau_{1/2}}{\tau_{shdsl}} = P(IE) \cdot N(IN|IE), \tag{5.39}$$

where $\tau_{1/2}$ is the median impulse duration, τ_{shdsl} is the bit-rate specific length of the symbol in SHDSL, and $\bar{t}$ is the mean impulse inter-arrival time. The impulse probability $P(IN)$ again has been represented as a product of the probability $P(IE) = \tau_{shdsl}/\bar{t}$ that an impulse event will occur, and the conditional coefficient $N(IN|IE) = \tau_{1/2}/\tau_{shdsl}$, which gives the number of SHDSL symbols that are likely to be affected by the impulse event.

For example, for $\bar{t} = 32.44\,s$, $\tau_{1/2} = 18\,\mu$s, and $\tau_{shdsl} = 1.46\,\mu\text{s} \Leftrightarrow R = 2.048$ Mbps, the total impulse probability $P(IN) = 5.55 \cdot 10^{-7}$, the probability for impulse event $P(IE) = 0.45 \cdot 10^{-7}$, and the conditional coefficient $N(IN|IE) = 12.33$.

5.5.4 SHDSL symbol error probability

Although SHDSL lacks the sophisticated formatting used in ADSL, it has a powerful trellis code [2] which is able to overcome long burst errors like those caused by impulse noise. The trellis code uses the two least significant bits to carry one encoded information bit, whereas the two most significant information bits remain unprotected (see Figure 2.10 on p. 25).

To reflect the fact that the unprotected two most significant bits in the PAM symbol have a lower error probability, they can be regarded as a smaller symbol of $k' = 2$ bits, and with a larger minimum distance $d' = 4 \cdot d$. If it is assumed that the trellis code corrects the errors in the least significant bit in the majority of cases, then the error probability for the unprotected bits would represent the error probability for the whole TC-PAM symbol.

For example, for 2 Mbps at a nominal transmit power of 13.5 dBm [2], and after attenuation on a 4 km long twisted pair with 4 mm wire, the symbol error probability (5.34) during an impulse event ($p = 1$) is $P_{s,PAM} = 0.6925$.

5.5.5 Byte error probability

Since one PAM symbol carries 3 bits in the SHDSL implementation, the alignment between the PAM symbols and bytes changes. An estimate of the bit error can be obtained from (5.37). Note that in this case $k = 3$ since a PAM symbol carries 3 information bits. The byte error probability $P_{B,shdsl}$ can then be expressed as:

$$P_{B,shdsl} = 1 - (1 - P_{b,PAM})^8. \tag{5.40}$$

Using the example above, the bit error probability during an impulse event will be $P_{b,PAM} = 0.231$, and the byte error probability $P_{B,shdsl} = 0.878$.

5.5.6 Data block error probability

As discussed earlier, the median duration of an error burst is given by $N(IN|IE) = \tau_{1/2}/\tau_{shdsl}$. Even in the extreme case of 2.312 Mbps data rate ($\tau_{shdsl} = 1.29\mu s$), an error burst in the median case would last 14 symbols, which is equivalent to 5.2 bytes. Such a burst is much shorter than the length of an ATM cell (53 bytes), and even smaller than the average length of an IP packet. Therefore, it can be assumed that the error burst falls entirely within one data block and does not affect neighbouring data blocks.

For a data block of length B_{data} bytes, the data block error probability will be:

$$P_{data,shdsl} = \frac{B_{data} \cdot 8/R}{\bar{t}} \cdot P_{burst}, \tag{5.41}$$

where R is the user bit rate in bits per second, and P_{burst} is the conditional error probability that the data block will be damaged because of an error burst. The probability P_{burst} can be calculated from:

$$P_{burst} = 1 - (1 - P_{B,shdsl})^{B_{err} \cdot R/(R+8)}, \tag{5.42}$$

where $P_{B,shdsl}$ is the byte error probability, B_{err} is the length of the error burst in bytes, and R is the data rate in kbps.

Using the example above, where it was calculated that $P_{B,shdsl} = 0.878$ for $R = 2.048$ Mbps, median error burst of $N(IN|IE) = 12.33$ symbols $\Leftrightarrow B_{err} = 4.62$ bytes, and setting the size of the data block to $B_{data} = 64$ bytes for the purpose of comparison with the case of ADSL, it

is obtained that $P_{burst} \approx 1$ and $P_{data,shdsl} = 7.71 \cdot 10^{-6}$.

5.5.7 Comparison between SHDSL and ADSL

The theoretically calculated ADSL frame error rates for 64 byte - frames (2 Mbps), is $P_{F,adsl} = 7.5 \cdot 10^{-6}$ without interleaving, and $P_{F,adsl} = 3 \cdot 10^{-9}$ with a maximum interleaving depth $D = 64$. It was calculated above that under the same bit rate and data block size, SHDSL exhibits a block error rate $P_{data,shdsl} = 7.71 \cdot 10^{-6}$. Obviously ADSL can mitigate impulse noise better than SHDSL when using the interleaving and error correction techniques, but this comes at the expense of a significantly increased latency and system complexity.

Note also that in a non-interleaved ADSL system, an impulse event typically damages the whole frame of 64 bytes, whereas in SHDSL the median burst length is 4.62 bytes. That is, for low latency applications which can utilise efficiently the bit stream, SHDSL offers a much better performance at the byte level than ADSL.

5.6 Conclusion

In this chapter, an analytical approach to estimating the errors due to impulse noise in DSL systems has been presented. A Bernoulli-Weibull impulse noise model at symbol level has been proposed, and it has been demonstrated that other models which assume Gaussian distribution of the impulse noise amplitudes or Rayleigh distribution of the noise powers give overly optimistic error estimates when used for evaluating impulse noise in telephone lines, due to their lighter tails in comparison with the Weibull distribution.

In order to allow for the analysis of orthogonal signals with the Bernoulli-Weibull noise model, a two-dimensional extension of the Weibull impulse amplitudes statistic has been introduced. The derived bivariate Weibull distribution has correlated variables, however a second type with independent variables has also been considered and it was found that the two distributions produce almost identical error estimates. The latter bivariate distribution was used to develop a numerical solution for the error probability in discrete multi-tone modulation, since a closed-form expression does not exist. A comparison between single and multi-carrier QAM showed that the spreading of noise power among the subcarriers in the process of multi-carrier demodulation is beneficial at high signal-to-noise ratios (SNR), when multi-carrier QAM performs

better, but detrimental at low SNR, when the multi-carrier performs worse than the single carrier QAM.

Further, a framework for calculation of data errors in ADSL has been developed on the basis of the temporal impulse statistics. The analytical solution was found to be close to the simulation results, which shows the accuracy of the underlying assumptions and expressions used for the analytical approach.

The Bernoulli-Weibull noise model was also applied to SHDSL and the data errors in SHDSL analysed. The performance of ADSL downstream was shown to be superior when the full interleaving depth and error correction were used. However, the SHDSL modulation and framing have advantages if a low latency and low byte error rate is required.

Chapter 6
Summary and conclusions

The primary aim of the work described in this thesis is to study the impact of impulse noise in telephone lines on the errors in DSL systems, and the way these errors affect higher layers of the protocol stack. Errors in ATM cells, ADSL frames, and MPEG2 bitstreams transmitted over ADSL have been investigated using simulations, and the errors in both ADSL and SHDSL have been studied through theoretical analysis. New results have been presented concerning impulse noise modelling, theoretical evaluation of errors due to impulse noise in the local loop, and the error patterns of higher layer data in ADSL. In this chapter, the main conclusions of the work are presented, some limitations are pointed out, and suggestions for future work are proposed.

6.1 Achievements of the work

A certain volume of the work has been devoted to justifying the use and describing the aspects of the impulse noise model used in the study. The selected BT/UE/DT model [3, 5, 82] mirrors impulse noise statistics in both the time and frequency domain and is the most suitable model for DSL study proposed to date. One of the contributions of Chapter 3 is a derivation of the distribution of impulse powers from the impulse amplitude statistics. It is shown that similar distributions of the impulse powers are obtained from both the generalised exponential and the Weibull amplitude models, and the latter model has the advantage that the derived impulse powers are also Weibull distributed, only with a different shape parameter from that for the impulse amplitudes. New work has also been presented in the area of impulse spectral modelling, namely a statistical analysis of autocorrelation functions of impulse samples measured in the DT telephone network. The results suggest that DT impulse spectral statistics can be modelled with sufficient accuracy with three spectral components, where either the three frequencies are described with a mixture of distributions, or each frequency - with a separate distribution, and the bandwidths are described with a single distribution.

The BT/UE/DT impulse noise model, together with crosstalk interference models, is exploited in Chapter 4 in a simulation of generic ADSL system. ADSL has been considered because of the outstanding issues with its performance despite its wide use, and the possibility of using the results for VDSL. In the process of designing the simulation platform, a new modification of a bit loading algorithm was developed to allow convergence with simultaneous trellis code constellation expansion and a restriction on the minimum number of bits per constellation. The algorithm operates by biasing the target bit rate upwards by the total number of bits in underloaded channels with less than the minimum allowed number of bits. After the algorithm has found a solution, these underloaded channels are declared as unused. Although no analysis of the conditions for convergence has been presented, extensive testing showed the algorithm is stable in all cases of practical interest.

The performance of ADSL downstream, which is more important from a user point of view than the upstream, is evaluated in terms of errors in ADSL frames, ATM cells, and MPEG2 video bit stream, assuming that the latter two are carried over an ADSL link. These performance measures have been chosen since they are likely to represent better the link error performance as perceived by the user. It is found that interleaving is only useful when set at its maximum depth. Intermediate depths degrade the performance of higher layers in comparison to no interleaving, and the latter is the best option if low latency is required. No such degradation is observed when combining several ADSL frames in one FEC codeword, but this burst error mitigation technique brings benefits only at low data rates due to framing restrictions in the ADSL standard. The trellis coding as implemented in ADSL is not efficient against impulse noise, leaving Reed-Solomon FEC coding as the only error correction technique in ADSL capable of improving the error performance in impulse noise environment. An investigation of the impact of crosstalk demonstrates that alien crosstalk in combination with impulse noise may worsen the error performance in ADSL, which shows the importance of spectral compatibility in an unbundled environment.

The clustering typical of inter-arrival times between impulses is also present in the distribution of error-free intervals between errored data blocks. This distribution depends on the bit rate if the intervals are measured in terms of data blocks, and therefore error-free data blocks may be a better performance measure from the user point of view than error-free seconds. The distribution of error-free intervals also depends on the degree to which a higher layer application can utilise isolated unerrored data blocks which occur between error bursts. In the case of

ATM cells, however, the error protected headers are less affected by impulse noise than the unprotected cell payload, which hinders the detection and subsequent use of such unerrored cells.

In addition to simulation, the problem of estimating errors caused in DSL systems by impulse noise in the local loop is also addressed analytically in Chapter 5. Various works have analysed the impact of impulse noise on modulation symbol errors assuming Gaussian distributed impulse amplitudes or Rayleigh distributed impulse powers [12–14]. Although such an assumption offers good mathematical tractability, it does not reflect the finding that impulse amplitudes in the local loop are better approximated with a generalised exponential or Weibull distribution [3]. Therefore, a novel DSL-specific Bernoulli-Weibull impulse noise model was introduced, which assumes Weibull distributed impulse amplitudes and Gaussian distributed background noise. Analysis of the symbol errors in single-carrier QAM showed that Gaussian or Rayleigh impulse models produce overly optimistic error estimates in comparison with the Weibull model.

A novel extension of the Weibull impulse amplitude model to two dimensions was derived for the case when orthogonal signals, such as QAM, need to be investigated. Since a closed-form expression for the symbol error probability of discrete multi-tone modulation does not exist, a numerical solution to this problem was developed. This solution is based on a bivariate Weibull distribution with independent variables, which was shown to produce error estimates almost identical to the originally derived bivariate Weibull distribution with correlated variables. Calculation of the symbol error in single and multi-carrier QAM using the Bernoulli-Weibull model showed that because of the impulse noise power spreading over the subcarriers, multi-carrier QAM performs better at high SNR, but worse at low SNR than single carrier QAM.

The temporal characteristics of impulse noise were then used to calculate the data errors in ADSL, with solutions close to the simulation results. Applying the same Bernoulli-Weibull and impulse time statistics approach to SHDSL, it is found that ADSL downstream performs better if maximum interleaving depth and strength of FEC code are used, but SHDSL has advantages if low latency and low byte rate are required.

On the basis of the results presented above, conclusions about the impact of noise on higher layers can be drawn. This impact is highly dependant on the specific protocols and applications transmitted over DSL. If lossless data transmission is required, any errors in the data stream

would result in retransmission requests and lower information throughput. Some real-time applications, however, such as audio and video streaming, cannot tolerate the delay caused by retransmission and any errors would result in information loss. In this case, high error rates would lead to noticable artifacts in the transmitted image/sound, as can be seen from the analysis of the MPEG2 video quality.

6.2 Limitations of the work and scope for further research

The contributions made by this study have shown that although impulse noise is a significant impairment for DSL transmission, various framing techniques can mitigate the impact of this noise to some extent depending on the requirements by the end user application. However, certain assumptions adopted in this study limit the conclusions of this work from providing a precise estimation of the errors in real DSL systems. Also, there are a number of areas where further investigation would be worthwhile.

Firstly, this study is based on the assumption of perfect synchronisation, timing, and an ideal channel. Obviously, these assumptions do not hold in most cases, but the influence of imperfect conditions can be compensated through front-end digital signal processing techniques. However, such techniques are vendor specific and their performance differs, i.e. modem chipsets from different manufacturers may exhibit different performance for the same framing parameters. Although the results of this thesis are indicative, it would be interesting in future research to evaluate the impact of imperfect channel conditions and specific front-end signal processing algorithms on the error performance in impulse noise.

Another point of interest is to extend the impulse noise model to generate impulses with more than one spectral component. This will make the impulse noise environment synthesised from this model more realistic, allowing for the direct use of the spectral statistics of DT impulses in impulse generation. A possible approach to model the statistical distributions of the components' frequencies and bandwidths has been suggested based on the DT data analysis. This approach now requires verification of its applicability and specific parametrisation for the case of DT or any other impulse data set.

It is also worth investigating the impact of crosstalk and radio-frequency interference in VDSL systems. Since VDSL utilises a much wider frequency band the the rest of the DSL technologies, these line noise impairments become a significant issue alongside impulse noise. An

analysis of the best approach to their mitigation can improve the VDSL capacity and reliability.

Finally, the analysis of higher protocol layers can be extended to include a larger variety of protocol stack configurations, including TCP/IP. The impact of impulse noise errors on the flow control is particularly important, as the flow control influences significantly the overall throughput of packet protocols. It is known that the congestion control of best-effort protocols, such as IP, does not function properly at high packet error rates, which results in a reduced throughput. Adapting flow control algorithms to high error rate would allow greater flexibility when choosing framing parameters in ADSL/VDSL, e.g. it could be possible to achieve lower latency without compromising the overall data throughput.

Appendix A
Power spectral densities of xDSL signals

The power spectral densities (PSD) of xDSL signals are useful for evaluating the level of crosstalk that these signals induce in other pairs of the same bundle. The analytical expressions for the nominal PSDs of the most common versions of ISDN, HDSL, ADSL, and SHDSL are as follows:

Power spectral density of ISDN signal

The nominal transmit PSD of 2B1Q-modulated ISDN [15–17] signal at 80 kbaud (160 kbps) is given by [6]:

$$S_{ISDN} = k_{ISDN} \times \frac{2}{f_0} \times \frac{\left[\sin\left(\frac{\pi f}{f_0}\right)\right]^2}{\left(\frac{\pi f}{f_0}\right)^2} \times \frac{1}{1+\left(\frac{f}{f_{3dB}}\right)^4}, \quad 0 \le f < \infty, \tag{A.1}$$

where $f_{3dB} = 80$ kHz, $f_0 = 80$ kHz, $k_{ISDN} = \frac{5}{9} \times \frac{V_p^2}{R}$, $V_p = 2.50$ V, and $R = 135\ \Omega$.

Power spectral density of HDSL signal

The nominal transmit PSD of 2B1Q-modulated HDSL [20, 22, 23] signal at 392 kbaud (784 kbps) per pair, full duplex, is defined as [6]:

$$S_{HDSL} = k_{HDSL} \times \frac{2}{f_0} \times \frac{\left[\sin\left(\frac{\pi f}{f_0}\right)\right]^2}{\left(\frac{\pi f}{f_0}\right)^2} \times \frac{1}{1+\left(\frac{f}{f_{3dB}}\right)^8}, \quad 0 \le f < \infty, \tag{A.2}$$

where $f_{3dB} = 196$ kHz, $f_0 = 392$ kHz, $k_{HDSL} = \frac{5}{9} \times \frac{V_p^2}{R}$, $V_p = 2.70$ V, and $R = 135\ \Omega$.

Power spectral density of ADSL signal

The spectrum of the DMT-modulated ADSL [1, 11, 24] signal is different for the downstream (central office to subscriber) and upstream (subscriber to central office) directions. It is assumed that ADSL uses all available subcarriers in each direction, and the total transmit power is such that the PSD would not exceed the maximum allowed PSD.

Downstream

The nominal transmit PSD mask of ADSL downstream signal that uses all 256 DMT subcarriers spaced at 4.3125 kHz and extending up to 1.104 MHz is given by [6]:

$$S_{ADSL,DS} = k_{ADSL,DS} \times \frac{2}{f_0} \times \frac{\left[\sin\left(\frac{\pi f}{f_0}\right)\right]^2}{\left(\frac{\pi f}{f_0}\right)^2} \times |LPF(f)|^2 \times |HPF(f)|^2, \quad 0 \le f < \infty, \tag{A.3}$$

where

$$f_0 = 2.208\,MHz,\ k_{ADSL,DS} = 0.1104\,mW;$$

$$|LPF(f)|^2 = \frac{f_{3dB}^{\alpha}}{f^{\alpha} + f_{3dB}^{\alpha}},\ f_{3dB} = 1.104MHz,\ \alpha = 8;$$

$$|HPF(f)|^2 = \frac{f^{\alpha}}{f^{\alpha} + f_{3dB}^{\alpha}},\ f_{3dB} = 20kHz,\ \alpha = 8;$$

Upstream

The nominal transmit PSD mask of ADSL upstream signal that uses all 32 DMT subcarriers spaced at 4.3125 kHz and extending up to 138 kHz is defined as [6]:

$$S_{ADSL,US} = k_{ADSL,US} \times \frac{2}{f_0} \times \frac{\left[\sin\left(\frac{\pi f}{f_0}\right)\right]^2}{\left(\frac{\pi f}{f_0}\right)^2}, \quad 0 \le f < \infty, \tag{A.4}$$

where $f_0 = 270$ kHz, and

$$k_{ADSL,US}(f) = \begin{cases} -38\ \ dBm/Hz & 28kHz \le f \le 138kHz \\ -38 - 24 \times \left(\frac{f-138000}{43125}\right) dBm/Hz & f > 138kHz \end{cases}.$$

Power spectral density of SHDSL signal

The spectrum of the 16-PAM SHDSL [2, 28, 29] signal is bit rate dependent and its nominal symmetrical transmit PSD is defined as [2]:

$$S_{SHDSL} = \begin{cases} 10^{\frac{-PBO}{10}} \times \frac{k_{SHDSL}}{135} \times \frac{1}{f_{sym}} \times \frac{\left[\sin\left(\frac{\pi f}{Nf_{sym}}\right)\right]^2}{\left(\frac{\pi f}{Nf_{sym}}\right)^2} \times \frac{1}{1+\left(\frac{f}{f_{3dB}}\right)^{2\times Order}} \times \frac{f^2}{f^2+f_c^2}, \ f < f_{int} \\ 0.5683 \times 10^{-4} \times f^{-1.5}, \ f_{int} \leq f \leq 1.1MHz \end{cases}, \tag{A.5}$$

where $f_c = 5$ kHz, f_{int} is the frequency of intersection of the two functions, PBO is the power back-off in dB (the nominal $PBO = 0$ dB), and the remaining parameters are given in Table A.1.

Payload data rate R, kbit/s	k_{SHDSL}	$Order$	N	f_{sym}, ksymb/s	f_{3dB}	P_{SHDS}, dBm
$R < 1536$	7.86	6	1	$(R+8)/3$	$1.0 \times f_{sym}/2$	$P1(R) \leq P_{SHDSL} \leq 13.5$
$R = \{1536, 1544\}$	8.32	6	1	$(R+8)/3$	$0.9 \times f_{sym}/2$	13.5
$R > 1544$	7.86	6	1	$(R+8)/3$	$1.0 \times f_{sym}/2$	13.5

$P1(R) = 0.3486 \log_2(R \times 1000 + 8000) + 6.06$ dBm.

Table A.1: *Parameters for symmetric PSD of SHDSL signal (after [2]).*

Appendix B
Weibull distributions

Although the Weibull distribution has been considered in the literature, it is necessary to make some comments related to its use for the analysis presented in this work.

B.1 Univariate Weibull distribution

In the general case the Weibull distribution has a probability density function (pdf) of the form:

$$f_{wb}(y) = \begin{cases} \alpha b y^{\alpha-1} e^{-by^{\alpha}} & \text{if } \; y \geq 0; \quad \alpha > 0; \quad b > 0 \\ 0 & \text{elsewhere} \end{cases}, \tag{B.1}$$

where α and b are shape parameters.

Moments

The moments $E[y^n]$ of the Weibull distribution are given by:

$$E[y^n] = \int_{-\infty}^{\infty} y^n f_{wb}(y) dy = b^{-n/\alpha} \Gamma\left(1 + \frac{n}{\alpha}\right), \tag{B.2}$$

where $\Gamma(z) = \int_0^{\infty} t^{z-1} e^{-t} dt$ is the gamma function. Hence the mean $\bar{y} = E[y^1]$ and the variance $\sigma_y^2 = E[y^2] - E^2[y^1]$ can be calculated.

Characteristic function

The characteristic function $\Phi(\omega)$ of the function $f(y)$ is defined in the general case as:

$$\Phi(\omega) = \int_{-\infty}^{\infty} e^{j\omega y} f(y) dy = \mathcal{L}[f(y)](-j\omega), \tag{B.3}$$

where $\mathcal{L}[f(y)](s)$ denotes the Laplace transform of the function $f(y)$ over the variable s.

The Weibull pdf, however, has a rather complicated general form of the Laplace transform, which for the function $f(x) = x^v e^{-ax^{l/k}}$ is given by [136]:

$$\mathcal{L}[f(x)](s) = \frac{k^{1/2} l^{v+1/2} s^{-v-1}}{(2\pi)^{(k+l)/2-1}} G_{l,k}^{k,l}\left[\frac{a^k l^l}{k^k s^l}\middle|\begin{matrix}\Delta(l,-v)\\ \Delta(k,0)\end{matrix}\right], \tag{B.4}$$
$$Re(v) > -1;\ Re(s) > 0 \text{ for } l < k,\ Re(a) > 0 \text{ for } l > k,\ Re(s+a) > 0 \text{ for } l = k,$$

where $G_{p,\,q}^{m,n}\left[x\middle|\begin{matrix}a_1,\ldots,a_p\\ b_1,\ldots,b_q\end{matrix}\right]$ is the Meijer's G-function defined as:

$$G_{p,\,q}^{m,n}\left[x\middle|\begin{matrix}a_1,\ldots,a_p\\ b_1,\ldots,b_q\end{matrix}\right] = \frac{1}{2\pi i} \times \int_{\gamma L} \frac{\prod_{j=1}^{m}\Gamma(b_j+s)\prod_{j=1}^{n}\Gamma(1-a_j-s)}{\prod_{j=n+1}^{p}\Gamma(a_j+s)\prod_{j=m+1}^{q}\Gamma(1-b_j-s)} x^{-s} ds. \tag{B.5}$$

More information about the Meijer's G-function and the general conditions for convergence can be found in e.g. [137].

Although the Laplace transform of the Weibull pdf can be simplified for certain special cases, the general form is obviously rather cumbersome. Note also that in the Weibull impulse amplitude models (see Section 3.2.3, p. 37 and [3]), the Weibull parameter α as in (B.1) is less than 1. The range $\alpha < 1$ corresponds to the case $l < k$, in which the Laplace transform (B.4) is defined only for a positive real part of the Laplace variable s. The condition $Re(s) > 0$, however, contradicts the definition of the characteristic function, which postulates that $s = -j\omega$ is purely imaginary. Therefore no explicit expression of the characteristic function is available for the analysis of the Weibull distributed impulse noise amplitudes (see also [98, 133]).

Double Weibull distribution

The double Weibull density, which is used in the impulse amplitude model instead of the original density (B.1) to ensure symmetry of the function around zero, has the form:

$$f_{wb}(u) = \frac{1}{2}\alpha b |u|^{\alpha-1} e^{-b|u|^\alpha}. \tag{B.6}$$

Note that in this case the mean is $\bar{u} = E[u^1] = 0$ and the variance $\sigma_u^2 = E[u^2] - E^2[u^1] = E[u^2]$.

B.2 Bivariate Weibull distributions

Two types of bivariate Weibull distributions have been employed in the theoretical analysis of the impact of impulse noise on orthogonal signals. A brief outline of these distributions is presented here. More information about multivariate Weibull distributions can be found in e.g. [135, 138].

Bivariate Weibull distribution of type I

One possible bivariate Weibull distribution, which will be referred to as type I, is characterised by the following ccdf:

$$\begin{aligned} \bar{F}_{wb,I}(x_1, x_2) &= Pr\left[X_1 > x_1, X_2 > x_2\right] = \\ &= e^{-b(x1^{\beta}+x_2^{\beta})^{\alpha/\beta}}, \;\; x_1, x_2 \geq 0, \; \alpha > 0, \; \beta > 0, \; b > 0, \end{aligned} \tag{B.7}$$

where α, β, and b are parameters.

The marginal ccdfs of this distribution are $\bar{F}_{1,2} = e^{-bx_{1,2}^{\alpha}}$ [135]. The random variables X_1 and X_2 are not independent and the correlation between $log(X_1)$ and $log(X_2)$ is $1 - \left(\frac{\alpha}{\beta}\right)^2$ [135].

The corresponding pdf is defined as:

$$\begin{aligned} f_{wb,I}(x_1, x_2) &= \frac{\partial^2 \bar{F}_{wb,I}(x_1, x_2)}{\partial x_1 \partial x_2} = \\ &= \alpha^2 x_1^{\beta-1} x_2^{\beta-1} e^{-b\,(x_1^{\beta}+x_2^{\beta})^{\alpha/\beta}} \times \\ &\quad \times \left[b^2 \left(x_1^{\beta} + x_2^{\beta}\right)^{2\frac{\alpha}{\beta}-2} + b\left(\frac{\beta}{\alpha} - 1\right)\left(x_1^{\beta} + x_2^{\beta}\right)^{\frac{\alpha}{\beta}-2} \right] \end{aligned} \tag{B.8}$$

In the particular case of the impulse noise model the parameter $\beta = 2$, and after an expansion of the pdf to four quadrants to achieve symmetry the expression becomes:

$$\begin{aligned} f_{wb,I}(u_R, u_I) &= \frac{1}{4} \cdot \alpha^2 \, |u_R| \, |u_I| \, e^{-b\,(u_R^2+u_I^2)^{\alpha/2}} \times \\ &\quad \times \left[b^2 \left(u_R^2 + u_I^2\right)^{\alpha-2} + b\left(\frac{2}{\alpha} - 1\right)\left(u_R^2 + u_I^2\right)^{\frac{\alpha}{2}-2} \right] \end{aligned} \tag{B.9}$$

Bivariate Weibull distribution of type II

Another form of bivariate Weibull distribution is given by:

$$\begin{aligned} \bar{F}_{wb,II}(x_1, x_2) &= Pr\left[X_1 > x_1, X_2 > x_2\right] = \\ &= e^{-b(x_1^\alpha + x_2^\alpha)}, \;\; x_1, x_2 \geq 0, \; \alpha > 0, \; b > 0, \end{aligned} \tag{B.10}$$

where α and b are parameters.

The marginal ccdfs of this distribution are again $\bar{F}_{1,2} = e^{-bx_{1,2}^\alpha}$. Unlike the type I bivariate Weibull, however, the random variables X_1 and X_2 here are independent.

The corresponding pdf is defined as:

$$\begin{aligned} f_{wb,II}(x_1, x_2) &= \frac{\partial^2 \bar{F}_{wb,II}(x_1, x_2)}{\partial x_1 \partial x_2} = \\ &= \alpha^2 \; b^2 \; x_1^{\alpha-1} x_2^{\alpha-1} e^{-b\,(x_1^\alpha + x_2^\alpha)}. \end{aligned} \tag{B.11}$$

After an expansion of the pdf to four quadrants to achieve the symmetry required by the impulse amplitude model the expression becomes:

$$f_{wb,II}(u_R, u_I) = \frac{1}{4} \cdot \alpha^2 \; b^2 \; |u_R|^{\alpha-1} |u_I|^{\alpha-1} e^{-b\,(|u_R|^\alpha + |u_I|^\alpha)} \tag{B.12}$$

Appendix C
Publications

The following papers have been either published or are due to appear in conference proceedings. Those marked by † are reproduced in this appendix.

N. Nedev, S. McLaughlin, D. Laurenson, and R. Daley, "ATM over DSL under the influence of impulse noise", *Proc. IEE Colloquium on New Access Network Technologies*, pp. 10/1 – 10/5, October 2000.

N. Nedev, S. McLaughlin, D. Laurenson, and R. Daley, "ATM cell error performance of xDSL under impulse noise", *Proc. IEEE International Conference on Communications*, vol. 4, pp. 1254 – 1258, June 2001. †

N. Nedev, S. McLaughlin, D. Laurenson, and R. Daley, "The impact of crosstalk in an unbundled environment on ATM and IP", *Proc. 14th International Symposium on Services and Local Access*, pp. 1 – 5, April 2002.

N. Nedev, S. McLaughlin, D. Laurenson, and R. Daley, "Data errors in ADSL and SHDSL systems due to impulse noise", *Proc. IEEE International Conference on Acoustics, Speech, and Signal Processing,*, vol. 4, pp. 4048 – 4051, May 2002.

N. Nedev, S. McLaughlin, D. Laurenson, and R. Daley, "Comparison between interleaving and multiple DMT symbols per RS codeword in ADSL systems", *Proc. IEEE Global Telecommunications Conference*, November 2002.

N. Nedev, S. McLaughlin, D. Laurenson, and D. Levey, "Impact of impulse noise on single and multi-carrier QAM in xDSL systems", to appear in *Proc. IEEE - EURASIP Workshop on Nonlinear Signal and Image Processing*, June, 2003. †

N. Nedev, S. McLaughlin, and D. Laurenson, "Estimating errors in xDSL due to impulse noise", submitted to *IEEE Global Telecommunications Conference*, November, 2003.

ATM Cell Error Performance of xDSL under Impulse Noise

Nedko Nedev[1], Stephen McLaughlin[2], David Laurenson[3], and Robert Daley[4]

[1,2,3]Dept. of Electrical Engineering, The University of Edinburgh,
King's Buildings, Edinburgh, EH9 3JL, UK
[4]Fujitsu Telecommunications Europe Ltd., Birmingham Business Park,
Birmingham, B37 7YU, UK
[1]nhn@ee.ed.ac.uk, [2]sml@ee.ed.ac.uk, [3]dil@ee.ed.ac.uk, [4]r.daley@ftel.co.uk

***Abstract*[*]–This paper considers the cell error performance of ATM over Digital Subscriber Lines (DSL) in the presence of impulse noise.**

In recent years there has been an increasing interest in xDSL technology due to its relatively broad bandwidth and ease of deployment. ATM is a preferred protocol over DSL. ATM, however, has been designed for low bit error rates. Despite error correction protocols, DSL cannot always overcome bursty errors, particularly impulse noise. Interest in DSL has triggered research into impulse noise. A new model has been developed based on surveys on experimental data. Using this model the impact of impulse noise on ATM cell error performance has been traced. Various DSL framings have been found to affect adversely the ATM stream. The interleave depth should be either 1 or large enough to correct the errors. The performance in terms of header and payload errors differs. Time between errored cells exhibits clustering like interarrival times. It is possible within one impulse event to have "good" cells between errored cells. And finally, for higher level applications error free cells is a more appropriate metric than error free seconds.

I. Introduction

In recent years DSL has been gaining popularity as a network access technology. A major impairment of DSL is impulse noise on the line. This prompted new research into this noise and its statistics. Proposals for an impulse noise model applicable to DSL have only recently been released [3-6].

A crucial aspect of a transmission technology is how it affects higher layers from the protocol stack. ATM is often quoted as one of the preferred protocols for transmission over DSL. Impulse noise introduces errors in the DSL system. ATM, however, has been primarily designed for an error free transmission medium. Thus the impact of errors at the DSL layer on ATM has to be determined precisely.

Different applications have different requirements on lower layers. Voice requires low latency and tolerable error rate, whereas data requires lossless transfers where errors can only be overcome by retransmission. If ATM is used as a link protocol it will be important to have information about the cell error performance.

This paper presents results of simulation of an ATM over ADSL system for different bit rates and framing on the DSL level. There has been similar research on influence of impulse noise on ATM/DSL with analysis of the end-to-end TCP/IP performance as well [8]. The current work gives further details about the behaviour and statistics of an ATM stream impaired by impulse noise, and the new and most accurate to date impulse noise model has been used [3,5,6]. Crosstalk from other pairs in the bundle has been accounted for. The performance metrics used are cell/header/payload error rate and statistics of interarrival times between errored cells.

II. Simulation design

Description. The simulation model (Fig. 1) is a generic ADSL modem as defined in [1] (except for trellis coding which is optional in the standards). Only the downstream direction is modelled since it is with larger bandwidth, in a higher frequency range and thus more susceptible to noise than the upstream. Up to four input channels are multiplexed either in a fast or in an interleaved path. Discrete Multi-Tone (DMT) modulation is used as defined in [1]. The noise models are described below.

Crosstalk is taken into account during DMT initialization. The specified bit loading algorithm is based on maximizing the system performance margin for a given bit rate [7]. We only consider kindred crosstalk, i.e. from other ADSL systems. The utilized crosstalk model is as described in [1] for worst case scenario with 49 interfering pairs in a bundle of 50 pairs.

Impulse noise. Several papers [3-6] suggest an impulse noise model suitable for the bandwidth and specifics of the DSL technology. It is based on two large-scale surveys of impulse noise on real telephone lines. These have been carried out independently by Deutsche Telekom and joint British Telecom/Edinburgh University teams. That model is considered the most up-to-date and accurate one. Therefore it has been used for the research presented in the current paper.

[*] This work was supported by Fujitsu Telecommunications Europe Ltd.

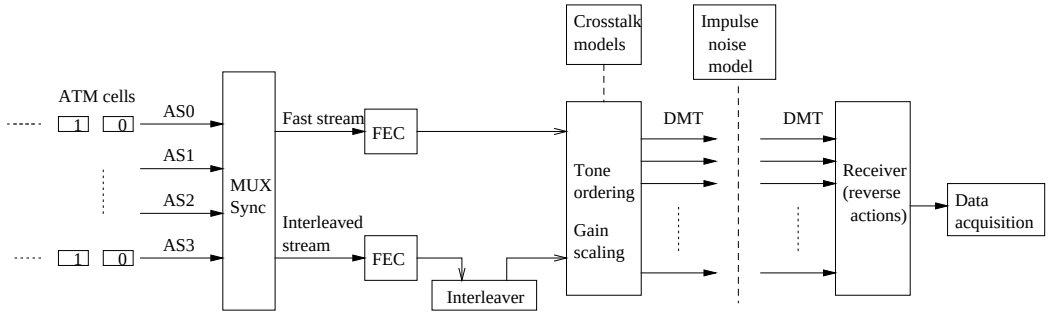

Fig. 1: Block diagram of the simulation software (ADSL modem - generic, downstream only).

In the utilized impulse noise model three statistics are used: pulse lengths, energies and interarrival times. Lengths and voltage amplitudes are modelled with the distributions defined by eq. (1) and (2) [5,6]

$$f_l(t) = B\frac{1}{\sqrt{2\pi}s_1 t}e^{-\frac{1}{2s_1^2}\ln^2(t/t_1)} + (1-B)\frac{1}{\sqrt{2\pi}s_2 t}e^{-\frac{1}{2s_2^2}\ln^2(t/t_2)} \quad (1)$$

$$f_i(u) = \frac{1}{140u_0}e^{-|u/u_0|^{1/5}} \quad (2)$$

where B, s_1, s_2, t_1, and t_2 are parameters for the distribution of impulse lengths t, and u_0 is a parameter in the distribution of impulse amplitude u.

Interarrival times between noise pulses have been found to exhibit a high degree of clustering. To take this into account a Markov chain is used. Each state matches a time region of the interarrival times. Different states are described by separately parameterized and possibly different distributions to fit best the experimental data. For our simulations a Markov chain with four states has been used as proposed in [3]. Each state resembles a Pareto distribution as defined by (3):

$$f_k(\tau) = \frac{\alpha\sigma^\alpha}{\tau^{\alpha+1}}, \tau \geq \sigma, \sigma > 0, \alpha > 0 \quad (3)$$

here α and σ are parameters, and τ is the interarrival time between pulses.

Symbol error probability. [1] postulates that Quadrature Amplitude Modulation (QAM) is used for each DMT subchannel. For an $M=2^k$-ary QAM and k-even, the symbol error probability is given [2] by eq. (4):

$$P_M = 1-\left(1-\left(1-\frac{1}{\sqrt{M}}\right)erfc\left(\sqrt{\frac{3SNR}{2(M-1)}}\right)\right)^2 \quad (4)$$

where erfc is the complementary error function and SNR is the signal to noise ratio. A tight upper bound is known for M-ary QAM for any k (including odd values), namely (5):

$$P_M \leq 2erfc\left(\sqrt{\frac{3kSNR}{2(M-1)}}\right) \quad (5)$$

This bound, however, is too pessimistic for low values of M, and it yields error probability larger than 1 for low SNR values. That is why eq. (4) is used to determine bit allocation and simulation of QAM symbol errors under specific noise levels for all values of k.

Simulation approach. The initialization period of the ADSL link is not considered. It is assumed that the DSL symbol and frame synchronizations remain stable despite the noise. Simulation runs are carried out for different interleaving depths, bit rates and strength of error correction code. All runs, including those with various bit rates, are over an equal number of DSL frames for the purpose of comparison.

III. Results

A. *Frame/cell error rate*

As can be seen (Fig. 2), interleaving makes sense only for depths large enough for the error correction code to cope. Services requiring low latency (voice, video-conferencing) should use no interleaving. For services tolerant to delay, e.g. video on demand, it will be more feasible to use large interleaving depths. The strength of the error correction code affects the performance at the cell level – it leads to lower "cut-off" interleaving depth. For applications using interleaving better error protection will reduce the boundary "cut-off" depth and is thus recommendable. Performance in terms of ATM cells differs from that of DSL multiplexed data frames (after deinterleaving if applicable and FEC). At the considered bit data rates (2 Mbps to 6 Mbps) DSL mux

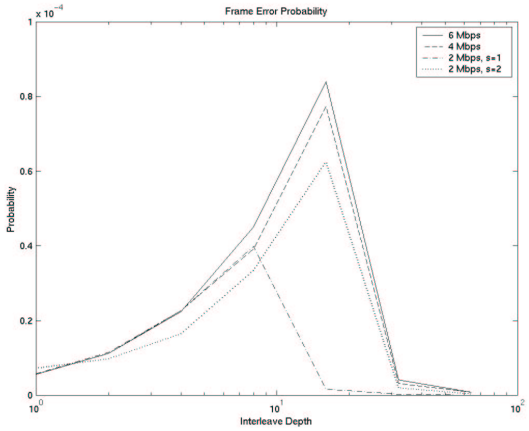

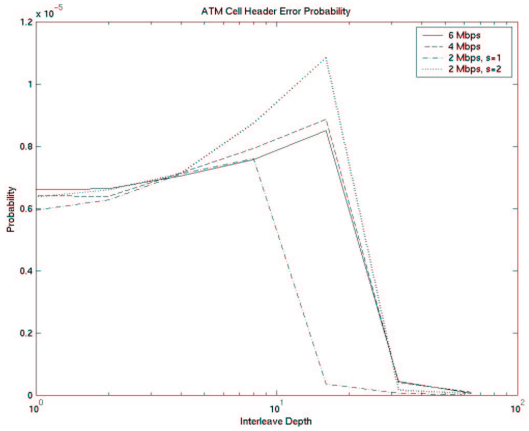

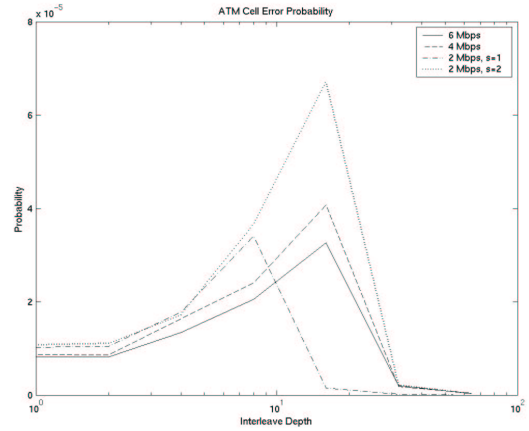

Fig. 2: Mux frame/cell error probability

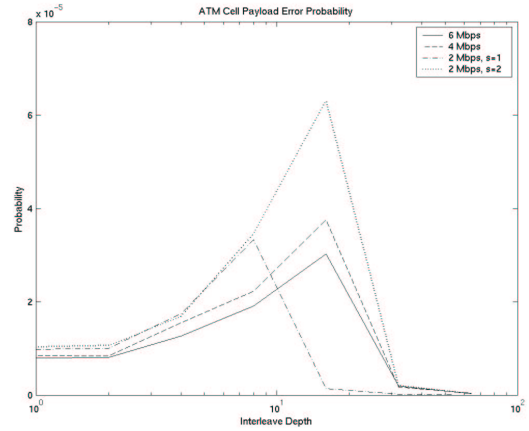

Fig. 3: Header/payload error probability

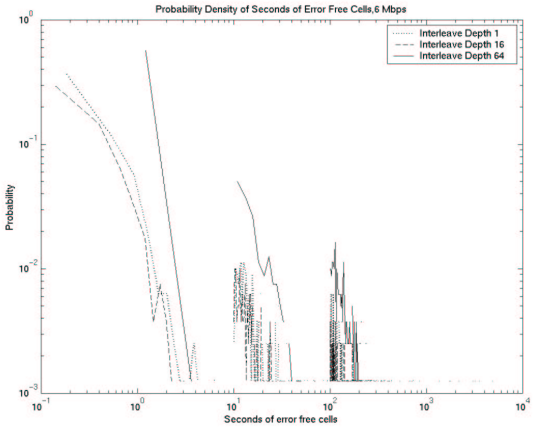

Fig. 4: Seconds of error free cells
6 Mbps, various interleaving depths

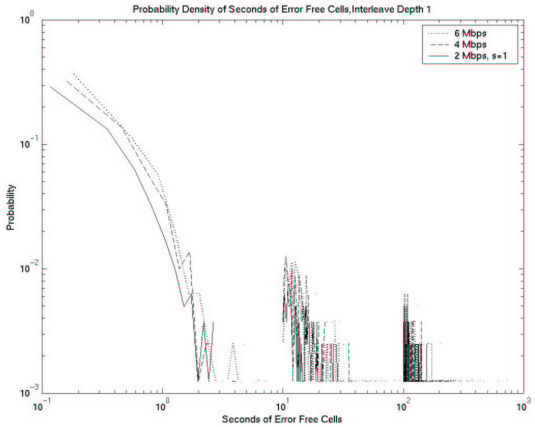

Fig. 5: Seconds of error free cells
ID=1, various bit rates

frames are larger and there is a higher probability that they will be damaged than ATM cells. If the performance of a DSL system is evaluated solely on the basis of errored DSL mux frames, the performance estimation will be inaccurate and pessimistic.

B. Header/payload error probability

Due to the smaller size of the headers their error probability is lower than the payload error probability (Fig. 3). Moreover, errors in headers are much less affected by changes in the interleaving depth than the payload. At the critical interleaving depth (with largest cell error rates) the discrepancy between header and payload error rates is largest. If a header is errored the cell is discarded. A significant proportion of the cells, however, have valid header but damaged payload. I.e., error detection and/or correction have to be provided at higher levels to avoid protocol/application confusions due to undiscovered errors. It should be pointed out that these results are for inter-cell interleaving.

C. Seconds of error free cells

For larger interleaving depths the error correction removes most of the errors and the graph shift towards larger number of error free cells (fig. 4). In general, for lower cell error probability (this trend is not unambiguously related to interleaving depth) the graphs shift to higher seconds of error free cells. It should be noted that despite these shifts the clustering remains as a characteristic.

The statistics of error free seconds do not change significantly with various bit rates (fig. 5), because at low interleaving depths (in this case 1) the cell error probabilities are similar. For the worst interleaving depths (close but lower than the cut-off value) larger dependence should be expected.

D. Minimum acceptable number of unerrored cells

Within one impulse event there may be several unerrored cells between the errored ones. It is up to the application running over ATM to utilize them. It is very unlikely that an IP packet can make use of them due to its much larger size. Other applications, however, such as voice based on AAL2, can benefit from such isolated unerrored cells. The statistics of seconds of error free cells change if a different minimum number of unerrored cells is tolerated. Most error free periods concentrate around smaller values and the graph is shifted downwards (fig. 6).

The changes in the shape of the distributions of error free seconds have to be taken into account if quality of service requirements are specified by means of graphs of such distributions.

Please note that the error free seconds in Fig. 4, 5, and 7 are derived for a minimum acceptable number of five unerrored cells. This relatively large number has been chosen for the purpose of comparison and clearer analysis. For the given DSL framing and ATM cell size, any smaller minimum number of unerrored cells will lead to excessive change in the shape of the distributions and will cover to some extent the impact of changes in other parameters.

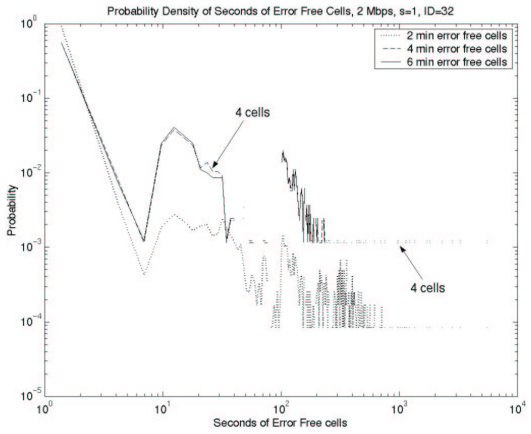

Fig. 6: Seconds of error free cells

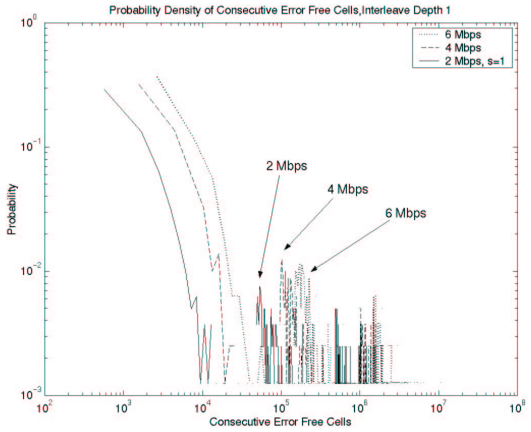

Fig. 7: Error free cells (vs. error free seconds , see fig. 5).

E. Error free seconds or error free cells

The metric error free seconds is very much preferred in the DSL world. From the point of view of higher level applications, however, this might not be the best metric. For different bit rates one unit of time contains a different number of cells. Thus the distribution of consecutive error free cells differs from that for seconds of error free cells. For larger bit rates the distribution shifts towards larger number of consecutive error free cells (compare Fig. 7 with fig. 5). Higher levels will rather be interested in error free cells or even payload bytes/bits.

IV. Conclusion

This work tries to analyze the impact of impulse noise on ATM when carried over DSL. The latest impulse noise models and current DSL standards have been utilized in the research.

The DSL framing has been found to have a very diverse impact on the cell error rate performance. The proper choice of interleaving depth (also reported in [8]) and error correction code need to be made if low cell error rates are to be obtained. The distribution of error free seconds exhibits a high degree of clustering, similar to the one shown by interarrival times of impulse noise.

Protocols transported over ATM may not utilize the ATM stream to full extent, if only few unerrored cells are found between errored ones. E.g. for Voice over ATM over DSL good use could be made of few unerrored cells between error bursts, whereas for applications based on IP over ATM this is not the case. The effective error free seconds' distribution as seen from higher layers varies according to the degree an application can utilize unerrored cells between error bursts.

The error free seconds, used widely to characterize a DSL system, are less suitable from the application point of view. For higher protocol layers, error free cells or even transported error free bytes would be more appropriate. This is to reflect the various bit rates one may come across among the DSL systems.

Acknowledgements

The authors would like to thank K. Jones and G. Cope from Fujitsu Telecom Europe Ltd. for their help and support in conducting the presented research.

References

[1] *Asymmetric Digital Subscriber Line (ADSL) Metallic Interface*, T1E1.4/98-007R5 ANSI 1998

[2] J.G. Proakis, *Digital Communications*, 3rd ed., New York: McGraw-Hill, 1995

[3] D.B. Levey, S. McLaughlin, "Statistics of impulse noise: Interarrival times", *ETSI WG TM6* TD19 993T19A0, 1999

[4] S. McLaughlin, D.B. Levey, "Statistics of impulse noise: Lengths and Energies", *ETSI WG TM6* TD20 993T20A0, 1999

[5] I. Mann, S. McLaughlin, "Appropriate models to represent impulsive noise inter-arrival times, duration, and amplitude statistics", *ETSI WG TM6* TD14, Vienna, Sept. 2000.

[6] W. Henkel, T. Kessler, "An Impulse-noise model - a proposal for SDSL", *ETSI WG TM6* TD45 992T45A0, 1999

[7] P.S. Chow, J.M. Cioffi, J.A.C. Bingham, "A practical discrete multitone transceiver loading algorithm for data transmission over spectrally shaped channels", *IEEE Trans. Commun.*, vol. 43 2 3, pp. 773 –775, Feb.-March-April 1995

[8] D. Laurenson, S. Mclaughlin, G. Cope, "Performance of TCP/IP over ADSL subjected to impulse noise", *Proc. International Signalling and Subscriber Loop Symposium*, Stockholm, 2000, Section 8:1.

IMPACT OF IMPULSE NOISE ON SINGLE AND MULTI-CARRIER QAM IN xDSL SYSTEMS

Nedko H Nedev[1], *Stephen McLaughlin*[2], *D. I. Laurenson*[3], *and David B Levey*[4]
School of Engineering and Electronics, The University of Edinburgh,
King's Buildings, Edinburgh, EH9 3JL, UK
[1]nhn@ee.ed.ac.uk, [2]sml@ee.ed.ac.uk, [3]dil@ee.ed.ac.uk, [4]dbl@ee.ed.ac.uk

ABSTRACT

This paper[1] uses amplitude statistics of impulse noise derived from recent studies in the German and British telephone network to develop a Bernoulli-Weibull model of impulse noise in the local loop. It is shown that earlier models that assume Gaussian distributed impulse amplitudes or Rayleigh distributed powers are not applicable to impulse noise in telephone lines. The Bernoulli-Weibull model is used to develop a closed form expression for the error probability of single carrier QAM. The performance of discrete multitone modulation is also analyzed using the same model and it is shown that multicarrier QAM performs better than single carrier systems but only for low impulse power and low impulse probability.

1 INTRODUCTION

In recent years digital subscriber line (DSL) has been gaining popularity as a high-speed network access technology, capable of the delivery of multimedia services. A limiting factor in the performance of DSL systems is impulse noise, because of its burstiness and potentially high noise power. There have been numerous studies on the statistical nature of impulse noise in telephone lines. Recent broadband noise measurements on the German [1] and British [2, 3] telephone networks have resulted in a new DSL-oriented statistical model of impulse noise [4]. The model includes separate specifications for the distributions of inter-arrival times, amplitudes and durations.

Earlier works have analysed the effect of impulse noise on QAM modulation [5, 6, 7] but with impulse noise models that do not apply to the impulse noise in telephone lines. In [8], the performance of a binary signal in telephones lines has been studied using the impulse noise model from [1]. This model has been modified in later works [4] and the results in this paper are based on the latter, modified version, a brief outline of which is presented in Section 2. The performance of single (SC) and multi-carrier (MC) QAM in impulse noise is analysed in Section 3, the results are discussed in Section 4, and conclusions are drawn in the final section.

[1]This work was supported by Fujitsu Telecommunications Europe Ltd. and British Telecommunications PLC.

2 IMPULSE NOISE MODEL

The salient impulse noise characteristics in the time domain are impulse interarrival times, durations and amplitudes [4]. The probability density function (pdf) of inter-arrival times can be modelled with a Markov renewal process, each state of which describes a time range with a specific distribution [2]. The impulse durations are described with a mixture of two lognormal densities [1]. Originally, it was proposed in [1] to model the amplitude statistics with a generalised exponential distribution of the form: $f_{ge}(u) = \frac{1}{240u_0}e^{-|u/u_0|^{1/5}}$, where u is the voltage and u_0 - a parameter. However, a double Weibull density has been proposed as an alternative since it is mathematically more easily tractable and also provides a good approximation of the amplitude densities [4]:

$$f_{wb}(u) = \frac{1}{2}\alpha b|u|^{\alpha-1}e^{-b|u|^{\alpha}}, \qquad (1)$$

where α and b are parameters. This expression can be extended to the complex space so that the impact of impulse noise on orthogonal signals can be evaluated. If the impulse noise amplitude u is Weibull distributed, then the complex impulse noise with real and imaginary components u_R and u_I will have a bivariate Weibull complementary cumulative distribution function (ccdf) of the form:

$$\bar{F}_{wb}(u_R, u_I) = e^{-b'(u_R^2+u_I^2)^{\alpha/2}}, \quad u_R, u_I \geq 0,\ \alpha > 0,\ b' > 0, \qquad (2)$$

where the parameter b has been scaled to $b' = 2^{\alpha/2}b$ to reflect the fact that both components of the complex impulse noise contribute to the noise power. The bivariate Weibull pdf, after expansion to four quadrants to allow for negative values of u_R and u_I, is defined as:

$$f_{wb}(u_R, u_I) = \tfrac{1}{4} \cdot \alpha^2 \, |u_R| \, |u_I| \, e^{-b' \, (u_R^2 + u_I^2)^{\alpha/2}} \times$$
$$\times \left[b'^2 \left(u_R^2 + u_I^2\right)^{\alpha-2} + b' \left(\tfrac{2}{\alpha} - 1\right) \left(u_R^2 + u_I^2\right)^{\frac{\alpha}{2}-2} \right] \quad (3)$$

A local loop - oriented noise model at symbol level shall now be introduced. The received signal $r(m)$ in the symbol domain can be expressed as:

$$r(m) = a(m) + n(m), \quad (4)$$

where $a(m)$ is the transmitted complex symbol drawn from the QAM constellation under consideration. Let us assume that the combined complex noise $n(m)$ at the receiver is a sum of an impulse Bernoulli-Weibull component and a background Gaussian componen, i.e.:

$$n(m) = bnl(m) \cdot w(m) + \overline{bnl}(m) \cdot g(m), \quad (5)$$

where w is a complex Weibull process with parameters α and b, g is a complex additive white Gaussian noise (AWGN) with mean zero and variance $2\sigma_g^2$, and bnl is a real Bernoulli process, i.e. an independent and identically distributed (i.i.d.) sequence of zeros and ones with probability $\Pr(bnl = 1) = p$. It is assumed that the process w refers to the combined effect of impulse noise and AWGN, because the distribution is derived from empirical data of this very combination. Note also that the real and imaginary parts u_R and u_I of the complex AWGN can be considered independent [6, 7] with joint pdf:

$$f_g(u_R, u_I) = \frac{1}{2\pi\sigma_g^2} e^{-(u_R^2 + u_I^2)/(2\sigma_g^2)}. \quad (6)$$

3 PERFORMANCE OF SC AND MC QAM IN IMPULSE NOISE

For a rectangular M-QAM constellation with M = $2^k, k = 2, 4, 6, ...$ points at distance d apart, the exact expression for symbol error probability is [6]:

$$P_{s,QAM} = 1 - \tfrac{1}{2^{k-2}} \Big[D_1 + (2^{\frac{k}{2}-1} - 1)^2 D_2 +$$
$$+ (2^{\frac{k}{2}-1} - 1) D_3 + (2^{\frac{k}{2}-1} - 1) D_4 \Big], \quad (7)$$

where D_1 is the probability of correct decision for the corner symbols, D_2 for the inner square, and D_3 and D_4 for the horizontal and vertical edges less the corners:

$$\begin{aligned} D_1 &= \Pr\left(n_R \geq -\frac{d}{2} \quad \& \quad n_I \geq -\frac{d}{2} \right), \\ D_2 &= \Pr\left(|n_R| \leq \frac{d}{2} \quad \& \quad |n_I| \leq \frac{d}{2} \right), \\ D_3 &= \Pr\left(|n_R| \leq \frac{d}{2} \quad \& \quad n_I \geq -\frac{d}{2} \right), \\ D_4 &= \Pr\left(n_R \geq -\frac{d}{2} \quad \& \quad |n_I| \leq \frac{d}{2} \right). \end{aligned} \quad (8)$$

The probability of symbol error can be converted into an equivalent probability of a binary digit error. For M-ary orthogonal signals with symbol error probability $P_{s,M}$, the bit error probability P_b is given by [9]:

$$P_b = \frac{2^{k-1}}{2^k - 1} P_{s,M}, \quad M = 2^k. \quad (9)$$

Error probability for single carrier QAM

Using the noise model from the previous section, it can be shown that for SC QAM the combined noise density is:

$$\begin{aligned} f_{n,SC}(n_R, n_I) &= p \cdot f_{wb}(n_R, n_I) + \\ &+ (1-p) f_g(n_R, n_I), \end{aligned} \quad (10)$$

where n_R and n_I are the real and imaginary noise components, and $f_{wb}(n_R, n_I)$ and $f_g(n_R, n_I)$ are the bivariate Weibull and bivariate Gaussian probability densities specified in the previous section.

By integrating $f_{n,SC}(n_R, n_I)$ in the appropriate limits as specified in (8), it is obtained:

$$\begin{aligned} D_1 &= p \left[1 - e^{-b' \left(\frac{d}{2}\right)^\alpha} + \tfrac{1}{4} e^{-b' \, 2^{\alpha/2} \left(\frac{d}{2}\right)^\alpha} \right] + \\ &+ (1-p) \left[1 - \mathcal{Q}\left(\tfrac{d}{2\sigma_g}\right) \right]^2, \\ D_2 &= p \left[1 - 2e^{-b' \left(\frac{d}{2}\right)^\alpha} + e^{-b' \, 2^{\alpha/2} \left(\frac{d}{2}\right)^\alpha} \right] + \\ &+ (1-p) \left[1 - 2\mathcal{Q}\left(\tfrac{d}{2\sigma_g}\right) \right]^2, \\ D_{3,4} &= p \left[1 - \tfrac{3}{2} e^{-b' \left(\frac{d}{2}\right)^\alpha} + \tfrac{1}{2} e^{-b' \, 2^{\alpha/2} \left(\frac{d}{2}\right)^\alpha} \right] + \\ &+ (1-p) \left[1 - \mathcal{Q}\left(\tfrac{d}{2\sigma_g}\right) \right] \left[1 - 2\mathcal{Q}\left(\tfrac{d}{2\sigma_g}\right) \right], \end{aligned} \quad (11)$$

where $\mathcal{Q}(x) = \frac{1}{\sqrt{2\pi}} \int_x^\infty e^{-y^2/2} dy$ is the $\mathcal{Q}$-function. The symbol error probability P_s and the bit error probability P_b can then be found using (7) and (9) respectively.

Note also that in all subsequent results the signal-to-background noise (SBR) ratio is defined as $\frac{\sigma_a^2}{2\sigma_g^2}$, and the signal-to-impulse noise ratio (SIR) - as $\frac{\sigma_a^2}{2\sigma_i^2}$.

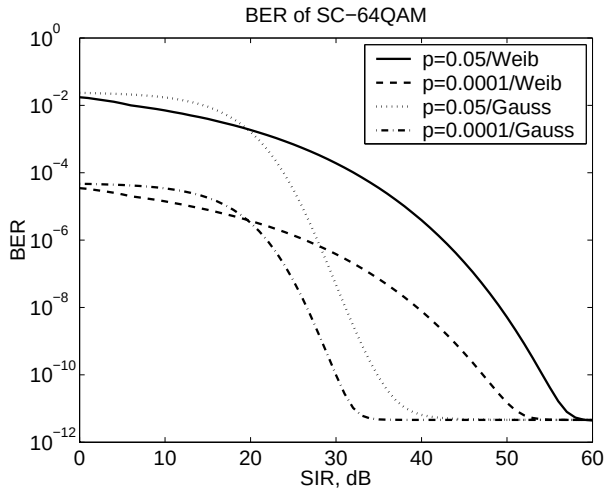

Figure 1: Comparison between the performance of SC-64QAM for Bernoulli-Weibull and Bernoulli-Gaussian impulse noise model with SBR = 30 dB.

It is interesting to compare the Bernoulli-Weibull model with the results obtained in [5, 6, 7] using Gaussian or Rayleigh impulse models. Fig. 1 shows plots of the performance in Bernoulli-Weibull and Bernoulli-Gaussian impulse noise. If the impulse amplitudes are Weibull distributed the performance of single carrier QAM remains poor for significantly higher signal-to-impulse noise ratios (SIR) than in the case of Gaussian impulse amplitudes. This is due to the fact that the Weibull distribution is more heavy-tailed than the Gaussian distribution. Therefore models which assume Gaussian impulse amplitudes, which are also equivallent to Rayleigh power distributions [6], offer less pessimistic results for the analysis of digital subscriber line systems.

Error probability for multi-carrier QAM

The most common MC-QAM version in DSL systems is discrete multi-tone (DMT), which is employed in Asymmetric DSL and Very high-speed DSL. DMT uses an inverse discrete Fourier transform (IDFT) to modulate the symbols.

Assuming perfect synchronisation, timing, and an ideal channel, the received symbol $r(m)$ for N-carrier DMT modulation is given by [10]:

$$r(m) = \frac{1}{\sqrt{N}} \sum_{i=0}^{N-1} a(i) e^{j2\pi im/N} + n(m), \quad m = 0, 1, \ldots, N-1, \qquad (12)$$

where again $a(m)$ is the transmitted QAM data symbol, and $n(m)$ is the combined complex noise defined in (5). Performing a discrete Fourier transform (DFT) on the received sequence $r(m)$ yields the recovered transmitted symbols $a(m)$ and a noise component $n_f(m)$:

$$n_f(m) = \frac{1}{\sqrt{N}} \sum_{i=0}^{N-1} n(i) e^{-j2\pi im/N}, \quad m = 0, 1, 2...N-1. \qquad (13)$$

Using (13), it is possible to derive an expression for the characteristic function (cf) of the complex noise component $n_f(m)$, namely:

$$\Phi_{n_f}(\omega_1, \omega_2) = \sum_{i=0}^{N} \binom{N}{i} p^i (1-p)^{N-i} \times \times \Phi_{wb}^i(\omega_1, \omega_2) \Phi_g^{N-i}(\omega_1, \omega_2) \qquad (14)$$

where $\Phi_{wb}(\omega_1, \omega_2)$ and $\Phi_g(\omega_1, \omega_2)$ are the characteristic functions of the bivariate Weibull and bivariate Gaussian distributions respectively.

The cf of a bivariate distribution with pdf $f(x_1, x_2)$ is given in the general case by the expression $\Phi(\omega_1, \omega_2) = \int_{-\infty}^{\infty} \int_{-\infty}^{\infty} e^{j\omega_1 x_1 + j\omega_2 x_2} f(x_1, x_2) dx_1 dx_2$. Hence the cf $\Phi_g(\omega_1, \omega_2)$ of the bivariate Gaussian distribution with pdf (6) is $\Phi_g(\omega_1, \omega_2) = e^{-\sigma_g^2(\omega_1^2 + \omega_2^2)/2}$.

For the Weibull cf, however, no explicit expressions are available if the shape parameter α is smaller than 1 [11], which is the case in impulse amplitude statistics [4]. That is why a numerical approach has been developed to calculate the noise pdf for multi-carrier QAM.

Since multiplication of cfs corresponds to convolution of pdfs, the pdf of the combined noise in the case of N-carrier DMT modulation can therefore be expressed as:

$$f_{n,MC}(n_R, n_I) = \sum_{i=0}^{N} \binom{N}{i} p^i (1-p)^{N-i} \times \times f_{wb}^{(*\,i)}(n_R, n_I) * \frac{1}{2\pi\sigma_{g,i}^2} e^{-(n_R^2 + n_I^2)/(\sigma_{g,i}^2)}, \qquad (15)$$

where $\sigma_{g,i}^2 = \frac{(N-i)\sigma_g^2}{N}$, and $f_{wb}^{(*\,i)}(n_R, n_I)$ denotes i-fold convolution of the function $f_{wb}(n_R, n_I)$.

The two-dimensional convolution of two functions $f_1(x, y)$ and $f_2(x, y)$ is defined in the general case as $f_1(x, y) * f_2(x, y) = \int_{-\infty}^{\infty} \int_{-\infty}^{\infty} f_1(v, w) f_2(x - v, y - w)\, dv\, dw$. Similarly to the Weibull characteristic function, no closed-form solution to the convolution of the Weibull probability densities can be found.

It is possible to evaluate the convolutions in (15) numerically. However, numerical convolution of two-dimensional functions poses significant computational and memory requirements when high precision is required. Therefore, a bivariate Weibull distribution of an alternative form has been considered,

which gives sufficiently accurate results for a significantly lower usage of computing resources.

Let us assume that the two orthogonal components of the complex impulse noise are independent and Weibull distributed with parameters α and b. The joint distribution of the two components is also Weibull of a form which will be referred to in this work as type II, and which has the following ccdf:

$$\bar{F}_{wb,II}(u_R, u_I) = e^{-b'(u_R^\alpha + u_I^\alpha)},\ u_R, u_I \geq 0, \quad (16)$$

The pdf of this distribution will simply be the product of the marginal pdfs, and after an expansion to four quadrants to allow for negative values of u_R and u_I has the form:

$$f_{wb,II}(u_R, u_I) = \tfrac{1}{4}\alpha^2 b'^2 |u_R|^{\alpha-1}|u_I|^{\alpha-1} \times \\ \times\ e^{-b'(|u_R|^\alpha + |u_I|^\alpha)}. \quad (17)$$

Going back to the original bivariate Weibull distribution with ccdf (3), which will be referred to as type I, there is a certain degree of dependence between its variables. The correlation between the random variables $\log U_R$ and $\log U_I$ is given by [12]: $1 - \left(\frac{\alpha}{2}\right)^2$. It has been found, however, that the error rates calculated using the original Weibull distribution do not differ significantly from the error rates based on the alternative Weibull model introduced in the current section, the latter producing a slightly more pessimistic estimates than the former. The type II distribution offers considerable computational advantages over type I, since the numerical convolution needs to be carried out only in one dimension. Therefore, the alternative bivariate Weibull distribution will be used for evalutating the performance of the multi-carrier QAM.

Using the alternative bivariate Weibull distribution of type II, the combined noise pdf for N-DMT modulation can be calculated from:

$$f_{nII,MC}(n_R, n_I) = \textstyle\sum_{i=0}^{N} \binom{N}{i} p^i (1-p)^{N-i} \times \\ \times\ f_{wb}^{(*\,i)}(n_R) * \tfrac{1}{\sqrt{2\pi}\sigma_{g,i}} e^{-n_R^2/\sigma_{g,i}^2} \times \\ \times\ f_{wb}^{(*\,i)}(n_I) * \tfrac{1}{\sqrt{2\pi}\sigma_{g,i}} e^{-n_I^2/\sigma_{g,i}^2}, \quad (18)$$

where $\sigma_{g,i}^2 = \frac{(N-i)\sigma_g^2}{N}$, the function $f_{wb}(x) = \frac{1}{2}\alpha b' |x|^{\alpha-1} e^{-b'|x|^\alpha}$ is the marginal pdf of the bivariate type II - Weibull distribution, and $f_{wb}^{(*\,i)}(x)$ denotes i-fold convolution of the function $f_{wb}(x)$.

Note that (18) specifies only one-dimensional convolution, which in the general case is defined as $f_1(x) * f_2(x) = \int_{-\infty}^{\infty} f_1(v) f_2(x-v) dv$. Therefore, this approach is computationally much less intensive than the one using the original type I - Weibull pdf.

After evaluating the noise pdf (18), it can be integrated numerically in the limits specified in (8), and then the probabilities of correct detection can be substituted in (7) to yield the symbol error probability.

4 ANALYTICAL RESULTS

The analysis in the previous section is used here to consider the bit error rate (BER) for single carrier 64QAM (Fig. 2), and for 256-carrier 64QAM (Fig. 3) for various values of p. As it can be seen from the two figures, MC QAM outperforms single carrier QAM for high values of SIR, because the DFT operation spreads the impulse over all N data symbols. For low SIR, however, MC QAM has a higher error rate than the single carrier QAM due to the fact the the noise level is high and after the spreading it affects the majority of subchannels. Note that for very low values of SIR, the error rate still remains higher than that of SC QAM even if the impulse probability p is small. This is a result of the heavy tail of the Weibull distribution, which is related to the tendency of impulse amplitudes to exhibit occasionally very high amplitudes.

5 CONCLUSIONS

The impact of impulse noise in the local loop on the error performance of QAM has been analysed in this paper. A closed-form expression for single carrier QAM has been derived and it has been shown that earlier impulse noise models that assume Gaussian or Rayleigh impulse distribution cannot be applied to impulse noise in telephone lines. The performance of multicarrier QAM has also been evaluated numerically from this model. It can be seen from the analysis in this paper that the performance of MC QAM depends on the impulse power, and to a lesser extent on the impulse probability. For low impulse power MC QAM performs better than single carrier. If, however, the impulse power is high and especially for high impulse probability, SC QAM is potentially a better option.

References

[1] W. Henkel and T. Kessler, "A wideband impulsive noise survey in the German telephone network: statistical description and modelling," *AEÜ*, vol. 48, pp. 277 – 288, November/December 1994.

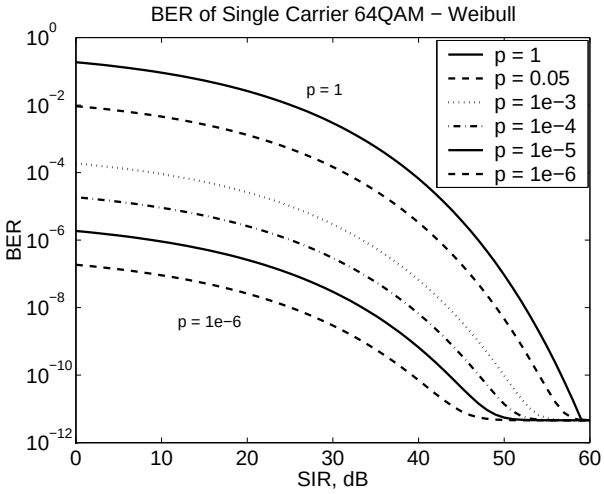

Figure 2: Analytical performance of SC-64QAM in local loop impulse noise with SBR = 30 dB.

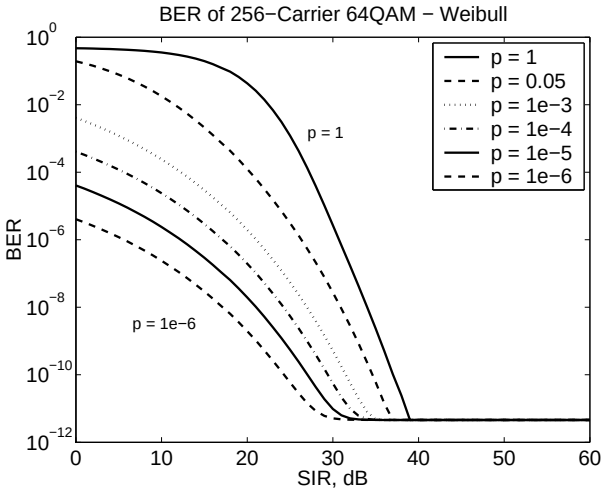

Figure 3: Analytical performance of 256-carrier 64QAM in local loop impulse noise with SBR = 30 dB.

[2] D. B. Levey and S. McLaughlin, "The statistical nature of impulse noise interarrival times in digital subscriber loop systems," *Signal Processing*, vol. 82, no. 3, pp. 329 – 351, 2002.

[3] S. McLaughlin and D. B. Levey, "Statistics of impulse noise: Lengths and energies," *Submission to ETSI WG TM6, TD20, 993T20A0*, September 1999.

[4] I. Mann, S. McLaughlin, W. Henkel, R. Kirkby, and T. Kessler, "Impulse generation with appropriate amplitude, length, inter-arrival, and spectral characteristics," *IEEE J. Select. Areas Commun.*, vol. 20, pp. 901 – 912, June 2002.

[5] S. A. Kosmopoulos, P. T. Mathiopoulos, and M. D. Gouta, "Fourier-Bessel error performance analysis and evaluation of M-ary QAM schemes in an impulsive noise environment," *IEEE Trans. Commun.*, vol. 39, pp. 398 – 404, March 1991.

[6] M. Ghosh, "Analysis of the effect of impulse noise on multicarrier and single carrier QAM systems," *IEEE Trans. Commun.*, vol. 44, pp. 145 – 147, February 1996.

[7] M. Hamza, H. T. Huynh, and P. Fortier, "Optimal detection of QAM in a man-made noise environment," in *Proc. IEEE VTC*, (Amsterdam, The Netherlands), pp. 1301 – 1306, July 1999.

[8] Y. H. Chew, T. T. Tjhung, T. He, and C. C. Ko, "Estimation of BER performance over an impulse noise channel," *IEE Electron. Lett.*, vol. 35, pp. 273 – 274, February 1999.

[9] J. G. Proakis, *Digital Communications*. McGraw-Hill, N.Y., 3rd ed., 1995.

[10] J. A. C. Bingham, "Multicarrier modulation for data transmission: an idea whose time has come," *IEEE Commun. Mag.*, vol. 28, pp. 5 – 14, May 1990.

[11] J. Abate and W. Whitt, "An operational calculus for probability distributions via Laplace transforms," *Advances in Applied Probability*, vol. 28, pp. 75 – 113, March 1996.

[12] P. Hougaard, "Fitting a multivariate failure time distribution," *IEEE Trans. Rel.*, vol. 38, pp. 444 – 448, October 1989.

Appendix D
CD

This appendix describes the contents of the CD accompanying the thesis. The CD contains files of MPEG-2 video bitstreams which illustrate the impact of impulse noise on the quality of video transmitted in the downlink of an ADSL system.

D.1 CD contents

The MPEG-2 video bitstream files are divided into two directories. The `mpeg2_1.5Mbps/` directory contains video files at 1.5 Mbps, and the `mpeg2_4.0Mbps/` directory - at 4 Mbps.

The files in both directories are labelled as `mpeg2test_bbbb_cccc.mpg` where:

- `bbbb` is the bitrate: `1.5M` = 1.5 Mbps, and `4.0M` = 4 Mbps.
- `cccc` is the bitstream type: `orig` = original [129], and `idNN` = transmitted, where `NN` = 01, 02, 04, 08, 16, 32, or 64 is the interleaving depth.

D.2 Software requirements

In order to view the video files supplied with this CD, you will need to have an MPEG-2 video bitstream player installed on your computer. A suitable shareware version of a such a player for the MS Windows 9x, Me, NT 4.0, 2000, and XP operating systems can be donwloaded free of charge from [139] (as of February, 2003).

Note that on encountering an error in the video bitstream, some video decoders jump to the next "good" video frame, rather than show images destorted by errors. In order to appreciate fully the impact of errors on the video quality, and the difference between this quality for different interleaving depths, you need to use a decoder which shows *all* (including the errored) video frames, such as the decoder suggested above.

References

[1] "Asymmetric digital subscriber line (ADSL) transceivers," *ITU Recommendation G.992.1*, 1999.

[2] "Single-pair high-speed digital subscriber line (SHDSL) transceivers," *ITU Recommendation G.991.2*, 2001.

[3] I. Mann, S. McLaughlin, W. Henkel, R. Kirkby, and T. Kessler, "Impulse generation with appropriate amplitude, length, inter-arrival, and spectral characteristics," *IEEE Journal on Selected Areas in Communications*, vol. 20, pp. 901 – 912, June 2002.

[4] S. McLaughlin, W. Henkel, R. Kirkby, and T. Kessler, "Text for realistic impulsive noise model," *Submission to ETSI WG TM6, TD20, 011T20*, February 2001.

[5] D. B. Levey and S. McLaughlin, "The statistical nature of impulse noise interarrival times in digital subscriber loop systems," *Signal Processing*, vol. 82, no. 3, pp. 329 – 351, 2002.

[6] T. Starr, J. M. Cioffi, and P. J. Silverman, *Understanding Digital Subscriber Line Technology*. Prentice Hall, Upper Saddle River, N.J., 1999.

[7] J.-J. Werner, "Impulse noise in the loop plant," in *Proceedings of the IEEE International Conference on Communications*, vol. 4, pp. 1734 – 1737, June 1990.

[8] P. Mertz, "Model of impulsive noise for data transmission," *IRE Transactions on Communications Systems*, vol. 9, no. 6, pp. 130 – 137, 1961.

[9] J. Berger and B. Mandelbrot, "A new model for error clustering in telephone circuits," *IBM Journal Research and Development*, vol. 7, pp. 224 – 236, 1963.

[10] "Interface between networks and customer installations - very-high speed digital subscriber lines (VDSL) metallic interface (trial-use standard)," *ANSI Standard T1.424-Trial Use*.

[11] "Network and customer installation interfaces - asymmetric digital subscriber line (ADSL) metallic interface," *ANSI Standard T1.413-1998*.

[12] S. A. Kosmopoulos, P. T. Mathiopoulos, and M. D. Gouta, "Fourier-Bessel error performance analysis and evaluation of M-ary QAM schemes in an impulsive noise environment," *IEEE Transactions on Communications*, vol. 39, pp. 398 – 404, March 1991.

[13] M. Ghosh, "Analysis of the effect of impulse noise on multicarrier and single carrier QAM systems," *IEEE Transactions on Communications*, vol. 44, pp. 145 – 147, February 1996.

[14] H. T. Huynh, P. Fortier, and B. Vo, "Influence of impulse rate on the QAM error probability in a non-gaussian noise environment," in *Sixth Communications Theory Mini-Conference in Conjunction with Globecom*, (Phoenix, Arizona), November 1997.

[15] "Digital transmission system on metallic local lines for ISDN basic rate access digital sections and digital line systems," *ITU Recommendation G.961(Rev 1)*, 2000.

[16] "ISDN basic access interface for use on metallic loops for application at the network side of NT, layer 1 specification," *ANSI Standard T1.601-1999*.

[17] "Transmission and multiplexing (TM) - integrated services digital network (ISDN) basic rate access; digital transmission systems on metallic local lines," *ETSI TS 102 080-v.1.3.2*, 2000.

[18] "Network and customer installation interfaces - DS1 - electrical interface," *ANSI Standard T1.403-1999*.

[19] "Physical/electrical characteristics of hierarchical digital interfaces," *ITU Recommendation G.703*, 2001.

[20] "High-bit-rate digital subscriber line (HDSL)," *ANSI Standard T1.TR.28-1994*.

[21] "High bit rate digital subscriber line - 2nd generation (HDSL2)," *ANSI Standard T1.418-2000*.

[22] "High speed digital subscriber line (HDSL) transceivers," *ITU Recommendation G.991.1*, 1998.

[23] "Transmission and multiplexing (TM) - high bit-rate digital subscriber line (HDSL) transmission systems on metallic local lines," *ETSI TS 101 135-v.1.5.3*, 2000.

[24] "Transmission and multiplexing (TM) - access transmission systems on metallic access cables; asymmetric digital subscriber line (ADSL) - european specific requirements," *ETSI TS 101 388-v.1.3.1*, 2002.

[25] "Splitterless asymmetric digital subscriber line (ADSL) transceivers," *ITU Recommendation G.992.2*, 1999.

[26] "Splitterless asymmetric digital subscriber line (ADSL) transceivers," *ANSI Standard T1.419-2000*.

[27] "Single-carrier rate adaptive digital subscriber line (RADSL)," *ANSI Standard T1.TR.59-1999*.

[28] "Transmission and multiplexing (TM) - access transmission systems on metallic access cables; symmetrical single pair high bit rate digital subscriber line (SDSL)," *ETSI TS 101 524-v.1.1.3*, 2001.

[29] "Single-pair high-speed digital subscriber line (SHDSL) transceivers," *ANSI Standard T1.422-2001*.

[30] "Very high speed digital subscriber line foundation," *ITU Recommendation G.993.1*, 2001.

[31] "Transmission and multiplexing (TM) - access transmission systems on metallic access cables; very high speed digital subscriber line (VDSL); part 1: Functional requirements," *ETSI TS 101 270-1-v.1.2.1*, 1999.

[32] J. A. C. Bingham, *ADSL, VDSL, and Multicarrier Modulation*. John Wiley & Sons, N.Y., 2000.

[33] D. J. Rauschmayer, *ADSL/VDSL Principles*. Macmillan Technical Publishing, IN, 1999.

[34] W. Goralski, *ADSL and DSL technologies*. McGraw-Hill, N.Y., 1998.

[35] J. A. C. Bingham, *The theory and practice of modem design*. John Wiley & Sons, N.Y., 1988.

[36] S. Lin and D. J. Costello, *Error control coding: fundamentals and applications*. Prentice Hall, Upper Saddle River, N.J., 1983.

[37] R. E. Blahut, *Theory and practice of error control codes*. Addison-Wesley, Boston, MA, 1983.

[38] J. M. Cioffi, "A multicarrier primer," *ANSI Contribution T1E1.4/91-157*, November 1991.

[39] S. B. Weinstein and P. M. Ebert, "Data transmission by frequency division multiplexing using discrete fourier transform," *IEEE Transactions on Communications*, vol. 19, pp. 628 – 634, October 1971.

[40] J. A. C. Bingham, "Multicarrier modulation for data transmission: an idea whose time has come," *IEEE Communications Magazine*, vol. 28, pp. 5 – 14, May 1990.

[41] L. F. Wei, "Rotationally invariant channel coding with expanded signal space," *IEEE Journal on Selected Areas in Communications*, pp. 659 – 668, September 1984.

[42] D. W. Decker, G. A. Anwyl, M. D. Dankberg, M. J. Miller, S. R. Hart, and K. A. Jaska, "Multi-channel trellis encoder/decoder," U.S. patent 4,980,897, December, 1990.

[43] D. Hughes-Hartogs, "Ensemble modem structure for imperfect transmission media," U.S. patents 4,679,227, July, 1987; 4,731,816, March 1988; and 4,833,706, May 1989.

[44] P. S. Chow, J. M. Cioffi, and J. A. C. Bingham, "A practical discrete multitone transceiver loading algorithm for data transmission over spectrally shaped channels," *IEEE Transactions on Communications*, vol. 43, pp. 773 – 775, Feb.-March-April 1995.

[45] R. F. H. Fischer and J. B. Huber, "A new loading algorithm for discrete multitone transmission," in *Proceedings of the IEEE Global Telecommunications Conference*, vol. 1, pp. 724 – 728, November 1996.

[46] W. Yu and J. M. Cioffi, "On constant power water-filling," in *Proceedings of the IEEE International Conference on Communications*, vol. 6, pp. 1665 – 1669, June 2001.

[47] A. Leke and J. M. Cioffi, "A maximum rate loading algorithm for discrete multitone modulation systems," in *Proceedings of the IEEE Global Telecommunications Conference*, vol. 3, pp. 1514 – 1518, November 1997.

[48] R. V. Sonalkar and R. R. Shively, "An efficient bit-loading algorithm for DMT applications," in *Proceedings of the IEEE Global Telecommunications Conference*, vol. 5, pp. 2683 – 2688, November 1998.

[49] B. S. Krongold, K. Ramchandran, and D. L. Jones, "Computationally efficient optimal power allocation algorithm for multicarrier communication systems," in *Proceedings of the IEEE International Conference on Communications*, vol. 2, pp. 1018 – 1022, June 1998.

[50] B. S. Krongold, K. Ramchandran, and D. L. Jones, "An efficient algorithm for optimal margin maximization in multicarrier communication systems," in *Proceedings of the IEEE Global Telecommunications Conference*, vol. 1b, pp. 899 – 903, November 1999.

[51] S. Kourtis, "Optimum bit allocation algorithm for dmt-based systems under minimum transmitted power constraint," *IEE Electronics Letters*, vol. 35, pp. 2181 – 2182, December 1999.

[52] J. Campello, "Optimal discrete bit loading for multicarrier modulation systems," in *Proceedings of the IEEE International Symposium on Information Theory*, p. 193, August 1998.

[53] J. Campello, "Practical bit loading for DMT," in *Proceedings of the IEEE International Conference on Communications*, vol. 2, pp. 801 – 805, June 1999.

[54] L. M. C. Hoo, J. Tellado, and J. M. Cioffi, "Dual QoS loading algorithms for multicarrier systems offering different CBR services," in *Proceedings of the IEEE International Symposium on Personal, Indoor and Mobile Radio Communications*, vol. 1, pp. 278 – 282, September 1998.

[55] L. M. C. Hoo, J. Tellado, and J. M. Cioffi, "Dual QoS loading algorithms for DMT systems offering CBR and VBR services," in *Proceedings of the IEEE Global Telecommunications Conference*, vol. 1, pp. 25 – 30, November 1998.

[56] M. Colin, C. Modlin, M. Gharbi, and M. Gazalet, "QoS considerations for DMT-based ADSL and VDSL systems," in *Proceedings of the IEEE International Conference on Acoustics, Speech and Signal Processing*, vol. 6, pp. 3437 – 3440, May 1998.

[57] L. M. C. Hoo, J. Tellado, and J. M. Cioffi, "Discrete dual QoS loading algorithms for multicarrier systems," in *Proceedings of the IEEE International Conference on Communications*, vol. 2, pp. 796 – 800, June 1999.

[58] H. Zheng and K. J. R. Liu, "Robust image and video transmission over spectrally shaped channels using multicarrier modulation," *IEEE Transactions on Multimedia*, vol. 1, pp. 88 – 103, March 1999.

[59] J. S. Chow, "Superframe-based bit allocation algorithms for DMT systems," in *Proceedings of the IEEE Global Telecommunications Conference*, vol. 5, pp. 2800 – 2805, November 1998.

[60] V. Oksman and J.-J. Werner, "Single-carrier modulation technology for very high-speed digital subscriber line," *IEEE Communications Magazine*, vol. 38, pp. 82 – 89, May 2000.

[61] B. R. Saltzberg, "Comparison of single-carrier and multitone digital modulation for ADSL applications," *IEEE Communications Magazine*, vol. 36, pp. 114 – 121, November 1998.

[62] M. A. Tzannes, M. C. Tzannes, J. Proakis, and P. N. Heller, "DMT systems, DWMT systems and digital filter banks," in *Proceedings of the IEEE International Conference on Communications*, vol. 1, pp. 311 – 315, May 1994.

[63] S. D. Sandberg and M. A. Tzannes, "Overlapped discrete multitone modulation for high speed copper wire communications," *IEEE Journal on Selected Areas in Communications*, vol. 13, pp. 1571 – 1585, December 1995.

[64] A. N. Akansu and X. Lin, "A comparative performance evaluation of DMT (OFDM) and DWMT (DSBMT) based DSL communications systems for single and multitone interference," in *Proceedings of the IEEE International Conference on Acoustics, Speech and Signal Processing*, vol. 6, pp. 3269 – 3272, May 1998.

[65] G. Cherubini, E. Eleftheriou, and S. Olcer, "Filtered multitone modulation for VDSL," in *Proceedings of the IEEE Global Telecommunications Conference*, vol. 2, pp. 1139 – 1144, November 1999.

[66] G. Cherubini, E. Eleftheriou, and S. Olcer, "Filtered multitone modulation for very high-speed digital subscriber lines," *IEEE Journal on Selected Areas in Communications*, vol. 20, pp. 1016 – 1028, June 2002.

[67] G. Cherubini, E. Eleftheriou, S. Olcer, and J. Cioffi, "Filter bank modulation techniques for very high speed digital subscriber lines," *IEEE Communications Magazine*, vol. 38, pp. 98 – 104, May 2000.

[68] F. Sjoberg, M. Isaksson, P. Deutgen, R. Nilsson, P. Odling, and P. O. Borjesson, "Performance evaluation of the Zipper duplex method," in *Proceedings of the IEEE International Conference on Communications*, vol. 2, pp. 1035 – 1039, June 1998.

[69] F. Sjoberg, R. Nilsson, M. Isaksson, P. Odling, and P. O. Borjesson, "Asynchronous Zipper [subscriber line duplex method]," in *Proceedings of the IEEE International Conference on Communications*, vol. 1, pp. 231 – 235, June 1999.

[70] F. Sjoberg, M. Isaksson, R. Nilsson, P. Odling, S. K. Wilson, and P. O. Borjesson, "Zipper: a duplex method for VDSL based on DMT," *IEEE Transactions on Communications*, vol. 47, pp. 1245 – 1252, August 1999.

[71] D. G. Mestdagh, M. R. Isaksson, and P. Odling, "Zipper VDSL: a solution for robust duplex communication over telephone lines," *IEEE Communications Magazine*, vol. 38, pp. 90 – 96, May 2000.

[72] J. H. Fennick, "Amplitude distribution of telephone channel noise and a model for impulse noise," *Bell System Technical Journal*, vol. 48, pp. 3243 – 3263, December 1969.

[73] B. W. Stuck and B. Kleiner, "A statistical analysis of telephone noise," *Bell System Technical Journal*, vol. 53, no. 7, pp. 1263 – 1320, 1974.

[74] S. J. M. Tol and W. van der Bijl, "Measured performance of ISDN transmission in the Dutch local telephone network," in *Proceedings of the International Symposium on Services and Local Access*, September 1986.

[75] K. Széchěnyi and K. Böhm, "Measured performance of ISDN transmission in the Dutch local telephone network," in *Proceedings of the International Symposium on Services and Local Access*, September 1988.

[76] R. A. McDonald, "Report on bellcore impulse noise study," *ANSI Contribution T1D1.3/87-256*, July 1987.

[77] K. Széchěnyi, "On the NEXT and impulse noise properties of subscriber loops," in *Proceedings of the IEEE Global Telecommunications Conference*, pp. 1569 – 1573, November 1989.

[78] C. F. Valenti and K. Kerpez, "Analysis of wideband noise measurements and implications for signal processing in ADSL environments," in *Proceedings of the IEEE International Conference on Communications*, pp. 826 – 832, May 1994.

[79] J. W. Cook, "Wideband impulsive noise survey of the access network," *BT Technology Journal*, vol. 11, pp. 155 – 162, July 1993.

[80] K. T. Foster, G. Young, and J. W. Cook, "Broadband multimedia delivery over copper," *BT Technology Journal*, vol. 13, pp. 78 – 98, October 1995.

[81] W. Henkel and T. Kessler, "Statistical description and modelling of impulsive noise on the German telephone network," *IEE Electronics Letters*, vol. 30, pp. 935 – 936, June 1994.

[82] W. Henkel and T. Kessler, "A wideband impulsive noise survey in the German telephone network: statistical description and modelling," *AEÜ*, vol. 48, pp. 277 – 288, November/December 1994.

[83] W. Henkel, T. Kessler, and H. Y. Chung, "Coded 64-CAP ADSL in an impulse-noise environment-modelling of impulse noise and first simulation results," *IEEE Journal on Selected Areas in Communications*, vol. 13, pp. 1611 – 1621, December 1995.

[84] D. B. Levey and S. McLaughlin, "Statistics of impulse noise: Interarrival times," *Submission to ETSI WG TM6, TD19, 993T19A0*, September 1999.

[85] S. McLaughlin and D. B. Levey, "Statistics of impulse noise: Lengths and energies," *Submission to ETSI WG TM6, TD20, 993T20A0*, September 1999.

[86] D. B. Levey and S. McLaughlin, "Statistics of impulse noise: Interarrival times," *Submission to ETSI WG TM6, TD54, 994TD54VA0*, November 1999.

[87] I. Mann, S. McLaughlin, and D. B. Levey, "A new statistic for impulse noise measurement," *Submission to ETSI WG TM6, TD55, 994TD55VA0*, November 1999.

[88] G. Komp, "Impulse noise measurements in the VDSL environment," *Submission to ETSI WG TM6, TD15, 972T15A0*, June 1997.

[89] W. Henkel and T. Kessler, "An impulse-noise model - a proposal for SDSL," *Submission to ETSI WG TM6, TD45, 992T45A0*, May 1999.

[90] R. J. A. Tough and K. D. Ward, "The correlation properties of gamma and other non-Gaussian processes generated by memoryless nonlinear transformation," *J. Physics D: Applied Physics*, vol. 32, pp. 3075 – 3084, December 1999.

[91] D. R. Cox and H. D. Miller, *The Theory of Stochastic Processes*. Methuen, London, 1965.

[92] D. R. Cox, *Renewal Theory*. Methuen, London, 1967.

[93] B. Mandelbrot, "Self-similar error clusters in communication systems and the concept of conditional stationarity," *IEEE Transactions on Communication Technology*, pp. 71 – 90, 1965.

[94] S. M. Sussman, "Analysis of the Pareto model for error statistics on telephone circuits," *IEEE Transactions on Communications Systems*, vol. 11, pp. 213 – 221, June 1963.

[95] R. M. Fano, "A theory of impulse noise in telephone networks," *IEEE Transactions on Communications*, vol. 25, pp. 577 – 588, June 1977.

[96] B. D. Fritchman, "A binary channel characterization using partitioned Markov chains," *IEEE Transactions on Information Theory*, vol. 13, pp. 221 – 227, April 1967.

[97] W. Mendenhall and T. Sincich, *Statistics for Engineering and the Sciences*. Macmillan Publishing, N.Y., 3rd ed., 1992.

[98] M. Kendall, A. Stuart, and J. K. Ord, *Kendall's Advanced Theory of Statistics*, vol. 1: Distribution Theory. Charles Griffin & Co., London, 5th ed., 1987.

[99] W. T. Cochran, A. L. Cudworth, E. E. Gross, R. A. Kaenel, W. W. Lang, and D. E. Nelson, "Recommended practices for burst measurements in the time domain," *IEEE Transactions on Audio and Electroacoustics*, vol. AU-14, pp. 115 – 121, September 1966.

[100] E. A. Lee and D. G. Messerschmitt, *Digital Communications*. Kluwer, Dordrecht, 2nd ed., 1994.

[101] A. Papoulis, *Probability, Random Variables, and Stochastic Processes*. McGraw-Hill, N.Y., 3rd ed., 1991.

[102] B. S. Everitt and D. J. Hand, *Finite Mixture Distributions*. Chapman and Hall, London, 1981.

[103] S. J. Russell and P. Norvig, *Artificial Intelligence: A Modern Approach*. Prentice Hall, N.J., 1995.

[104] R. A. Howard, *Dynamic Probabilistic Systems*, vol. 1: Markov Models. John Wiley & Sons, N.Y., 1971.

[105] R. A. Howard, *Dynamic Probabilistic Systems*, vol. 2: Semi-Markov and Decision Processes. John Wiley & Sons, N.Y., 1971.

[106] D. R. Cox and P. A. W. Lewis, *The Statistical Analysis of Series of Events*. Methuen, London, 1966.

[107] P. Billingsley, "Statistical methods in Markov chains," *Annals on Mathematical Statistics*, vol. 32, pp. 12 – 40, 1961.

[108] J. A. Rice, *Mathematical Statistics and Data Analysis*. Wadsworth & Brooks/Cole, Ca., 1988.

[109] K. J. Kerpez, "Near end crosstalk is almost Gaussian," *IEEE Transactions on Communications*, vol. 41, pp. 670 – 672, May 1993.

[110] B. Pederson and D. Falconer, "Minimum mean square equalization in cyclostationary and stationary interference analysis and subscriber line calculations," *IEEE Journal on Selected Areas in Communications*, vol. 9, pp. 931 – 940, August 1991.

[111] S. H. Lin, "Statistical behavior of multipair crosstalk," *Bell System Technical Journal*, vol. 59, pp. 955 – 974, July/Aug. 1980.

[112] M. Pollakowski, "Eigenschaften symmetrischer Ortanschlusskabel im Frequenzbereich bis 30 MHz," *Der Fernmelde Ingenieur*, vol. 9/10, September 1995.

[113] C. Valenti, "Cable crosstalk parameters and models," *ANSI Contribution T1E1.4/97-302*, September 1997.

[114] J. H. W. Unger, "Near-end crosstalk model for line studies," *ANSI Contribution T1D1.3/85-244*, November 1985.

[115] G. Huang and J.-J. Werner, "Cable characteristics," *ANSI Contribution T1E1.4/97-169*, May 1997.

[116] G. Zimmerman, "On the importance of crosstalk from mixed sources," *ANSI Contribution T1E1.4/97-181*, June 1997.

[117] S. Galli and K. J. Kerpez, "Methods of summing crosstalk from mixed sources. II. Performance results," *IEEE Transactions on Communications*, vol. 50, pp. 600 – 607, April 2002.

[118] K. T. Foster, "VDSL noise model philosophy," *Submission to ETSI WG TM6, TD17, 973T17R0*, October 1997.

[119] R. Persico, L. Magnone, and FSAN Group, "A new analytical method for NEXT and FEXT noise calculation in multi-access architecture," *Submission to ETSI WG TM6, TD04, 983T04A0*, June 1998.

[120] J. Cook, L. Magnone, M. Friese, and M. Isaksson, "FSAN noise combination method versus mean PSD method: comparison using cable couplings," *ANSI Contribution T1E1.4/99-015*, 1999.

[121] "Spectrum management for loop transmission systems," *ANSI Standard T1.417-2001*.

[122] S. Galli and K. J. Kerpez, "The problem of summing crosstalk from mixed sources," *IEEE Communications Letters*, vol. 4, pp. 325 – 327, November 2000.

[123] S. Galli and K. J. Kerpez, "Methods of summing crosstalk from mixed sources. I. Theoretical analysis," *IEEE Transactions on Communications*, vol. 50, pp. 453 – 461, March 2002.

[124] "Access to bandwidth: determination on the access network frequency plan (ANFP) for BTs metallic access network," *Office of Telecommunications, UK*, October 2000.

[125] J. G. Proakis, *Digital Communications*. McGraw-Hill, N.Y., 3rd ed., 1995.

[126] D. I. Laurenson, S. McLaughlin, and G. Cope, "Performance of TCP/IP over ADSL subjected to impulse noise," in *Proceedings of the International Symposium on Services and Local Access*.

[127] M. Zorzi and R. R. Rao, "On the impact of burst errors on wireless atm," *IEEE Personal Communications*, vol. 6, pp. 65 – 76, August 1999.

[128] Y. Wei, G. Ginis, and J. M. Cioffi, "Distributed multiuser power control for digital subscriber lines," *IEEE Journal on Selected Areas in Communications*, vol. 20, pp. 1105 – 1115, June 2002.

[129] (2003, February) Tektronix MPEG2 video test bitstreams. [Online]. Available: ftp://ftp.tek.com/tv/test/streams/Element/index.html.

[130] H. T. Huynh, V. Bach, and P. Fortier, "Performance analysis of M-QAM in a non-gaussian environment," *International Journal of Electronics and Communications*, pp. 255 – 262, September 1997.

[131] Y. H. Chew, T. T. Tjhung, T. He, and C. C. Ko, "Estimation of BER performance over an impulse noise channel," *IEE Electronics Letters*, vol. 35, pp. 273 – 274, February 1999.

[132] P. Hougaard, "A class of multivariate failure time distributions," *Biometrika*, vol. 73, pp. 671 – 678, December 1986.

[133] J. Abate and W. Whitt, "An operational calculus for probability distributions via Laplace transforms," *Advances in Applied Probability*, vol. 28, pp. 75 – 113, March 1996.

[134] R. C. Gonzalez and R. E. Woods, *Digital Image Processing*. Addison-Wesley, Reading, MA, 1992.

[135] P. Hougaard, "Fitting a multivariate failure time distribution," *IEEE Transactions on Reliability*, vol. 38, pp. 444 – 448, October 1989.

[136] A. P. Prudnikov, Y. A. Brychkov, and O. I. Marichev, *Integrals and series*, vol. 4: Direct Laplace Transforms. OPA (Amsterdam) B.V., 1992.

[137] A. P. Prudnikov, Y. A. Brychkov, and O. I. Marichev, *Integrals and series*, vol. 3: More special functions. OPA (Amsterdam) B.V., 1990.

[138] S. Kotz, N. Balakrishnan, and N. L. Johnson, *Continuous Multivariate Distributions*, vol. 1: Models and Applications. John Wiley & Sons, N.Y., 2nd ed., 2000.

[139] (2003, February) Elecard MPEG2 player 2.0. [Online]. Available: http://www.elecard.com/products/mpeg2player.shtml.